

First-principles calculation of alloy phase diagrams: The renormalized-interaction approach

L. G. Ferreira, Su-Huai Wei, and Alex Zunger
Solar Energy Research Institute, Golden, Colorado 80401
(Received 3 January 1989)

We present a formalism for calculating the temperature-composition phase diagrams of isostructural solid alloys from a microscopic theory of electronic interactions. *First*, the internal energy of the alloy is expanded in a series of volume-dependent multiatom interaction energies. These are determined from self-consistent total-energy calculations on periodic compounds described within the local-density formalism. *Second*, distant-neighbor interactions are renormalized into composition- and volume-dependent effective near-neighbor multisite interactions. *Finally*, approximate solutions to the general Ising model (using the tetrahedron cluster variation method) underlying these effective interactions provide the excess enthalpy ΔH , entropy ΔS , and hence the phase diagram. The method is illustrated for two prototype semiconductor fcc alloys: one with a large size mismatch ($\text{GaAs}_x\text{Sb}_{1-x}$) and one with a small size mismatch ($\text{Al}_{1-x}\text{Ga}_x\text{As}$), producing excellent agreement with the measured miscibility temperature and excess enthalpies. For lattice-mismatched systems, we find $0 < \Delta H^O < \Delta H^D$, where O denotes some ordered Landau-Lifshitz (LL) structures, and D denotes the disordered phase. We hence predict that such alloys will disproportionate at low-temperature equilibrium into the binary constituents, but if disproportionation is kinetically inhibited, some special ordered phases (i.e., chalcopyrite) will be thermodynamically stabler below a critical temperature than the disordered phase of the same composition. For the lattice-matched systems, we find $0 < \Delta H^D < \Delta H^O$ for all LL structures, so that only a phase-separating behavior is predicted. However, in these systems, longer-period ordered superlattices are found to be stabler, at low temperatures, than the disordered alloy.

I. INTRODUCTION

A. Modeling isostructural phase diagrams as a generalized Ising problem

The existence of finite interactions between atoms A and B on a lattice leads to either phase separation or ordering of the solid A_xB_{1-x} alloy at low temperatures. As the temperature is raised, ordered or phase-separated forms could transform into a homogeneous disordered structure. The great diversity of such configurational arrangements underlying the crystalline solid state, evidenced by the voluminous catalogs of phase phenomena,¹⁻⁶ has naturally led to many attempts to systematize these effects in terms of microscopic quantities.⁷⁻¹³ Whereas the competition between various possible *ordered* phases at $T=0$ has been partially rationalized in terms of either elemental structural diagrams^{1,13} or quantum-mechanical total-energy calculations for crystals,¹⁴ these approaches have generally not described the additional, temperature-mediated competition with disordered phases, partially ordered structures, or multiple-phase coexistences occurring at *finite* temperatures.

The composition-temperature (x, T) phase diagrams^{15,16} of isovalent octet compounds $A_x^{8-\lambda}B_{1-x}^{8-\lambda}C^\lambda$ ($4 \leq \lambda \leq 7$) have received special attention due to the ability to tune their technologically significant electronic properties through adjustments of the compositions x . Alkali halides ($\lambda=7$) alloys exhibit¹⁵ in their phase dia-

gram miscibility gaps, partial solubility, and even insolubility accompanied by compound formation (CsLiF_2 , RbLiF_2). Until recently, thermodynamic studies¹⁷⁻²³ suggested that both II-VI pseudobinary alloys ($\lambda=6$) and III-V pseudobinary alloys ($\lambda=5$) exhibit mostly "solid solubility above a miscibility gap," as well as limited solubility, but no compound formation. However, recent predictions²⁴⁻²⁶ and subsequent experiments²⁷⁻³³ have observed at low temperatures the formation of inter semiconductor isovalent compounds $A_n^{8-\lambda}B_{4-n}^{8-\lambda}C_4^\lambda$ for $n=1, 2$, and 3 . Similarly, despite the very limited solid solubility of the nonisovalent octet compounds $(A^{\text{III}}B^{\text{V}})_x(C^{\text{IV}})_{1-x}$ or $(A^{\text{II}}C^{\text{VI}})_x(B^{\text{III}}D^{\text{V}})_{1-x}$, long-range-ordered compounds have been reported.³⁴

Whereas simple phenomenological models involving the size and electronegativity mismatch between the alloyed atoms and A and B have traditionally been used to systematize the propensity of the components to form solid solutions,^{9,11,12,35} theoretical descriptions of the full temperature-composition phase diagrams have been sought through lattice models. There,^{26,36-38} one considers the 2^N possible arrangements ("configuration," or "microstates") of atoms A and B on a fixed lattice of N points, characterizing each configuration σ by its excess internal energy (at a given external volume V) with respect to equivalent amounts of the solid constituents A and B at their equilibrium volumes,

$$\Delta E(\sigma, V) = E(\sigma, V) - \frac{N_A}{N} E_A - \frac{N_B}{N} E_B, \quad (1.1)$$

where N_A and N_B are the number of A and B atoms, respectively. Each lattice site i can be occupied either by a B atom (in which case the spin variable is denoted $\hat{S}_i = 1$) or by an A atom (where $\hat{S}_i = -1$). One then seeks to find for each (x, T) the density matrix $\rho(\sigma, V)$ and from it the ensemble average (over configurations) of the internal energy $\langle \Delta E(\gamma, V) \rangle$ and entropy, for all phases γ (disordered, ordered, phase coexistence, etc.). The solutions which are energy minimizing both with respect to volume and probability distributions define the excess enthalpy and entropy

$$\begin{aligned} \Delta H(\gamma, T) &= H(\gamma, T) - xH_A(T) - (1-x)H_B(T), \\ \Delta S(\gamma, T) &= S(\gamma, T) - xS_A(T) - (1-x)S_B(T) \end{aligned} \quad (1.2)$$

for each phase γ . Using the conventional common tangent construction³⁷ (seeking x and T where the free energies of two phases equilibrate) one then constructs the phase diagram.

Even neglecting excess vibrational energies and limiting the discussion to phase interconversions on the same type of lattice at all compositions, this is still a formidable task, involving 2^N calculations of $\Delta E(\sigma, V)$ at each V and performing a statistical ensemble average on such systems (indeed, no exact calculation of the partition function exists for three-dimensional infinite systems). Hence, the standard lattice theory approach³⁶⁻³⁸ proceeds by making two central approximations.

First, instead of attempting a direct evaluation of the total energy $\Delta E(\sigma, V)$ of the 2^N possible arrangements of atoms A and B on N sites, one expands $\Delta E(\sigma, V)$ in a series of "figures" f consisting of k vertices and up to m neighbors. Denoting by $J_f(V)$ the simultaneous interaction energy of a figure $f = (k, m)$ and by $\Pi_f(l_f, \sigma)$ the product of the spin variables \hat{S} at the vertices of the figure f located at l , one has

$$\Delta E(\sigma, V) = \sum_f \sum_{l_f} J_f(V) \Pi_f(l_f, \sigma). \quad (1.3)$$

Note that in Eq. (1.3) l_f denotes the lattice site l and the equivalent figures f at that site. The following sum rules are observed:

$$\sum_{l_f} 1 = ND_f, \quad (1.4a)$$

$$\sum_f ND_f = 2^N, \quad (1.4b)$$

where D_f is the average number of figures of type f per site. The definition of a figure depends on the space group associated with the structure. Two figures (f, l) and (f', l') are equivalent if there is a space-group operation transforming (f, l) into (f', l') . For example, in an fcc lattice of N sites with the full space group (i.e., that of pure A , pure B , or the disordered alloy) there are $6N$ nearest-neighbor pairs, $8N$ nearest-neighbor triangles, and $2N$ nearest-neighbor tetrahedra (i.e., $D_f = 6, 8, 2$ respectively). In this case all figures belonging to a given type (nearest-neighbor pairs, triangles, tetrahedra, etc.) are equivalent. However, this equivalency is generally lifted in ordered structures, since the space group of or-

dered structures is a subgroup of that of the disordered phase. In this case we will have more figures and smaller D_f 's.

In a coherent binary ($A_x B_{1-x}$) or pseudobinary ($A_x B_{1-x} C$) system, the substituting species (A and B) are restricted to reside on the ideal lattice site, in which case a single external volume V defines uniquely the size and shape of each figure f . Hence, $J_f(V)$ is independent on the space group of the system (or on the equivalence or inequivalence of the figure f). In this case, one can define the "average in lattice product"

$$\bar{\Pi}_f(\sigma) = \frac{1}{ND_f} \sum_{l_f} \Pi_f(l_f, \sigma), \quad (1.5)$$

where the figures f (and their equivalent partners) are defined with respect to the full space group of the disordered alloy. Equation (1.3) then reads

$$\Delta E(\sigma, V) = N \sum_f D_f \bar{\Pi}_f(\sigma) J_f(V). \quad (1.6)$$

In contrast, in the case of incoherence (e.g., when lattice relaxation displaces the A, B atoms off their ideal sites), the volume alone does not suffice to define the size and shape of each figure and the degeneracy of the J_f 's could split. In this case, one can still use Eq. (1.6) and the definitions surrounding it, as long as an appropriate average over those figures which are equivalent in the disordered alloy is taken to equate (1.3) to Eq. (1.6).

The utility of the expansion (1.3) or (1.6) in actual calculations rests in the truncation of the size of the largest figure F to a computationally tractable small value. This implies that a correspondingly small set of interaction energies $\{J_f(V)\}$ can capture through a linear superposition construct the essential energetics of any configuration σ of (N_A, N_B) atoms on the $N = N_A + N_B$ sites. The reader will recognize Eq. (1.3) to be the generalized three-dimensional Ising model³⁶ with up to F spin interactions.

To calculate thermodynamic quantities, one needs to take the configurational averages of $\Delta E(\sigma, V)$ for particular phases γ (ordered or disordered). The ensemble average of a function $\psi(\sigma)$ is

$$\langle \psi(\sigma) \rangle_\gamma = \sum_\sigma \rho_\gamma(\sigma) \psi(\sigma), \quad (1.7)$$

where $\rho_\gamma(\sigma)$ is the density matrix for phase γ . The ensemble average of $\Pi_f(l_f, \sigma)$ of Eq. (1.3) is the "multisite correlation function"

$$\langle \Pi_f \rangle_\gamma = \sum_\sigma \rho_\gamma(\sigma) \Pi_f(l_f, \sigma), \quad (1.8)$$

which does not depend on l since $\rho_\gamma(\sigma)$ has the space-group symmetry of γ , (defining among others the figures and their inequivalence). The density matrix can be obtained by using the "orthogonality condition"^{39,40} given by Sanchez *et al.*⁴⁰ as

$$\rho(\sigma) = \frac{1}{2^N} \sum_f \sum_{l_f} \langle \Pi_f \rangle \Pi_f(l_f, \sigma) \quad (1.9)$$

for any one of the 2^N configurations. The sum in Eq. (1.9) is taken over all topologically different figures f located anywhere in the lattice (including the "empty" figure $f=0$, with no sites, for which $\Pi_f=1$). Combining Eqs. (1.3) and (1.8) we obtain

$$\langle \Delta E(V) \rangle = N \sum_f D_f J_f(V) \langle \Pi_f \rangle. \quad (1.10)$$

Equation (1.10) provides a practical form for calculating ensemble average energies in terms of a limited number of figures, provided that the sum over 2^N terms involved in the calculation of the correlation functions $\langle \Pi_f \rangle$ can be made tractable. This leads to the second class of key approximation. While many different strategies exist, we briefly discuss the cluster variation method⁴¹⁻⁴³ (CVM) which we use to this end. Here one selects the largest figure F (and all of its subfigures g) to be used in approximating the *statistical* sum of Eq. (1.9) (the multisite correlation function $\langle \Pi_f \rangle$ for figures larger than F will be expressed in Sec. II in terms of those of figures contained in F). This choice, implying a distance d_{stat} beyond which statistical correlations are neglected, is distinct from the choice of the maximum interaction distance d_{int} , within which the interaction energies J_f are retained. Denoting by n the configuration of spins at the vertices of a subfigure g at l , one then defines the reduced density matrix⁴⁰

$$\rho_g(n) = \sum_{\sigma} \rho(\sigma), \quad (1.11)$$

where the primed sum over σ denotes a multiple sum over all configurations σ containing n at the vertices of subfigure g at l . The simplification is achieved by decomposing the subfigure g into a hierarchy of *its* subfigures h , hence, like Eq. (1.9), Eq. (1.11) can be written as a sum over the subfigures h (contained in g , and therefore in F):

$$\rho_g(n) = \frac{1}{2^k} \sum_{(h,l') \subset (g,l)} \langle \Pi_h \rangle \Pi_h(l', n), \quad (1.12)$$

where k is the number of vertices of figure g . This approximation of the density matrix affords a hierarchial calculation of the multisite correlation functions $\langle \Pi_g \rangle$ of Eq. (1.8). Using Eq. (1.10), this then gives the ensemble average of the internal energy $\langle \Delta E(V) \rangle$. The analogous result for the excess entropy is similarly expressed in terms of the reduced density matrix as

$$\Delta S = -k_B N \sum_{g \subset F} a_g \sum_n \rho_g(n) \ln \rho_g(n), \quad (1.13)$$

where a_g are geometrical constants obtained by the procedure of Barker.⁴²

The two central approximation—(i) the superposition ansatz of Eq. (1.3) for the interaction energies $J_f(V)$ (truncated at an interaction distance d_{int}), and (ii) the approximation of the configurational sum in Eq. (1.8) (truncated at a statistical counting distance d_{stat})—enable a calculation of the thermodynamic functions of Eq. (1.2)

and hence the phase diagram. Much of the effort in this field has focused on (i) developing approximate methods for evaluation of $\langle \Pi_g \rangle$ of Eq. (1.8) and (ii) characterizing the type of ground states *given* a fixed (and usually small) set of interaction energies $\{J_f\}$. It is clear, however, that the understanding of actual phase diagrams requires, in addition,^{37,40} (i) a microscopic formulation of the interaction energies $\{J_f(V)\}$ in terms of the properties of A and B , and (ii) an understanding of the physical content of the length scales (e.g., d_{int} , d_{stat}) of the problem, combined with tractable formulations for incorporating contributions to the free energy within these lengths. We turn next to the latter issue.

B. Length scales of the problem

Three distinct length scales appear in formulating a first-principles theory of phase diagrams. *First*, the calculation of the interaction energies J_f by integrating the electronic (elec) degrees of freedom often involves matrix elements between atomic orbitals separated by a maximum distance d_{elec} . Tight-binding models,⁴⁴ for example, often truncate d_{elec} at first- or second-neighbor hopping integrals. *Second*, the expansion of the Born-Oppenheimer energy of Eq. (1.3) in terms of multiatom interactions J_f involves a distance d_{int} beyond which atoms are assumed to have a negligible interaction (int). d_{int} involves both the order k of simultaneous many-atom interactions retained ($k=1,2,3,4$ corresponding to simultaneous one-, two-, three-, and four-body interactions, respectively) and the maximum interatomic separation within which interactions are calculated ($m=1,2,3,4$ corresponding to first-, second-, third-, and fourth-neighbor interactions, respectively). The simplest Ising model (see review in Ref. 36) involves pair interactions within first neighbors ($k \leq 2, m=1$). *Third*, the statistical calculation of the correlation functions $\langle \Pi_g \rangle$ of Eq. (1.8) for a given set $\{J_f\}$ involves a statistical (stat) counting range d_{stat} , i.e., the size of the largest topological "figures" whose contributions to the entropy [Eqs. (1.11)–(1.13)] are counted. The sites-only statistical range corresponds to the Bragg-Williams approximation;⁴⁵ the sites plus pairs statistical range corresponds to the Bethe approximation,⁴⁶ etc.

Many of the currently used lattice models of phase diagrams can be characterized by the values of the three length scales used. For example, the tight-binding CPA-GPM (coherent-potential approximation-generalized perturbation method)⁴⁷ generally uses first neighbors for d_{elec} and few-neighbors pair interactions for d_{int} . The superposition model of Wei *et al.*⁴⁸ involves essentially an infinite range for d_{elec} , and a first-neighbor and up to four-body interaction ($m_{\text{max}}=1, k_{\text{max}}=4$) for d_{int} and four-site nearest-neighbor range for d_{stat} .

Experience from calculation of band structure of solids⁴⁹ shows that limiting d_{elec} to first neighbors rarely suffices to capture many of the physically significant details of the cohesive and structural energies, simply because the dimensions of the outer atomic orbitals in broad band solids often exceed the nearest-neighbor interatomic separations. Limiting the calculation to an iso-

lated subband^{44,47,50} (e.g., narrow d bands in transition metals) or empirical parametrization of the near-neighbor Hamiltonian matrix elements^{44,51} are often used to partially avoid this problem. The advances in modern electronic-structure computational techniques,^{52,53} however, make it now unnecessary to limit d_{elec} to a small value.

Statistical solutions to an Ising Hamiltonian with d_{int} fixed at the first nearest neighbor and varying d_{stat} have shown³⁷ that most aspects of the phase diagram are accurately captured when d_{stat} includes four-body counting figures. For example, the reduced transition temperature $k_B T_t / 12J_2$ for a nearest-neighbor pair-interaction fcc Ising ferromagnet is³⁷ 1.0, 0.9142, 0.8354, 0.84045, 0.83394, and 0.82981 if d_{stat} includes sites, pairs, tetrahedra, double tetrahedra, the tetrahedron-octahedron, and the double tetrahedron-octahedron, respectively, compared with the numerically accurate value of 0.81627 obtained in high-temperature expansions.³⁷ Hence, relative to the latter value, the errors in $k_B T_t / 12J_2$ are 22.5%, 12%, and 2.3% for sites, pairs, and tetrahedra, respectively. For many applications, an error of 2–5% can be tolerated. Note, however, that we do not know the effect on T_t of increasing d_{stat} when the interaction range d_{int} itself is long (e.g., $d_{\text{stat}} \cong d_{\text{int}}$ is equal to a few neighbor distances). This important question remains open at the present time.

The minimum range d_{int} of multiatom interactions needed to capture the essential physical characteristics of phase diagrams is more difficult to assess on a general basis. Past experience for fcc systems⁵⁴ (using volume-independent interactions) has shown that three-body interactions (or composition-dependent effect pair interactions)^{47(b)} are needed to explain the often observed asymmetry of the phase diagram about $x = 0.5$, that the general hierarchy of interactions for (fcc) systems is⁵⁵ $|J_{m=1}| \gg |J_{m \geq 2}|$, and that certain ordered phases (e.g., chalcopyrite and famatinite) can become ground-state structures only if $J_{m \geq 2}$ is included.^{56,57}

This discussion suggests to us that for fcc alloys, d_{elec} should be extended to large values, d_{stat} could be kept at four-body terms with little loss, and that d_{int} should include at least terms up to a few neighbor interactions. This realization leads us to our first (of two) developments: keep d_{stat} at fixed value (e.g., including up to four-body terms) and find a way to renormalize for the disordered phase the J_f 's for $d_{\text{int}} > d_{\text{stat}}$ into the \mathcal{J} 's for $d_{\text{int}} \leq d_{\text{stat}}$, by making a physically motivated approximation on the statistical correlations beyond d_{stat} . (For *ordered* phases we retain the full set of J_f 's so that chalcopyrite has a different energy than CuAu-I, and famatinite has a different energy than luzonite, etc.) We find that (see Sec. II B) if we assume that spin variables of a figure with sites separated by more than d_{stat} are statistically uncorrelated, we can renormalize analytically the effect of the \mathcal{J} 's beyond d_{stat} into those for $d \leq d_{\text{stat}}$. This contrasts with the conventional lattice theory approach to phase diagram calculations.^{37,47,56} There, the maximum figure F is used *both* for the definition of the range of J_f in the energy expansion [Eq. (1.3)] and for the statistical

calculation of the entropy [Eq. (1.13)]. When $d_{\text{int}} > d_{\text{stat}}$, one increases the size of the maximum figure used in the calculation of the entropy³⁷ (to capture $d_{\text{stat}} \leq d_{\text{int}}$), leading to a substantial complication and loss of transparency.

Our second development rests on the recent realization^{24–26,58} that in alloys of size-mismatched constituents (i.e., when the molar volumes V_A and V_B are unequal), there is no reason to believe that the interaction energies J_f of Eq. (1.3) are fixed, volume-independent constants as has been assumed in virtually all Ising model approaches to phase diagrams.^{36–38,40,45–47} Since the energy $E(V)$ of either ordered or disordered alloys depends, in general, on V , surely the J_f 's of Eq. (1.9) do too. The introduction of a volume dependence into $J_f(V)$ indeed changes significantly the phase diagram.²⁶

We therefore describe in Secs. II–IV (i) the way in which the volume-dependent functions $\{J_f(V)\}$ can be extracted from first-principles total-energy calculations on prototype ordered phases and (ii) the manner in which a large set of such $J_f(V)$'s can be renormalized into a smaller set of effective $\tilde{J}_f(x, V)$ under our statistical approximation. Applications of these effective interaction energies to the calculation of phase diagrams of III-V semiconductor alloys are described in Secs. V–VIII.

II. THE BASIC IDEAS

A. Obtaining $J_f(V)$ from the total energy of periodic structures

We start this section with two observations.^{24,48,58} (i) for certain high-symmetry states of order s (e.g., simple periodic crystals), the correlation functions $\bar{\Pi}_f(s)$ of Eq. (1.6) are geometrical constants which can be obtained directly by inspection, and (ii) the total excess energy $\Delta E(s, V)$ for these special structures $\{s\}$ can be calculated with high precision as a function of volume directly from self-consistent first-principles local-density methods,^{52,53} incorporating a long range of d_{elect} . These observations imply that one can specialize Eq. (1.6) to a few (say, M) ordered periodic structures $\{s\}$ of stoichiometry $A_n B_{N-n}$:

$$\Delta E(s, V) = N \sum_f D_f J_f(V) \bar{\Pi}_f(s), \quad (2.1)$$

where the excess total energy of crystal s with respect to equivalent amounts of its constituent solids A and B at equilibrium is

$$\Delta E(s, V) = E(s, V) - nE_A[V_A] - (N-n)E_B[V_B]. \quad (2.2)$$

We can now use the set of M linearly independent structures, and invert Eq. (2.1) to yield M interaction energy functions⁵⁸ $J_f(V)$:

$$J_f(V) = \frac{1}{ND_f} \sum_s [\bar{\Pi}_f(s)]^{-1} \Delta E(s, V). \quad (2.3)$$

We will assume below that the interaction energies $\{J_f(V)\}$ extracted from a set of prototype ordered periodic structures are transferrable to other phases γ of

the same system, provided that those phases differ from the set of ordered structures only by *substitutional* order. This is our first (of two) key approximations.

Connolly and Williams⁵⁸ have implemented this approach using five fcc ordered structures for $\{s\}$, i.e., limiting d_{int} to first fcc nearest neighbors. This selection is unconstrained in that (i) it does not provide information on the magnitude and importance of the interactions neglected or on the completeness of this set of interactions, and (ii) in selecting this value of d_{int} , the method leads to a degeneracy of the energies of those ordered structures which are distinguished by interactions beyond d_{int} (e.g., $L1_2$ versus DO_{22}). We avoid both problems by developing below (Sec. V E) a simple method of associating a set of M structures $\{s\}$ with a set of M interaction energies $\{J_f\}$, retaining in J_f interactions beyond the first fcc nearest neighbors. We will investigate in detail how the transferability can be affected by making the interaction energies volume dependent, by including a sufficiently large interaction range d_{int} , and by selecting an appropriate set of prototype structures $\{s\}$.

B. Expressing the configuration-averaged energies $\langle \Delta E(V) \rangle$ in terms of energies of periodic structures

Since $\{J_f(V)\}$ is linearly related through Eq. (2.3) to the excess energy of periodic structures $\{\Delta E(s, V)\}$, one can alternatively express $\Delta E(\sigma, V)$ of Eq. (1.6) as a superposition of $\Delta E(s, V)$

$$\Delta E(\sigma, V) = \sum_s \xi_s(\sigma) \Delta E(s, V), \quad (2.4a)$$

where the weights are

$$\xi_s(\sigma) = \sum_f [\bar{\Pi}_f(s)]^{-1} \bar{\Pi}_f(\sigma). \quad (2.4b)$$

In this case, the alloy excess energy becomes

$$\langle \Delta E(V) \rangle = \sum_s Q_s \Delta E(s, V), \quad (2.5)$$

where

$$Q_s = \langle \xi_s(\sigma) \rangle = \sum_f [\bar{\Pi}_f(s)]^{-1} \langle \bar{\Pi}_f \rangle. \quad (2.6)$$

Observe that in Eq. (2.6) the figures are defined with respect to the full space group, while the ensemble averages are taken with the space groups that are reduced in the case of the ordered phases. In the latter case, the independent variables used to minimize the free energy are not $\langle \bar{\Pi}_f \rangle$ but rather $\langle \Pi_f \rangle$ because the latter, not the former, define through Eqs. (1.12) and (1.13) the entropy.

In the general case, the weights Q_s of Eq. (2.5) cannot be interpreted as probabilities because they are not positive definite. However, in a special case we can interpret Q_s as probabilities. Consider the case where the maximum figure F is defined as a translational repeat unit U . This figure has k vertices which are labeled 1 to k ; all lattice sites are labeled accordingly. The space group of the labeled lattice is reduced with respect to that of the original unlabeled lattice. The number of subfigures of U is

2^k , corresponding to the different ways of selecting k sites. If (i) the figures are defined with this reduced space group, and (ii) if the ordered periodic structures $\{s\}$ can be described as a superposition of cells n (a particular arrangement of atoms A and B at the vertices of U), we may rewrite (2.4) as

$$\Delta E(\sigma, V) = \sum_n \xi_n(\sigma) \Delta E(n, V), \quad (2.7a)$$

where

$$\xi_n(\sigma) = \sum_{g \subset U} [\bar{\Pi}_g(n)]^{-1} \bar{\Pi}_g(\sigma) \quad (2.7b)$$

for the 2^k periodic structures n . In this case, the weights $\xi_n(\sigma)$ in Eq. (2.7b) have a simple interpretation as follows. First observe that, for a periodic structure n obeying the superposition assumption above,

$$\bar{\Pi}_g(n) = \Pi_g(l, n). \quad (2.8)$$

Second, analogously to the orthogonality relation,^{39,40} one has

$$\sum_n \Pi_g(l, n) \Pi_{g'}(l, n) = 2^k \delta_{g, g'}, \quad (2.9)$$

thus

$$[\bar{\Pi}_g(n)]^{-1} = 2^{-k} \Pi_g(l, n). \quad (2.10)$$

By Eq. (2.7b)

$$\xi_n(\sigma) = 2^{-k} \sum_{g \subset U} \Pi_g(l, n) \bar{\Pi}_g(\sigma). \quad (2.11)$$

The thermal average $P_n = \langle \xi_n \rangle$ can be written as

$$P_n = 2^{-k} \sum_{g \subset U} \langle \Pi_g \rangle \Pi_g(l, n) = \rho_U(n), \quad (2.12)$$

coinciding with the reduced density matrix of Eq. (1.12). Then the volume-dependent ensemble average energy of Eq. (1.10) becomes

$$\langle \Delta E(V) \rangle = \sum_n P_n \Delta E(n, V), \quad (2.13)$$

where the density-matrix elements P_n are positive and add up to 1. Thus *the ensemble average of the alloy energy can be interpreted as a statistical average of energies of these representative ordered periodic structures*. This is a powerful relationship since, as will be seen below, the thermodynamics of alloys could be expressed in terms of readily calculated equations of state $\Delta E(n, V)$ of ordered compounds.^{24-26,48,59-61} The remaining problem is to establish a set of structures used in Eq. (2.5) which produces rapid convergence of Eq. (2.13). We next describe a practical method for folding distant-neighbor interactions into a smaller set of interaction parameters, contained in U , enabling the construction of a rapidly convergent series.

C. Renormalization of distant-neighbor interactions into effective near-neighbor interactions in the disordered phase

Since there is no reason to believe that the interaction energies $\{J_f(V)\}$ are negligible beyond first-nearest neigh-

bors, we will “fold” distant-neighbor interactions into *effective* volume- and composition-dependent interactions⁶² $\{\tilde{J}_f(x, V)\}$ within the figure U . In the present illustration U is taken as the fcc tetrahedron of nearest neighbors. This folding is performed under a statistical assumption—our second key approximation—stating that if a figure has two spin variables separated by a distance larger than d_{stat} they will be assumed to be *statistically uncorrelated* in the following sense. Consider a figure ϕ consisting of sites $\alpha, \beta, \dots, \omega$. By the definition surrounding Eq. (1.3) its spin product is

$$\Pi_\phi = \hat{S}_\alpha \hat{S}_\beta \cdots \hat{S}_\omega, \quad (2.14)$$

where \hat{S} are the spin variables (taking up values of ± 1). If the figure ϕ is not contained in U , we assume no correlation and set

$$\langle (\hat{S}_\alpha - q_\alpha)(\hat{S}_\beta - q_\beta) \cdots (\hat{S}_\omega - q_\omega) \rangle = 0, \quad (2.15)$$

where

$$q_\alpha = \langle \hat{S}_\alpha \rangle \quad (2.16)$$

(with a similar definition for spins on other sites). In the case of the *disordered phase*,

$$q_\alpha = q_\beta = \cdots = q_\omega = q = 2x - 1, \quad (2.17)$$

where x is the concentration of B atoms. Equation (2.15) results from the natural assumption that the average product of Eq. (2.15) should be zero either if there are many spins participating (i.e., if ϕ is a large figure) or if the spins are far removed from each other. It allows us to write the correlation function $\langle \Pi_\phi \rangle$ as a combination of correlation functions of subfigures of ϕ times homogeneous polynomial functions of the sublattice concentrations. If any subfigures of ϕ is not yet contained in U , the process is repeated. In the case of the *disordered phase*, the result of this reduction is

$$\langle \Pi_\phi \rangle = \sum_{f \subset U} C_\phi^f (2x - 1)^{k_\phi - k_f} \langle \Pi_f \rangle, \quad (2.18)$$

where k_ϕ and k_f are the number of vertices in the figures ϕ and f , respectively, and C_ϕ^f are coefficients derived below from the expansion of the left-hand side of Eq. (2.15). Equation (2.18) will be used to evaluate the expression for the density matrix [Eq. (1.9)] and the alloy internal energy [Eq. (1.10)]. The latter becomes for the disordered phase

$$\langle \Delta E(V) \rangle = N \sum_{f \subset U} D_f J_f(V) \langle \Pi_f \rangle + N \sum_{\phi \not\subset U} D_\phi J_\phi(V) \langle \Pi_\phi \rangle. \quad (2.19)$$

Analogy with Eq. (1.10) permits the definition of *effective* interactions \tilde{J}_f satisfying

$$\langle \Delta E(V) \rangle \equiv N \sum_{f \subset U} D_f \tilde{J}_f(x, V) \langle \Pi_f \rangle. \quad (2.20)$$

The *effective interactions* $\tilde{J}_f(x, V)$ contained in the unit cell U are hence given as a simple superposition of all interactions both inside and outside U with known coefficients:

$$\tilde{J}_f(x, V) = J_f(V) + \sum_{\phi \not\subset U} \frac{D_\phi}{D_f} C_\phi^f (2x - 1)^{k_\phi - k_f} J_\phi(V). \quad (2.21)$$

Use of the orthogonality relation (2.9) and Eq. (2.12) to write the correlation functions $\langle \Pi_f \rangle$ in terms of the probabilities P_n gives

$$\langle \Pi_f \rangle = \sum_n \bar{\Pi}_f(n) P_n. \quad (2.22)$$

Using this result in Eq. (2.20) we arrive at

$$\langle \Delta E(V) \rangle = \sum_n P_n \Delta \bar{E}(n, x, V), \quad (2.23)$$

where

$$\Delta \bar{E}(n, x, V) = N \sum_{f \subset U} D_f \bar{\Pi}_f(n) \tilde{J}_f(x, V). \quad (2.24)$$

Our method [Eq. (2.15)] of calculating the correlation functions $\langle \Pi_\phi \rangle$ of figures not contained in the unit cell U differs from the proposal of Morita.⁴³ Only in the case of second-neighbor pair interaction do they give the same result, i.e.,

$$\langle \hat{S}_\alpha \hat{S}_\beta \rangle = \langle \hat{S}_\alpha \rangle \langle \hat{S}_\beta \rangle. \quad (2.25)$$

For *ordered* phases (which have lower-symmetry space groups than the parent disordered phase), we retain the full set of interactions $\{J_f\}$ so that structures which differ by interactions beyond first neighbors have distinct energies.

D. Effective equation of state and equilibrium condition

In our final step we use the expression (2.23) for the energy, the CVM expression for the entropy [Eq. (1.13)] and (i) minimize the ensemble average of the energy with respect to the volume

$$\frac{\partial \langle \Delta E \rangle}{\partial V} = 0 \quad (2.26)$$

[giving the equilibrium volume $V_{\text{eq}}(x)$] and (ii) the free energy with respect to P_n (or $\langle \Pi_f \rangle$). This produces the thermodynamic functions of Eq. (1.2).

Instead of minimizing the free energy with respect to the correlation functions⁶³ $\langle \Pi_f \rangle$, we prefer the minimization with respect to the reduced density-matrix elements P_n , as originally proposed by Kikuchi.⁴¹ Using P_n as the independent variables allows a powerful method of solution for the coupled transcendental equations (the natural iterations method).⁶⁴ This requires rewriting Eq. (2.23) as

$$\langle \Delta E \rangle = \sum_n P_n \bar{\epsilon}_n(P, V), \quad (2.27)$$

where $\bar{\epsilon}_n(P, V)$ are the *effective equations of state* which depend on the probabilities $P = \{P_i\}$, such that

$$\sum_n P_n \bar{\epsilon}_n(P, V) = \sum_n P_n \Delta \bar{E}(n, x, V) \quad (2.28)$$

and

$$\sum_n P_n \frac{\partial \bar{\epsilon}_n(P, V)}{\partial P_i} = 0. \quad (2.29)$$

Equation (2.29), for any i , is required because, in the Kikuchi minimization of the free energy,⁶⁴ the energy parameters ϵ_n are taken to be independent of the probabilities $\{P_i\}$ while ours depend on it through the relationship between the concentration x of atoms B in the alloy and the concentration X_n of atom B in the ordered structure n :

$$x = \sum_n P_n X_n. \quad (2.30)$$

A solution to Eqs. (2.28) and (2.29) is

$$\begin{aligned} \bar{\epsilon}_n(P, V) = & \Delta \bar{E}(n, x, V) + \sum_i P_i \frac{\partial \Delta \bar{E}(i, x, V)}{\partial P_n} \\ & - \sum_{i,j} P_i P_j \frac{\partial \Delta \bar{E}(i, x, V)}{\partial P_j}. \end{aligned} \quad (2.31)$$

In the special case where $\Delta \bar{E}$ depends on $\{P_i\}$ only through Eq. (2.30), Eq. (2.31) reduces to

$$\bar{\epsilon}_n(P, V) = \Delta \bar{E}(n, x, V) + (X_n - x) \sum_i P_i \frac{\partial \Delta \bar{E}(i, x, V)}{\partial x}. \quad (2.32)$$

In summary, our method consists of the following steps.

(i) Calculate (e.g., from the self-consistent local-density approach) the total-excess-energy functions $\Delta E(s, V)$ for M periodic prototype structures $\{s\}$, and extract from these through Eq. (2.3) M values of the interaction energies $J_f(V)$. The selection of the ordered structures and typical values for $\Delta E(s, V)$ and $J_f(V)$ are discussed in Secs. IV and V C, respectively.

(ii) Verify that this set $\{J_f(V)\}$ extending up to d_{int} predicts, through Eq. (2.4a) to within a prescribed maximum error, the directly calculated total energies of a set of structures $\{s'\} \neq \{s\}$. This procedure for examining the completeness of the sets $\{s\}$ and $\{J_f(V)\}$ (i.e., also the needed value of d_{int}) is described in Sec. V E.

(iii) Compute the expansion coefficients C_ϕ^f of Eqs. (2.18) and (2.21) giving m effective interaction energies $\bar{J}_f(x, V)$ in terms of a larger number (M) of conventional interaction energies $\{J_f(V)\}$. The expansion coefficient of $\bar{J}_f(x, V)$ in terms of $J_f(V)$ are given in Sec. VI A.

(iv) Expand the set of m effective equation of states $\bar{\epsilon}_n$ of Eq. (2.32) in terms of $\bar{J}_f(x, V)$.

(v) Compute the enthalpy $\Delta H = \langle \Delta E(V_{\text{eq}}) \rangle$ from Eqs. (2.26), (2.27), and (2.32) and the entropy from Eq. (1.13). From these, construct the complete temperature-composition phase diagrams.

Equations (2.18)–(2.20) describe the renormalization method for the *disordered* phase, having the full space-group symmetry. For *ordered* structures similar procedures can be used by noticing that for fixed d_{stat} the number of figures will increase (consistent with the lower space group). In this case $\langle \Pi_f \rangle$ of Eq. (1.10) are used as independent variables to calculate the enthalpy and en-

trophy within d_{int} and d_{stat} , respectively, using standard CVM. For longer-range correlations, we again assume spin independence [Eq. (2.15), where q_α is now site dependent], consistent with the treatment of the disordered phase.

III. ADVANTAGES AND LIMITATIONS

A. Advantages

The use of first-principles total-energy method to obtain $\{\Delta E(s, V)\}$ allows us to avoid many of the approximations used previously.

(i) *Nature of electronic Hamiltonian.* Since only ground-state properties are sought, the powerful local-density formalism^{65,66} can be used to integrate the electronic degrees of freedom in obtaining $\Delta E(s, V)$, instead of either phenomenological⁶⁷ or highly simplified⁴⁴ independent-particle Hamiltonians. Density-dependent electron correlations, Coulomb interactions, and exchange, spin-polarization, and relativistic terms are most naturally included.^{14,24–26,48,52,53,58–61} The total energy^{14,58} $\Delta E(s, V)$ includes not only the sum of effective single-particle energies (the only term used in many alloy calculations, e.g., Ref. 44), but also explicit electron-electron, electron-ion, ion-ion terms.^{52,53}

(ii) *Nature of solutions to the electronic Hamiltonian.* The periodicity of the structures $\{s\}$ affords the use of powerful band-theory techniques^{52,53} to evaluate $\Delta E(s, V)$ for any given Bloch Hamiltonian. In particular, the use of self-consistent pseudopotential⁵² or all-electron methods⁵³ avoids the use of minimal basis set tight binding⁴⁴ or spherical potential representations [Korringa-Kohn-Sham (KKR)],⁶⁸ the neglect of part⁴⁴ or all of the multiatom and multiorbital s - p - d hybridization, the truncation⁶⁹ or the neglect⁵⁰ of *true* (i.e., position-dependent) charge self-consistency, shape approximations (e.g., muffin tin) on the crystal density and potential,⁶⁸ or simplifying assumptions on the energy dependence of the density of states.⁴⁴ The method is applicable to metals, semiconductors and insulators alike as it does not assume any particular form of the wave functions, bandwidth, degree of charge transfer, screening, or the subband structure of the density of states. Arbitrarily strong scattering potentials (difference between the potentials of the end-point constituents) can be treated. Artificial idealizations of the true atomic arrangements (e.g., Bethe lattices⁷⁰) are avoided.

(iii) *Relaxation of structural degrees of freedom.* Recent advances in formulating rapidly convergent forms for the total energy,^{52,53} forces on atoms⁵² and stresses⁷¹ afford rapid and accurate relaxations of the structural degrees of freedom in calculating $\Delta E(s, V)$. Hence, not only is $J_f(V)$ obtained as a function of the cell volume V , but for each volume, both the cell-internal bond length and bond angle coordinates^{72,73} and the cell-external structural parameters (characterizing the mixed A - B sublattice) are allowed to relax to equilibrium. As was recently demonstrated,^{26,48,51,61} the dependence of J_f on volume and atomic relaxations had dramatic effects on the phase diagram *even*⁵⁰ if Vegard's rule is approximate-

ly satisfied: even *constant-volume* bond relaxations greatly affect the values of $\Delta E(s, V)$, and hence $J_f(V)$.

(iv) *Nature of the ground-state structures.* The nature of the $T=0$ ground-state ordered structures can be found in conventional methods^{56,57} only if a small number of J 's are retained in Eq. (2.1). Having calculated the left-hand side of Eq. (2.1), the prediction of the lowest-energy ordered phases at $T=0$ among the set $\{s\}$ is available at the outset, *independently* of any truncation of the sum of Eq. (2.1) to a few J 's.

(v) *Statistical correlations.* The inclusion of many-spin statistical correlations within a range d_{stat} transcends the limited statistical correlations used in simpler models. The method developed here permits therefore the consideration of rather general forms of "chemical disorder" (through inclusion of variational, nonrandom correlation functions) as well as "positional disorder" (through relaxation of atomic position vectors in minimizing the total energy).

(vi) *Control over types of interactions included.* Interaction parameters J_f are included in a hierarchical manner, based on their established magnitudes, not in an *ad hoc* fashion. For a sufficiently large set of interactions, the resulting phase diagram is unique.

B. Limitations

There are two main limitations to our method

(i) *The choice of $\{J_f(V)\}$.* Many calculations of alloy phase diagrams are based on the assertion³⁶⁻³⁸ that interactions corresponding to a "small" number of bodies k and a "few" neighbors m are sufficient to obtain a converged representation of the internal energy. These assertions are often based on the success of fitting certain features of the phase diagrams (e.g.,⁷⁴ order-disorder temperatures for $\text{Cu}_{1-x}\text{Au}_x$) using just nearest-neighbor interactions. However, first-principles calculations of $J_f(V)$ reveal (e.g., see Fig. 2 below) that one may have to keep many $J_f(V)$'s in the expansion of Eq. (1.10). Furthermore, to treat an incoherent system (e.g., a lattice-mismatched superlattice), one may have to include even more J_f 's because of the removal of the degeneracy of the J_f 's. In fact, the only method that is reasonably safe here is to attempt different choices of interaction range and observe numerically the convergence of the result (see below), a rather laborious procedure. Note, however, that in our formulation $J_f(V)$ is expressed as total energies, not interaction potentials, hence the convergence of the energy expansion is rather fast.

(ii) *Number and choice of special structures.* The number of $J_f(V)$'s determined by the range m_{max} of neighboring interactions decides the number of structures needed. For instance, inclusion of all interactions up to $k_{\text{max}}=4$ requires for $m_{\text{max}}=1$ (nearest neighbors) $3m_{\text{max}}+2=5$ structures, for $m_{\text{max}}=2$ it requires 8 structures, and for $m_{\text{max}}=3$ it requires 11 structures. Hence, calculation of $\Delta E(s, V)$ for a sizable number (4-10) of supercells (see Sec. V) is needed for systems exhibiting a slow rate of decay of $J_f(V)$. Note, however, that the definition of the special structures $\{s\}$ is rather general and could include periodic supercells within which the atomic positions are

rather "disordered."

Throughout the present work we apply our method to purely fcc systems, neglecting the *excess* vibrational entropy. Incoherent systems exhibiting mixed lattices (e.g., fcc and bcc) would require corrections due to vibrational entropy.

IV. CHOICE OF STRUCTURES AND INTERACTION PARAMETERS

The association of a set of M ordered structures with a set of M interaction energies [Eq. (2.3)] is performed in two steps. First, select a "large" set of structures, obtain a correspondingly "large" set of interaction energies through Eq. (2.3), and establish from this which interactions need to be retained to assure that the error in $\Delta E(s, V)$ does not exceed a prescribed tolerance. Second, to establish a smaller set of structures for future, computationally less expensive calculations, find combinations of structures $\{s\}$ and interactions $\{J_f(V)\}$ which reproduce, through the series expansion of Eq. (2.1), the directly calculated (via the self-consistent local-density approach) total energies of structures $\{s'\} \neq \{s\}$ to within a prescribed tolerance. This is discussed in Sec. V E.

To select the "large" set of structures, one needs to include, at the very least, the end-point structures A and B . Since we study here phase transformations which do not alter the Bravais lattice ("coherent" phase diagrams), all members of $\{s\}$ must be subgroups of the space group of A or B . Since we wish to study both ordered and disordered phases, the set $\{s\}$ must include structures exhibiting the most important *local* geometries which are possible in the disordered phase. For example, studying alloys of fourfold-coordinated (tetrahedrally bonded) semiconductors AC and BC , one selects structures $\{s\}$ exhibiting around C at least all the local configurations $(C)A_4$, $(C)A_3B$, $(C)A_2B_2$, $(C)AB_3$, and $(C)B_4$. Having established in exploratory calculations the relative equilibrium total energies $\Delta E(s, V_s)$ of some of these small-cell Landau-Lifshitz⁷⁵ or Kanamori⁵⁷ structures, one is sure to include in the set $\{s\}$ the *lowest-energy* structures. Finally, we include in the set structures exhibiting ordering along a range of the principal directions, [e.g., $(0,0,1)$, $\frac{1}{2}(2,0,1)$, and $\frac{1}{2}(1,1,1)$], and a range of stoichiometries ($X_n = n/4$ in $A_nB_{4-n}C_4$, covering $0, \frac{1}{4}, \frac{1}{2}, \frac{3}{4}$, and 1).

This preliminary screening resulted in a set of ten tentative structures for fcc symmetry in fourfold coordination, depicted in Table I. Table II gives the lattice average expansion coefficients $\bar{\Pi}_{k,m}(s)$ for these structures. These ten structures can be arranged in groups according to the basic ordering vectors: $\frac{1}{2}(0,0,1)$, $\frac{1}{2}(2,0,1)$ and $\frac{1}{2}(1,1,1)$.

For $(0,0,1)$ structures, we have at 50%-50% composition (ABC_2) the layered tetragonal structure (CuAu-I-like, or CA), and at 25%-75% composition (AB_3C_4) and 75%-25% composition (A_3BC_4) the "luzonite" structures (denoted $L1$ and $L3$, respectively). In the absence of the common sublattice C , these are the L_{10} (for CA) and L_{12} (for $L1, L3$) structures familiar from metallurgy.^{1,2} Note that the CA structure is actually an alternate monolayer superlattice $(AC)_1(BC)_1$ oriented along (001) .

We include in this group also the two-layer $(AC)_2(BC)_2$ superlattice, also along (001) (denoted Z2).

For (2,0,1) structures, we have at 50%-50% composition (ABC_2) the chalcopyrite (CH) structure, whereas at compositions of 25%-75% and 75%-25% we have the famatinitite structures ($F1$ and $F3$, respectively). In the absence of the common sublattice C , these are the $tI8$ (for chalcopyrite) and $D0_{22}$ (for famatinitite) structures familiar in metallurgy.^{1,2} Note from Table II that the (0,0,1) structures differ from the (2,0,1) structures by interactions beyond first neighbors.

Finally, for the (1,1,1) structures, we have at 50%-50% composition the layered trigonal, CuPt-like (CP) structure ($L1_1$, in the absence of sublattice C), while for compositions of 25%-75% and 75%-25% we have the $X1$ and $X3$ structures, respectively. Table II also gives the correlation functions for the perfectly random $(R) A_x B_{1-x} C$ alloy, showing the useful identity

$$\Delta E_R(x = \frac{1}{2}) = J_{0,1} [V(x = \frac{1}{2})] = \frac{1}{N} \sum_s [\bar{\Pi}_{0,1}(s)]^{-1} \Delta E [s, V(x = \frac{1}{2})]. \quad (4.1)$$

Regarding the selection of a set of interaction parameters, one notes that in zinc-blende-based structures ternary-based structures the pair interactions between atoms A and B in the mixed sublattice are mediated by the common C atom. This suggests a natural cutoff in the interaction range. Starting from an atom (A or B) at the origin, this can be illustrated as follows.

(i) First-neighbor interactions ($J_{2,1} \equiv J_2$) pass through only one C atom [e.g., that at $(\frac{1}{4}, \frac{1}{4}, \frac{1}{4})$ then to A or B at $(\frac{1}{2}, \frac{1}{2}, 0)$]. This interaction is usually the most important.

(ii) Second-to fourth-neighbor interactions ($J_{2,2} = K_2$, $J_{2,2} = L_2$, and $J_{2,4} = M_2$) pass through two C atoms. For example, the K_2 interaction between an atom at (0,0,0)

TABLE I. Ternary Landau-Lifshitz fcc structures discussed in this work. Along with the crystal structure we give the space group in the International Tables, Schoenflies, Strukturbericht, and the Pearson symbol. Atomic position vectors are given in the notation of the International Tables. The table also gives analogous information for the binary $A_n B_{4-n}$ structures.

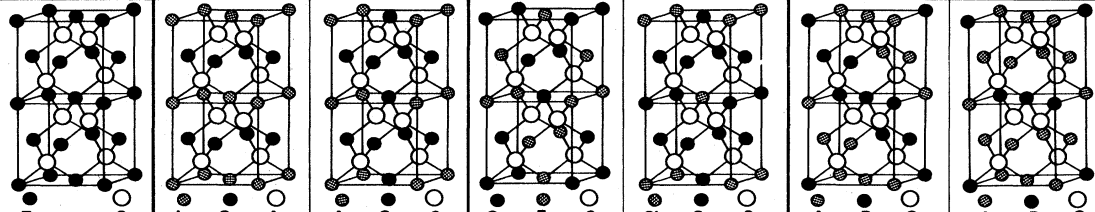
Ordering Vectors	(0,0,0)	(0,0,1)		(2,0,1)		(1,1,1)	
Name (ternary)	Zincblende (Sphalerite)	Layered Tetragonal	"Luzonite"	Chalcopyrite	Famatinitite	Layered Trigonal	"X"
Formula:	$n = 0,4; AC$	$n = 2; ABC_2$	$n = 1,3; A_3BC_4$	$n = 2; ABC_2$	$n = 1,3; A_3BC_4$	$n = 2; ABC_2$	$n = 1,3; A_3BC_4$
	Zn S	In Ga As	As Cu S	Cu Fe S	Sb Cu S	A B C	A B C
Example: (ternary)	ZnS-type	InGaAs ₂ -type	Cu ₃ AsS ₄ -type	CuFeS ₂ -type	Cu ₃ SbS ₄ -type	CrCuS ₂ -type (Na V S ₂)	
Bravais Lattice:	Face centered cubic	Simple tetragonal	Simple cubic	Body centered tetragonal	Body centered tetragonal	Rhombohedral	Orthorhombic
Space Group	$F\bar{4}3m$	$P\bar{4}m2$	$P\bar{4}3m$	$I\bar{4}2d$	$I\bar{4}2m$	$R\bar{3}m$	
Int. Tables:	T_d^2	D_{2d}^5	T_d^1	D_{2d}^{12}	D_{2d}^{11}	C_{3v}^5	
Schoenflies:	216	115	215	122	121	160	
Number:	B3	—	H2 ₄	E1 ₁	H2 _a		
Strukturbericht	CF8	—	CP8	t16	t16	hR4	
Pearson symbol:							
Atomic positions: (ternary)	Zn: 4 a $\bar{4}3m$ S: 4 c $\bar{4}3m$	1A: 1 a $\bar{4}2m$ 1B: 1 c $\bar{4}2m$ 2C: 2 g mm	3 Cu: 3 c $\bar{4}2m$ 1 As: 1 a $\bar{4}3m$ 4 S: 4 e 3m	2 Cu: 4 a $\bar{4}$ 2 Fe: 4 b $\bar{4}$ 4 S: 8 d 2	1 Cu: 2 b $\bar{4}2m$ 2 Cu: 4 d $\bar{4}$ 1 Sb: 2 a $\bar{4}2m$ 4 S: 8 i m	1 A: 1 a 3m 1 B: 1 a 3m 1 C: 1 a 3m 1 C: 1 a 3m	
Equivalent superlattice:	None	(1,1) in [0 0 1] direction	None	(2,2) in [2 0 1] direction	(1,3) in [2 0 1] direction	(1,1) in [1 1 1] direction	None
Space group and type (binary)							
Int. Tables:	$Fm\bar{3}m$	$P4/mmm$	$Pm\bar{3}m$	$I4_1/amd$	$I4/mmm$	$R\bar{3}m$	$Cmmm$
Schoenflies:	O_h^5	D_{4h}^1	O_h^1	D_{4h}^{19}	D_{4h}^{17}	D_{3d}^5	D_{2h}^{19}
Number:	225	123	121	141	139	166	65
Strukturbericht	A1	L1 ₀	L1 ₂	—	DO ₂₂	L1 ₁	—
Pearson symbol	CF ₄	tp4	Cp4	t18	t18	hR32	—
Examples (binary)	Cu, Ag, Au	CuAuI	Cu ₃ Au Au ₃ Cu	NbP(?)	Al ₃ Tl, Ni ₃ V	Cu Pt, SiGe	None

TABLE II. Lattice average spin products $\bar{\Pi}_{k,m}(s)$ [Eq. (1.5)] for the ordered structures of Table I and the Z2 structure. For the random structure $q = 2x - 1$.

	Interaction $J_{k,m}$	Figure	$D_{k,m}$	$\bar{\Pi}_{k,m}(s)$													
				AC	L1 A_3B	CuAu AB	L3 AB_3	BC	Chal. ABC_2	CuPt ABC_2	F1 A_3B	F3 AB_3	Z2 ABC_2	X1 A_3B	X3 AB_3	Rand	
0	$J_0=J_{0,1}$		1	1	1	1	1	1	1	1	1	1	1	1	1	1	1
1	$J_1=J_{1,1}$		1	-1	-1/2	0	1/2	1	0	0	-1/2	1/2	0	-1/2	1/2	q	
2	$J_2=J_{2,1}$		6	1	0	-1/3	0	1	-1/3	0	0	0	1/3	1/6	1/6	q^2	
3	$J_3=J_{3,1}$		8	-1	1/2	0	-1/2	1	0	0	1/2	-1/2	0	0	0	q^3	
4	$J_4=J_{4,1}$		2	1	-1	1	-1	1	1	-1	-1	-1	1	0	0	q^4	
5	$K_2=J_{2,2}$		3	1	1	1	1	1	1/3	-1	2/3	2/3	1/3	0	0	q^2	
6	$M_2=J_{2,4}$		6	1	1	1	1	1	-1/3	1	1/3	1/3	-1/3	1	1	q^2	
7	$K_3=J_{3,2}$		12	-1	-1/2	0	1/2	1	0	0	-1/6	1/6	0	1/6	-1/6	q^3	
8	$K_4=J_{4,2}$		12	1	0	-1/3	0	1	1/3	0	-1/3	-1/3	-1/3	-1/6	-1/6	q^4	
9	$L_2=J_{2,3}$		12	1	0	-1/3	0	1	1/3	0	1/3	1/3	-1/3	1/6	1/6	q^2	
10	$L_3=J_{3,3}$		24	-1	1/2	0	-1/2	1	0	0	1/6	-1/6	0	0	0	q^3	

and one at $(1,0,0)$ passes through the C atom at $(\frac{1}{4}, \frac{1}{4}, \frac{1}{4})$ to A (or B) at $(\frac{1}{2}, \frac{1}{2}, 0)$ then to C at $(\frac{3}{4}, \frac{1}{4}, -\frac{1}{4})$. The L_2 interaction between an atom at $(0,0,0)$ and one at $(1, \frac{1}{2}, \frac{1}{2})$ passes through C at $(\frac{1}{4}, \frac{1}{4}, \frac{1}{4})$ to A (or B) at $(\frac{1}{2}, \frac{1}{2}, 0)$ to C at $(\frac{3}{4}, \frac{3}{4}, \frac{1}{4})$. The M_2 interaction between an atom at $(0,0,0)$ and one at $(1,1,0)$ passes through C at $(\frac{1}{4}, \frac{1}{4}, \frac{1}{4})$ to A (or B) at $(\frac{1}{2}, \frac{1}{2}, 0)$ then to C at $(\frac{3}{4}, \frac{3}{4}, \frac{1}{4})$. All of these three interactions are similarly important and will be treated on the same footing.

(iii) Any longer-range interactions pass through more than two C atoms and, hence, are likely to be weaker.

Before describing the interaction energies obtained from these structures, we review the method used to calculate $\Delta E(s, V)$.

V. ENERGIES $\Delta E(s, V)$ OF ORDERED STRUCTURES

A. Method of calculation

We have previously used two first-principles, self-consistent approaches^{65,66} to the local-density formalism to calculate the excess energies $\Delta E(s, V)$ of ordered, periodic structures: the plane-wave nonlocal pseudopotential^{24,25,52,61,73} and the general-potential linear augmented-plane-wave^{48,53,72} (LAPW) methods. When applied to the same system (e.g., Ref. 59) both produce numerically similar results. The LAPW approach converges faster for systems containing active d bands (e.g.,

noble⁴⁸ and transition metals, or II-VI compound semiconductors⁷²).

In this study we have applied the general-potential LAPW method to ordered phases $A_{4-n}B_nC_4$ formed between the binary constituents $AC=GaAs$ and $BC=GaSb$ (using the Ceperly-Alder exchange-correlation functional as parametrized by Perdew and Zunger⁷⁶) or $AC=GaAs$ and $BC=AlAs$ (using the Hedin-Lundqvist⁷⁷ exchange-correlation functional). These systems were selected because they exhibit the lowest and one of the highest mixing enthalpies and lattice-parameter mismatches known among the III-V compound semiconductors, and because they are experimentally among the best studied semiconductor alloys. For GaAs we find that the two exchange-correlation functionals give very similar results (to within 0.01 eV in band energies and 0.05 eV in cohesive energies). Scalar relativistic effects are included in the calculation. All (core and valence) states are calculated self-consistently. The core states at energies equal and lower than the inner d orbitals are calculated using a spherically averaged potential, whereas all other states are calculated retaining the full potential. The muffin-tin (MT) radii we used were $R_{MT}(Ga)=2.3548$ a.u., $R_{MT}(As)=2.178$ a.u., and $R_{MT}(Sb)=2.532$ a.u. for the Ga(As,Sb) system and $R_{MT}=2.265$ a.u. for the As(Al,Ga) system. The basic consideration in choosing the MT-sphere radii is to increase the convergence but avoid overlapping MT

TABLE III. Calculated formation enthalpies $\Delta H^{(n)}$ of ordered phases $\text{Ga}_4\text{As}_n\text{Sb}_{4-n}$ and $\text{Ga}_n\text{Al}_{4-n}\text{As}_4$, equilibrium lattice constants $a_{\text{eq}}^{(n)}$ and volumes $V_{\text{eq}}^{(n)}$, bulk moduli $B_{(n)}$ and their pressure derivatives $B'_{(n)}$. The ordered structures are depicted in Table I.

Structure	Formula	$\Delta H^{(n)}$ [meV/(4 atoms)]	$a_{\text{eq}}^{(n)}$ (Å)	$V_{\text{eq}}^{(n)} = \frac{1}{4}a^3$ (Å ³)	B_n (GPa)	B'_n	Formula	$\Delta H^{(n)}$ [meV/(4 atoms)]
Zinc-blende ($n=0$)	Ga_4Sb_4	0.0	6.1068	56.935	51.8	4.43	Al_4As_4	0.0
Luzonite ($L1$; $n=1$)	Ga_4AsSb_3	88	6.0071	54.192	54.0	4.37	Al_3GaAs_4	8.7
CuAu-I (CA ; $n=2$)	$\text{Ga}_4\text{As}_2\text{Sb}_2$	115	5.8927	51.154	61.0	5.05	$\text{Al}_2\text{Ga}_2\text{As}_4$	11.5
Luzonite ($L3$; $n=3$)	$\text{Ga}_4\text{As}_3\text{Sb}$	100	5.7852	48.406	65.2	6.71	AlGa_3As_4	8.4
Zinc-blende ($n=4$)	Ga_4As_4	0.0	5.6816	45.851	74.6	6.67	Ga_4As_4	0.0
CuPt (CP ; $n=2$)	$\text{Ga}_4\text{As}_2\text{Sb}_2$	132	5.8974	51.277	59.6	5.29	$\text{Al}_2\text{Ga}_2\text{As}_4$	7.5
Chalcopyrite (CH ; $n=2$)	$\text{Ga}_4\text{As}_2\text{Sb}_2$	52	5.8922	51.141	59.2	5.21	$\text{Al}_2\text{Ga}_2\text{As}_4$	9.8
Famatinite ($F1$; $n=1$)	Ga_4AsSb_3	60	6.0046	54.124	53.1	4.47	Al_3GaAs_4	7.7
Famatinite ($F3$; $n=3$)	$\text{Ga}_4\text{As}_3\text{Sb}$	68	5.7823	48.333	65.8	5.82	AlGa_3As_4	7.3
Superlatt. ($Z2$; $n=2$)	$\text{Ga}_4\text{As}_2\text{Sb}_2$	97	5.8983	51.300	59.1	5.13	$\text{Al}_2\text{Ga}_2\text{As}_4$	2.85

spheres. The final result is insensitive to the choice of MT radii. The small amount of Ga 3d electrons outside the MT spheres is treated exactly without further approximation.^{53(b)} A rapid convergence in the interaction process is achieved by using Broyden's method.^{53(c)}

The numerically calculated excess energy functions $\Delta E(s, V)$ have been fitted for convenience of use to Murnaghan's equation of state⁷⁸

$$\Delta E(s, V) = \frac{B_s V}{B'_s} \left[\frac{(V_s/V)^{B'_s}}{B'_s - 1} + 1 \right] + \text{const}, \quad (5.1)$$

where B_s and B'_s are the bulk modulus and its pressure derivative at the equilibrium volume V_s . The fitting procedure is similar to that given in Ref. 48. To find the equilibrium structural parameters we have minimized the total energy with respect to *all* cell-internal structural degrees of freedom. Finding that symmetry-allowed tetragonal or trigonal distortions of the unit-cell vector are small for these systems (< 1%) we neglected them.

Table III gives the calculated parameters of Eq. (5.1) for GaAs-GaSb and for GaAs-AlAs; Fig. 1 shows $\Delta E(s, V)$ for the five $\text{Ga}_4\text{As}_n\text{Sb}_{4-n}$ structures corresponding to (0,0,0) and (0,0,1) ordering vectors. Table IV gives

TABLE IV. Calculated lattice constants, cell-internal relaxation parameters, and Ga-As and Ga-Sb bond lengths for the Ga(As,Sb) system. See Table I and III for the definition of the ordered structures. The numbers in parentheses are the numbers of inequivalent bonds in the tetrahedron. The atomic position in the unit cell determined by cell-internal parameter $\{u\}$ can be found in Ref. 61.

Formula and structure	a_{eq} (Å)	$\{u_{\text{eq}}\}$	$R(\text{Ga-Sb})$ (Å)	$R(\text{Ga-As})$ (Å)
Ga_4Sb_4 (ZB)	6.1068	0.25	2.6443	
Ga_4AsSb_3 (L1)	6.0071	0.2417	2.6313	2.5146
$\text{Ga}_4\text{As}_2\text{Sb}_2$ (CA)	5.8927	0.2336	2.6085	2.4971
$\text{Ga}_4\text{As}_3\text{Sb}$ (L3)	5.7852	0.2579	2.5844	2.4797
Ga_4As_4 (ZB)	5.6816	0.25		2.4602
$\text{Ga}_4\text{As}_2\text{Sb}_2$ (CP)	5.8974	$u1=0.2410$ $u2=0.2590$	2.5857($\times 3$) 2.6456($\times 1$)	2.4617($\times 1$) 2.5245($\times 3$)
$\text{Ga}_4\text{As}_2\text{Sb}_2$ (CH)	5.8922	0.2294	2.6233	2.4833
Ga_4AsSb_3 (F1)	6.0046	$u=0.2404$ $2v=0.2423$	2.6413($\times 1$) 2.6283($\times 2$)	2.5068
$\text{Ga}_4\text{As}_3\text{Sb}$ (F3)	5.7823	$u=0.2604$ $2v=0.2584$	2.6013	2.4640($\times 1$) 2.4776($\times 2$)

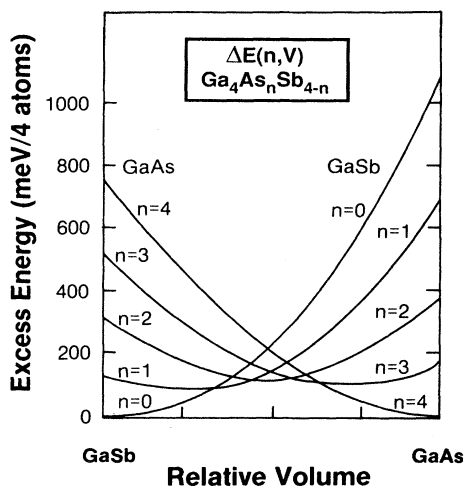


FIG. 1. Total excess energy of ordered $\text{Ga}_4\text{As}_n\text{Sb}_{4-n}$ structures belonging to the (0,0,1) ordering vector ($n=1,2,3$) and for the end-point compounds ($n=0,4$).

the values of the cell-internal structural parameters of GaAs-GaSb at equilibrium. Since GaAs and AIAs have nearly the same lattice parameter, the small volume dependence of their $\Delta E(s)$ was neglected.

B. Energy scales and precision

Equations (2.3), (2.4), and (2.27) show that the scale of the internal energy of the alloy is determined by $\Delta E(s, V)$. There are three characteristic energies: (i) the *formation enthalpy* of the perfectly ordered structure s is given by

$$\Delta H(s) = \Delta E(s, V_s), \quad (5.2)$$

where V_s is the volume which minimizes $\Delta E(s, V)$ of Eq. (2.2), where all other, cell-internal degrees of freedom are also at equilibrium; (ii) the *structural-preference energy*, i.e., the difference between the formation enthalpies of two different structures of the same compositions

$$\delta\Delta H(s, s') = \Delta E(s, V_s) - \Delta E(s', V_{s'}); \quad (5.3)$$

and (iii) the *mixing enthalpy* of the disordered phase $\Delta H^D(x, T)$ [i.e., Eq. (2.27), evaluated for the disordered system at $V_{\text{eq}}(x)$]. Table III shows that (i) formation enthalpies of ordered inter semiconductor compounds are around 10^{-1} – 10^{-2} eV per four atoms, and (ii) structural preference energies (e.g., CuAu versus chalcopyrite, or luzonite versus famatinite) are around $\sim 10^{-2}$ eV. (iii) Our results below (Sec. VII E) or the experimental data^{17–22} show that semiconductor alloy mixing enthalpies are typically of the order of 10^{-1} – 10^{-2} eV for lattice-mismatched semiconductors at $x=0.5$.

Since the pertinent energy scale involved is $\leq 10^{-2}$ eV/atom, energy differences must be calculated with equal or higher precision. In our formulation of the problem neither the energies of the free atoms nor the cohesive energy of solid phases enter, as we focus the study on *relative* free energies with respect to the phase-separated solid system $AC + BC$. This can be achieved by calculating in Eq. (2.2) the energy $E(s, V)$ of $A_{4-n}B_nC_4$, the energy E_A of $A_{4-n}A_nC_4$ and the energy E_B of $B_{4-n}B_nC_4$ in precisely the same \mathbf{k} -point sampling basis sets and integration grid points, assuring best cancellation of numerical errors. Cancellation between large constant terms, common to $A_{4-n}B_nC_4$ and $\frac{1}{4}(4-n)A_{4-n}A_nC_4 + \frac{1}{4}nB_{4-n}B_nC_4$ (core energies, Madelung energies, etc.) are hence affected algebraically. In this work we have used two special \mathbf{k} -points for the ZB structure and their equivalent \mathbf{k} -points for the ternary structures.⁷⁹ By comparing results with an equivalent ten \mathbf{k} -points we find that the convergence error of the excess energy due to the two- \mathbf{k} -point sampling is about 5 meV/per four atoms (0.06 kcal/mol).

C. Properties of the interaction energies $J_f(V)$ in prototype semiconductor alloys

Figure 2 shows, as a function of volume, the interaction energies $J_{k,m}(V)$ obtained for GaAs-GaSb using the large set of ten ordered structures $A, B, CA, CH, CP, Z2, L1, L3, F1,$ and $F3$, and Eq. (2.3). We give for comparison the results for the five ordered structures $A, B, CA, L1,$ and $L3$ used previously.^{24,25,48} Table V gives the

TABLE V. Interaction energies (in meV) obtained using Eq. (2.3) from ten structures (Table II) of $\text{Ga}_4\text{As}_n\text{Sb}_{4-n}$ and $\text{Ga}_n\text{Al}_{4-n}\text{As}_4$. \bar{V} is the average of the GaAs and GaSb cell volumes.

Interaction	GaAs-GaSb			GaAs-AIAs volume- independent
	at V_{GaAs}	at \bar{V}	at V_{GaSb}	
J_0	176.02	44.34	139.98	3.30
J_1	-256.13	-3.75	194.38	-0.15
J_2	7.98	5.97	4.58	-0.79
J_3	-0.36	-0.28	-0.33	0.01
J_4	-0.64	0.09	0.14	0.01
K_2	1.33	0.62	0.04	0.09
L_2	0.65	0.14	-0.09	0.03
M_2	4.78	3.95	3.40	0.12
K_3	-0.31	-0.25	-0.38	0.01
K_4	-0.03	0.03	0.00	0.01

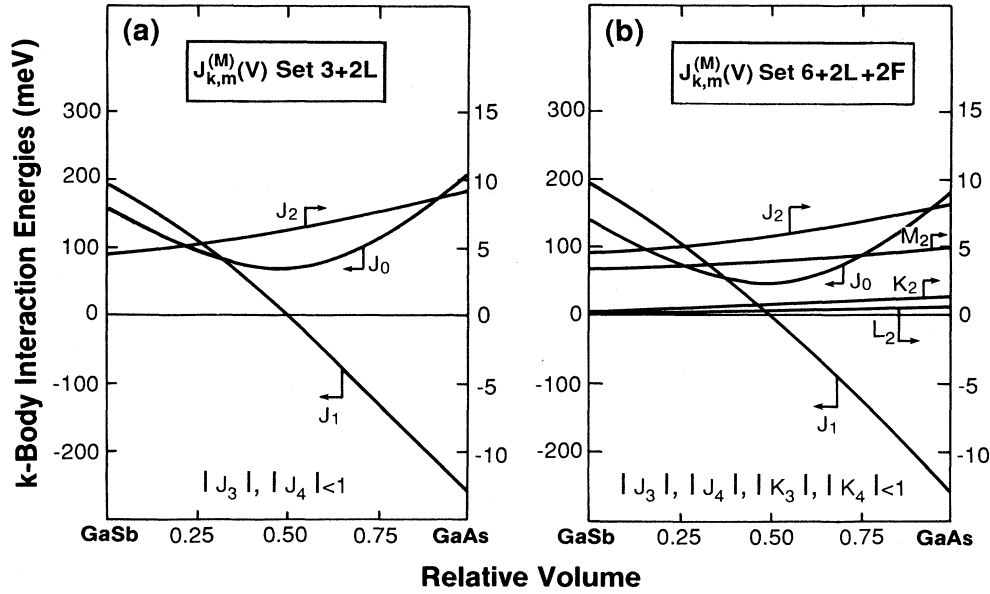


FIG. 2. Volume-dependent interaction energies $J_{k,m}(V)$ for GaAs-GaSb extracted from two different structure sets.

value of $J_f(V)$ for these two systems at a few volumes.

These results show that (i) these systems are dominated by pair interactions J_2 , K_2 , L_2 , and M_2 between first, second, third, and fourth fcc neighbors, respectively, but (ii) the magnitude of these energies does not decrease monotonically with the corresponding interaction range, e.g., $M_2 > L_2$, and (iii) when the size mismatch between the constituents is non-negligible (GaAs-GaSb), so is the volume dependence of $J_{k,m}(V)$. (iv) For AlAs-GaAs we find that $J_2 < 0$ but $K_2 > 0$; hence the system is spin frustrated. GaAs-GaSb shows $J_2, K_2 > 0$. This leads also to spin frustration (since in this case an A atom prefers to have all of its first-shell and second-shell atoms to be of type B , yet some of the second-shell atoms are first neighbors to first-shell atoms). (v) The calculated interaction energies and the correlation functions of Table II make possible the assessment of the contribution of a certain type of interaction to the total energy. For example, the largest correlation function $D_f \bar{\Pi}_f(s)$ associated with J_4 is 2; hence, omitting this interaction leads to errors of the order of only 0.2 meV for GaAs-GaSb and ~ 0.02 meV for GaAs-AlAs.

D. Properties of the excess energy $\Delta E(s, V)$ in prototype semiconductor alloys

Our results for the formation enthalpies $\Delta H_s = \Delta E(s, V_s)$ of the ordered inter semiconductor compounds (Table III) show some general features.

(i) The ΔH_s of all ordered inter semiconductor structures of GaAs-GaSb and GaAs-AlAs considered here are *positive*, hence these systems are less stable than equivalent amounts of the (phase-separated) binary constituents at equilibrium. At $T=0$ equilibrium these systems would yield a phase-separated ground state (analogous to ferromagnetism).

gous to ferromagnetism).

(ii) For the lattice-matched system AlAs-GaAs the sequence of energies of the different ordered modifications at $x=0.5$ is

$$\Delta H(CA) > \Delta H(CH) > \Delta H(CP), \quad (5.4a)$$

and

$$\Delta H(L) > \Delta H(F). \quad (5.4b)$$

(iii) For the lattice-mismatched system GaAs-GaSb the sequence is

$$\Delta H(CP) > \Delta H(CA) > \Delta H(CH), \quad (5.5)$$

and

$$\Delta H(L) > \Delta H(F). \quad (5.6)$$

Recent valence force field (VFF) calculations by Bernard *et al.*⁶⁰ for 18 III-V and 18 II-VI alloys have shown that Eqs. (5.5) and (5.6) hold in all cases.

For our method of selecting interaction parameters to have a general validity for other semiconductor systems, we need to examine whether the behavior outlined in Eqs. (5.4)–(5.6) is accidental or not. To do so, we follow Srivastava *et al.*²⁴ and decompose the excess energy $\Delta E(s, V)$ of a structure s into three physically recognizable contributions. *First*, compress and dilate, respectively, AC and BC from their equilibrium volumes V_{AC} and V_{BC} to the intermediate volume V , investing thereby the “volume deformation” (VD) energy

$$\begin{aligned} \Delta E_{VD}(n, V) = & \frac{1}{4}(4-n)[E_{AC}(V) - E_{AC}(V_{AC})] \\ & + \frac{1}{4}n[E_{BC}(V) - E_{BC}(V_{BC})]. \end{aligned} \quad (5.7)$$

Second, bring together AC and BC , both at the volume V ,

to form $A_{4-n}B_nC_4$, also at the volume V . The “charge exchange (CE) energy involved is

$$\Delta E_{CE}(s, n, V) = E_{A_{4-n}B_nC_4}(s, V, \{u_0\}) - \frac{1}{4}(4-n)E_{AC}(V) - \frac{1}{4}nE_{BC}(V). \quad (5.8)$$

In this step we do not relax the cell-internal degrees of freedom (denoted as $\{u\}$). *Third*, allow the cell-internal structural freedom to relax from $\{u_0\}$ to $\{u_{eq}\}$. The structural (S) energy involved is

$$\Delta E_S(s, n, V) = E_{A_{4-n}B_nC_4}(s, V, \{u_{eq}\}) - E_{A_{4-n}B_nC_4}(s, V, \{u_0\}). \quad (5.9)$$

The total excess energy $\Delta E(s, V)$ of Eq. (2.2) is the sum of the three terms of Eqs. (5.7)–(5.9), i.e.,

$$\begin{aligned} \Delta E(s, n, V) &= \Delta E_{VD}(n, V) + \Delta E_{CE}(s, n, V) + \Delta E_S(s, n, V) \\ &= E_{A_{4-n}B_nC_4}(s, V, \{u_{eq}\}) - \frac{1}{4}(4-n)E_{AC}(V_{AC}) - \frac{1}{4}nE_{BC}(V_{BC}). \end{aligned} \quad (5.10)$$

The formation enthalpy $\Delta H(s, n)$ of ordered phase n is the value of $\Delta E(s, n, V)$ at the equilibrium volume V_n which minimizes $\Delta E(n, V)$.

Figure 3 depicts the three functions $\Delta E_{VD}(n, V)$, $\Delta E_{CE}(s, n, V)$, and $\Delta E_S(s, n, V)$ for a few structures s of $Ga_4As_nSb_{4-n}$. Their sum [Eq. (5.10)] is shown in Fig. 1, whereas Table III gives their values at equilibrium. This analysis demonstrates the following points.

(i) Since $\Delta E_{VD}(n, V)$ is common to all structures of a fixed stoichiometry X_n (e.g., for $s = CA, CH$, and CP at $X_n = \frac{1}{2}$), structural preference energies in lattice-

mismatched systems are decided by $\Delta E_S(s, n) + \Delta E_{CE}(s, n)$. Since $\Delta E_{VD} = \Delta E_S = 0$ in lattice-matched systems, the structural preference energies are determined by $\Delta E_{CE}(s, n)$ alone.

(ii) All such *ternary* semiconductor phases are *structurally frustrated* in the sense that it is impossible to have, at the same time, “ideal” (tetrahedral) bond angles and “ideal” (i.e., zinc-blende) bond lengths. *Binary AB* tetrahedral compounds (e.g., zinc-blende or $L1_2$) can be strain free in this sense.⁸⁰ This is the principal reason why *binary* intersemiconductor isovalent compounds can have $\Delta H(s, n) < 0$ when ΔE_{CE} is sufficiently negative (e.g.,⁸⁰ zinc-blende SiC), whereas for most such *ternary* compounds $\Delta H(s, n) > 0$.

(iii) $\Delta E_{CE}(s, n)$ is positive to these ternary semiconducting alloys [although, in general, it could be negative, e.g., in ferromagnetic CdTe-MnTe (Ref. 81)] and about an order of magnitude smaller than $\Delta E_S(n)$ or $\Delta E_{VD}(n)$ of the lattice-mismatched systems. Hence, in the lattice-matched GaAs-AlAs system the formation enthalpies are about an order of magnitude smaller than those in lattice-mismatched systems since only $\Delta E_{CE}(s, n)$ is at play in the former case.

(iv) The chemical energy $\Delta E_{CE}(s, n)$ is nearly volume independent. It is smaller in mixed-*cation* systems (e.g., 7.5 meV in the CuPt structures of $GaAlAs_2$) relative to mixed-*anion* systems (e.g., 19 meV in the same CuPt structure of Ga_2AsAb). This reflects the fact that the valence-band wave functions of covalent semiconductors are mostly anion-derived, hence mixed-anion systems strongly perturb the occupied valence band, whereas mixed-cation systems do so to far lesser extent (they perturb greatly, instead, the empty conduction bands).

(v) The order of $\Delta H(s, n)$ in lattice-matched systems is consistent with that obtained by retaining $\Delta E_{CE}(s, n)$

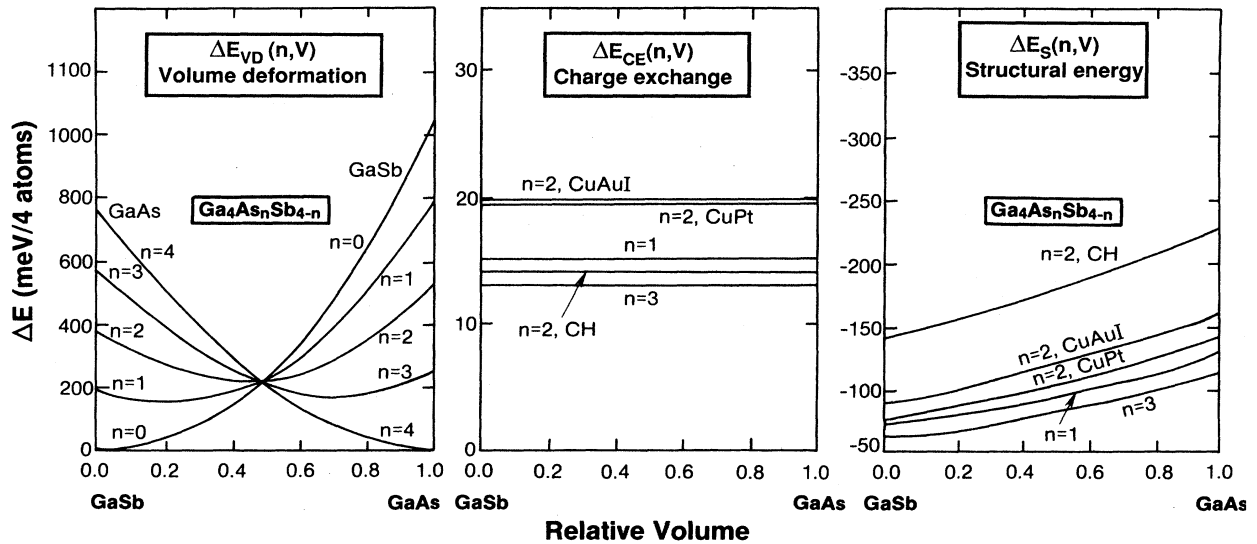


FIG. 3. Decomposition of the formation enthalpy of ordered $Ga_4As_nSb_{4-n}$ structures into volume deformation [Eq. (5.7)], charge-exchange [Eq. (5.8)], and structural relaxation [Eq. (5.9)] contributions.

alone and modeling it by the excess electrostatic Madelung energy $\Delta E_{\text{Madelung}}$ of the ordered structures with respect to equivalent amounts of zinc-blende $AC+BC$. A simple electrostatic model gives the excess Madelung energy (per four-atom cell)

$$\Delta E_{\text{Madelung}}(s,2) = \frac{1}{2d}(\alpha_{\text{ZB}}\Delta q^2 - 4\beta_s\Delta Q^2), \quad (5.11)$$

where d is the bond length, $\Delta q = q_A(AC) - q_B(BC)$ is the difference in charge between the binary compounds, and $\Delta Q = Q_A(ABC_2) - Q_B(ABC_2)$ is the corresponding difference in the ternary ordered phase, and where

$$\begin{aligned} \alpha_{\text{ZB}} &= 1.6381, \\ \beta_{\text{CA}} &= 0.1220, \\ \beta_{\text{CH}} &= 0.1253, \\ \beta_{\text{CP}} &= 0.1868 \end{aligned} \quad (5.12)$$

are geometrical constants.⁸² Clearly, only if the charge exchange ΔQ in the ternary phase exceeds that in the binary structures by more than a critical value $(\Delta Q/\Delta q)_{\text{crit}}$ can the ternary phase have $\Delta E_{\text{Madelung}} < 0$. We find

$$(\Delta Q/\Delta q)_{\text{crit}} = \begin{cases} 1.83, & \text{CuAu-I} \\ 1.81, & \text{chalcopyrite} \\ 1.48, & \text{CuPt} \end{cases} \quad (5.13)$$

In GaAs-GaSb and GaAs-AlAs, $\Delta Q/\Delta q$ does not exceed these critical values, hence $\Delta E_{\text{Madelung}} > 0$. The order of stability of Eq. (5.4) obtained in our total-energy calculations (Table III) is consistent with the values of β_s given in Eq. (5.12). This suggests that other contributions to $\Delta E_{\text{CE}}(s,n)$ (e.g., on-site Coulomb energy)⁸³ are less important.

(vi) The order of stabilities in lattice-mismatched systems [Eq. (5.5)] is decided primarily by $\Delta E_s(n)$ of Fig. 3 [since $\Delta E_{\text{CE}}(s,n)$ is relatively small and nearly constant in these systems]. This reflects the fact that for a fixed internal displacement of atom C the chalcopyrite structure has a smaller bond-angle distortion, hence, it can better accommodate dissimilar bond lengths R_{A-C} and R_{B-C} than, say, the CuAu-I structure.⁶⁰ This is seen in Table IV, showing smaller bond distortions $R_{AC} - R_{AC}^0$ in chalcopyrite relative to that in the CuAu-I structure. We will see below that the chalcopyrite structure emerges indeed as a metastable ordered phase in the phase diagram of lattice-mismatched isovalent semiconductor alloys. The CuPt structure has larger strain because it must accommodate in the same lattice two clusters, $A_3B(C)$ and $AB_3(C)$, with different sizes. We have found that the calculated $\Delta E(s,n,V)$ has a larger magnitude at $V=V(\text{GaAs})$ than at $V=V(\text{GaSb})$ (Fig. 3), in contrast with the result obtained by VFF.⁶⁰ This reflects the fact that the VFF is essentially a harmonic theory while our calculation includes anharmonic effects.

We conclude that the relative stability of the *lattice-matched* ordered isovalent semiconductor phase is decided primarily by the small charge-exchange energies ΔE_{CE}

reflecting largely the relative electrostatic energies of different lattices, whereas the relative stabilities of *lattice-mismatched* isovalent semiconductor phases is decided by the structural energies ΔE_s reflecting the different abilities of the various structures to minimize the *strain* energies by accommodating spatially different bond lengths. These conclusions are supported by recent total-energy calculations for the inter semiconductor systems, CdTe-HgTe,⁷² CdTe-ZnTe,⁷² HgTe-ZnTe,⁷² GaP-InP,⁸⁴ and InAs-GaAs, yielding excess energies [in meV/(4 atoms)] of 12.3, 54.2, 42.3, 91.0, and 66.7 in the CA structure; 11.3, 19.2, 11.4, 19.0, and 16.5 in the CH structure, and 9.8, 103.5, 155.4, and 108.4 in the CP structure, respectively. These LAPW calculated values exhibit the anticipated trends of Eq. (5.4) for lattice-matched systems (AlAs-GaAs and CdTe-HgTe) and that of Eq. (5.5) for all lattice-mismatched systems.

E. Optimal choices of minimal sets of ordered structures: Test of completeness and linear independence

Our foregoing discussion suggests that the *order* of energies of various phases [e.g., Eqs. (5.4)–(5.6)] is likely to hold, quite generally, for reasons discussed in Sec. V D, for a wide range of isovalent zinc-blende semiconductor systems. This suggests that a choice of a set of structures (hence, also interaction parameters) for the prototype zinc-blende semiconductors treated in this work might be useful for other zinc-blende semiconductor alloys as well. We hence discuss next how such sets can be selected.

Having calculated self-consistently the total excess energies of a “large” set of ordered GaAs-GaSb compounds as well as that of the random alloy [Eq. (4.1)], we can now seek smaller sets of structures, examining the extent to which the interaction energies extracted from them reproduce the *directly calculated* energies of structures outside these “small” sets. Since the systems under consideration here are dominated by pair interactions, we discuss these first.

Define as the bare minimum set the interactions J_0, J_1 , and J_2 , and the end-point structures AC and BC . Now add to this set of structures one of the remaining structures, so that the 3×3 problem can be inverted through Eq. (2.3) to find the values of the interaction energies. The first four lines of Table VI show the four combinations of (a total of $M=3$) structures possible and identifies the structures *outside* each of these small sets. We now predict the energies of the structures *outside* each of these small sets using the interaction energies extracted from the small set and Eq. (2.1). Table VII shows the ratio between the predicted energy [using series expansion of Eq. (2.1)] and the directly calculated energy (using the LAPW method). This procedure can be extended to a total of $M=4$ structures (giving 18 sets), $M=5$ structures (12 sets), etc. The results for the predicted-to-calculated energy ratios are given in Table VII for all sets.

Inspection of these results reveals the (i) to get correctly the energy of the random structure, it is essential in all cases to include the fourth-neighbor pair interaction M_2 , (ii) the smallest set guaranteeing a maximum error of $\sim 6\%$ for all structures is $M=4$, and (iii) the canonical

Connolly-Williams set ($A, B, CA, L1$, and $L3$) used previously in a number of phase diagrams calculations is *not* optimal, leading to errors as large as 58%, 30%, 121%, and 71% for R, \bar{F}, CH , and $Z2$, respectively.

Table VIII gives for each $M \geq 4$ the best set of structures and interaction parameters as well as the previously used set (A, B, CA) for $M=3$. In Sec. VIII we will present detailed phase diagrams for these sets (including also interactions beyond pairs), demonstrating convergence of the properties of the *disordered* alloy. For *random* (R) alloys, however, it is possible to examine, analytically the rate of convergence of the excess energy $\Delta E(R, V)$ by noting that at $x=0.5$ [Eq. (4.1)] this is given by $J_0[V(x=0.5)]$, and that the latter quantity is a superposition of energies $\Delta E[s, V(x=0.5)]$ of ordered structures. Table IX gives the expansion coefficients $\eta_0(s, M) = [\bar{\Pi}_{0,1}(s)]^{-1}$ of Eq. (2.3) for $J_0[V(x=\frac{1}{2})] = \Delta E(R, x=\frac{1}{2})$ for some sets of M structures indicated in Table VIII, as well as for those obtained by adding $L1$ and $L3$ to each set. The caption to Table IX gives the LAPW calculated values of $\Delta E(s, \bar{V})$ at $\bar{V} = V_s(CA)$. Using these, one can calculate the energy of the random alloy at \bar{V}

$$\Delta E(R, \bar{V}, M) = \sum_s \eta_0(s, M) \Delta E(s, \bar{V}) \quad (5.14)$$

as a function of the number of structures M included. This is shown in the last column of Table IX. The results exhibit a rapid convergence of $\Delta E(R, \bar{V})$ with M and reveal that the converged result is rather unique, in that different combinations of structures result (past $M=5$) in virtually identical alloy energies. It is interesting to note

from Table IX that the major effect of including more interactions M is to gradually reduce the values of $\eta_0(s, M)$ for the high-energy structures $s=CA, L1$, and $L3$, and to increase $\eta_0(s, M)$ for the stabler, low-energy structures $CH, Z2, F1$, and $F3$.

While this test identifies the rate of convergence with M , it does not address the issue of the *sensitivity* of the expansion of Eq. (2.1) to certain $\Delta E(s, V)$ values: when a large number of structures is included, one may expect in general that eventually some linear dependence will develop. We can define a "quality parameter" K reflecting this effect for a full composition range. Using Eqs. (2.5) and (2.6), one can write Eq. (5.14) for any $V(x)$ as

$$\Delta E[R, V(x), M] = \sum_s Q_s(x, M) \Delta E(s, V), \quad (5.15)$$

where

$$Q_s(x, M) = \sum_f [\bar{\Pi}_f(s)]_M^{-1} \bar{\Pi}_f(R, x). \quad (5.16)$$

For the expansion (5.15) to be stable, we wish to exclude structures s which are nearly linearly dependent, so that the convergence of (5.15) with M will be regular. Since $d\Delta E/d\Delta E(s, V) = Q_s$ and $\bar{\Pi}_0(s) = 1$, we have the sum rule

$$\begin{aligned} \sum_s Q_s(x) &= \sum_{s,f} (2x-1)^{k_f} [\bar{\Pi}_f(s)]^{-1} \bar{\Pi}_0(s) \\ &= \sum_f (2x-1)^{k_f} \delta_{f,0} = 1, \end{aligned} \quad (5.17)$$

where (Table III) $\bar{\Pi}_f(R) = (2x-1)^{k_f}$. This sum rule can be verified for $x=\frac{1}{2}$ from Table IX by summing the entries in a given row. This suggests that a good criteria for

TABLE VI. Sets of structures and their association with interaction parameters. Here we indicate the "structures added" to the two end-point structures of AC and BC , and the interaction energies (J) added to J_0, J_1 , and J_2 . In each case we indicate as energies to be predicted those structures *not* included in a given set. Their predicted relative energies are given in Table VII. \bar{F} and \bar{L} denote the averages of $F1+F3$ and $L1+L3$, respectively. R denotes the random alloys.

M	Structures added	J 's added	Structures whose energies are to be predicted
3 (4 sets)	CA		$R, CH, CP, Z2, \bar{F}, \bar{L}$
	CH		$R, CA, CP, Z2, \bar{F}, \bar{L}$
	CP		$R, CA, CH, Z2, \bar{F}, \bar{L}$
	Z2		$R, CA, CH, CP, \bar{F}, \bar{L}$
4 (18 sets)	CA, CH	$K_2/L_2/M_2$	$R, CP, Z2, \bar{F}, \bar{L}$
	CA, CP	$K_2/L_2/M_2$	$R, CH, Z2, \bar{F}, \bar{L}$
	CA, Z2	$K_2/L_2/M_2$	$R, CH, CP, \bar{F}, \bar{L}$
	CH, CP	$K_2/L_2/M_2$	$R, CA, Z2, \bar{F}, \bar{L}$
	CH, Z2	$K_2/L_2/M_2$	$R, CA, CP, \bar{F}, \bar{L}$
	CP, Z2	$K_2/L_2/M_2$	$R, CA, CH, \bar{F}, \bar{L}$
5 (12 sets)	CA, CH, CP	$M_2K_2/M_2L_2/K_2L_2$	$R, Z2, \bar{F}, \bar{L}$
	CA, CH, Z2	$M_2K_2/M_2L_2/K_2L_2$	R, CP, \bar{F}, \bar{L}
	CA, CP, Z2	$M_2K_2/M_2L_2/K_2L_2$	R, CH, \bar{F}, \bar{L}
	CH, CP, Z2	$M_2K_2/M_2L_2/K_2L_2$	R, CA, \bar{F}, \bar{L}
6 (1 set)	CA, CH, CP, Z2	K_2, L_2, M_2	R, \bar{F}, \bar{L}

TABLE VII. This table gives, for each set of GaAs-GaSb structures and its corresponding set of interaction parameters (listed in Table VI), the ratio between the predicted energy [using the series expansion of Eq. (2.1)] and the directly calculated (via LAPW) energy, both at the 50%-50% volume. The symbols identifying the structures are given in the first column of Table III. A entry "S" indicates that Eq. (2.3) is singular, hence, not invertible. The energy of the random alloy at $x = \frac{1}{2}$ (R) is calculated within the LAPW method from Eq. (4.1).

$M=3$															
Structures added	Predicted energy ratios														
	R	\bar{F}	\bar{L}	J_0, J_1, J_2	ABC_2										
CA	1.58	1.30	1.00	CH=2.21	Z2=1.71	CP=1.06									
CH	1.05	0.86	0.66	CA=0.45	Z2=1.38	CP=0.70									
CP	1.49	1.22	0.94	CA=0.90	Z2=1.65	CH=2.0									
Z2	0.42	0.35	0.27	CA=-0.19	CH=-0.42	CP=0.28									
$M=4$															
Structures added	Predicted energy ratios														
	R	\bar{F}	J_0, J_1, J_2, K_2	\bar{L}	ABC_2	R	J_0, J_1, J_2, L_2	\bar{F}	\bar{L}	ABC_2	R	J_0, J_1, J_2, M_2	\bar{F}	\bar{L}	ABC_2
CA, CH	0.51	1.01	1.00	CP=-0.37	Z2=1.06	1.58	1.01	1.00	CP=1.06	Z2=1.77	1.05	1.01	1.00	CP=1.06	Z2=1.06
CA, CP	1.53	1.28	1.00	CH=2.16	Z2=1.68	S	S	S	S	S	S	S	S	S	S
CA, Z2	0.42	0.98	1.00	CH=0.69	CP=-0.49	1.58	1.62	1.00	CH=3.53	CP=1.06	1.00	0.98	1.00	CH=0.89	CP=1.06
CH, CP	1.20	0.82	0.57	CA=0.30	Z2=1.47	1.49	0.98	0.94	CA=0.90	Z2=2.19	1.05	0.98	0.94	CA=0.90	Z2=1.11
CH, Z2	0.42	1.03	1.06	CA=1.1	CP=-0.56	0.84	0.80	0.53	CA=0.24	CP=0.56	1.05	1.03	1.06	CA=1.10	CP=1.12
CP, Z2	0.42	-0.23	-0.41	CA=-1.29	CH=-1.63	1.49	1.51	0.94	CA=0.90	CH=3.21	0.965	0.93	0.94	CA=0.90	CH=0.79
$M=5$															
Structures added	Predicted energy ratios														
	R	\bar{F}	J_0, J_1, J_2, M_2, K_2	\bar{L}	ABC_2	R	J_0, J_1, J_2, M_2, L_2	\bar{F}	\bar{L}	ABC_2	R	J_0, J_1, J_2, K_2, L_2	\bar{F}	\bar{L}	ABC_2
CA, CH, CP	1.03	1.01	1.00	Z2=1.06	S	S	S	S	S	1.53	1.01	1.00	Z2=2.30		
CA, CH, Z2	S	S	S	S	1.03	1.01	1.00	CP=1.06	0.47	1.01	1.00	Z2=-0.43			
CA, CP, Z2	0.98	0.98	1.00	CH=0.89	S	S	S	S	1.53	1.94	1.00	CH=3.42			
CH, CP, Z2	1.00	1.03	1.06	CA=1.09	1.00	0.98	0.94	CA=0.90	1.00	0.87	0.33	CA=-0.10			
$M=6$															
Structures added	Predicted energy ratios														
	R	\bar{F}	$J_0, J_1, J_2, M_2, K_2, L_2$	\bar{L}	ABC_2										
CA, CH															
CP, Z2	1.00	1.00	1.00												

TABLE VIII. Sets associating a group of ordered structures with a group of interaction parameters, and the quality parameter K [Eq. (5.19)] for some of the best sets. The stabler sets have smaller K values.

M	Structures	Interaction parameters	K	K	K	K
				$(M+2L)$	$(M+2F)$	$(M+2L+2F)$
3	A, B, CA	J_0, J_1, J_2	0.62	0.41	0.41	0.94
4	A, B, CA, CH	J_0, J_1, J_2, M_2	0.62	0.75	0.48	1.08
5	A, B, CA, CH, CP	J_0, J_1, J_2, K_2, M_2	0.65	0.72	0.55	1.18
6	A, B, CA, CH, CP, Z2	$J_0, J_1, J_2, L_2, M_2, K_2$	0.45	0.48	0.40	0.90

TABLE IX. Expansion coefficients ($\times 16$) of $J_0(V)$ in terms of the energies $\Delta E(s, V)$ of different ordered structures s , see Eq. (4.1). The different sets of structures follow those used in Fig. 8. In the last column, we give the value of $2J_0$ (in meV) computed for $\text{GaAs}_{0.5}\text{Sb}_{0.5}$ at a 50%-50% volume \bar{V} . This is obtained using Eq. (5.14) and the LAPW energies [in meV/(4 atoms), at \bar{V}] 198, 234, 135, 115, 144, 52, 132, 97, 105, and 110 for $A, B, L1, CA, L3, CH, CP, Z2, F1$, and $F3$, respectively. Note the fast convergence of J_0 .

	A	B	$L1$	CA	$L3$	CH	CP	$Z2$	$F1$	$F3$	$2J_0(\bar{V})$
Set 3	2	2	0	12	0	0	0	0	0	0	140.25
Set 3+2L	1	1	4	6	4	0	0	0	0	0	139.88
Set 4	2	2	0	0	0	12	0	0	0	0	93.00
Set 4+2L	1	1	4	-6	4	12	0	0	0	0	92.63
Set 5	$\frac{3}{2}$	$\frac{3}{2}$	0	-3	0	12	4	0	0	0	90.94
Set 5+2L	1	1	2	-6	2	12	4	0	0	0	90.75
Set 6	0	0	0	0	0	6	4	6	0	0	88.88
Set 6+2F	$-\frac{1}{2}$	$-\frac{1}{2}$	0	-1	0	4	4	6	2	2	88.56
Set 6+2L	$-\frac{1}{2}$	$-\frac{1}{2}$	2	-3	2	6	4	6	0	0	88.69
Set 10	$-\frac{1}{2}$	$-\frac{1}{2}$	2	-3	2	6	4	6	0	0	88.69

the stability of the expansion (5.15) is that

$$K(M) = \sum_s^M \int_0^1 Q_s^2(x, M) dx = \text{minimum}. \quad (5.18)$$

This gives

$$K(M) = \sum_{f, f'} \sum_s [\bar{\Pi}_f(s)]^{-1} [\bar{\Pi}_{f'}(s)]^{-1} \times \frac{1 - (-1)^{k_f + k_{f'} + 1}}{2(k_f + k_{f'} + 1)} = \text{minimum}. \quad (5.19)$$

Table VIII gives the values of the quality parameter K , also including results obtained by adding the 1:3 and 3:1 structures (L and F) along with the many-body terms J_3, J_4, K_3, K_4 . This demonstrates that (i) the set $M=6$ is indeed the stablest pair interaction set ($K=0.45$); (ii) the set $M=6+2F$ is the stablest set which includes many-body effects ($K=0.40$), although the set $M=6+2L$ is similar in quality; and (iii) inclusion of $2L+2F$ along with J_3, K_3, J_4, K_4 causes some approximate linear dependence (K increases), hence such combinations should be avoided. (iv) Using $\kappa_1 = \sum_s^M |[\bar{\Pi}_1(s)]^{-1}|$ as a ‘‘quality parameter’’ which measures the stability of a set M in describing the asymmetry of the phase diagram (dictated by $J_{f=1}$), we find that $\kappa_1=5.5$ for all $M+2L+2F$ sets (i.e., a very large sensitivity), whereas $\kappa_1=1.5$ for all $M+2L$ or $M+2F$ sets, and $\kappa_1=1.0$ for all sets which do not include either the structures L and F . This also suggests that sets including both $L1, L3$ and $F1, F3$ should be avoided.

The demonstrated transferability of the set of interactions obtained from a given set of small unit-cell structures to the prediction of the energies of other structures can be applied to the interesting case of lattice-matched superlattices. Recently, Wei *et al.*^{85(a)} have generalized this procedure to longer-period $(\text{AlAs})_p/(\text{GaAs})_p$ superlattices in various orientations, finding that the interesting parameters extracted from *short-period* ($p \sim 1-2$) ordered structures (Table VIII) accurately described directly calculated superlattice energies for longer-period structures.^{85(b)}

VI. FOLDING HIGHER-ORDER INTERACTIONS INTO LOWER ORDERS: DISORDERED fcc ALLOYS

In this section we apply the formalism developed in Sec. II together with the interaction parameters described in Sec. V to ‘‘pseudobinary’’ fcc $\text{GaAs}_x\text{Sb}_{1-x}$ and $\text{Al}_{1-x}\text{Ga}_x\text{As}$ alloys. To illustrate our method we fix the statistical counting range d_{stat} to include first neighbors ($m=1$), up to four-body interactions ($k=4$), or, in other words, the first five clusters of Table II, comprising a tetrahedral figure U . We use eight successively increasing ranges for d_{int} corresponding to $M=3, 4, 5$, and 6 of Table VIII (pair interactions only) and $M=3+2L, 4+2L, 5+2L$, and $6+2L$ resulting from adding to these the two ($L1, L3$) luzonite structures and the interaction parameters J_3 and J_4 .

A. The determination of C_ϕ^f

To determine the effective equations of state [Eq. (2.32)] we first reduce the figures not contained in the range d_{stat} (i.e., not contained in U) according to Eq. (2.18), finding the coefficients C_ϕ^f of Eq. (2.18) to be used later in Eq. (2.21) to determine the effective interactions. The method of reduction is given by Eq. (2.15), which is used whenever the figure made of the sites is not a subfigure of U . We consider only the disordered phase.

1. Pair interactions $K_2 \equiv J_{2,2}, L_2 \equiv J_{2,3}$ and $M_2 \equiv J_{2,4}$

The reduction follows Eq. (2.25). In general, we have for the m th pair interaction

$$\langle \Pi_{2,m} \rangle = q^2 = (2x - 1)^2. \quad (6.1)$$

For K_2 , we have

$$C_{2,2}^{1,1} = 1, \text{ others null}. \quad (6.2)$$

For L_2 , we have

$$C_{2,3}^{1,1} = 1, \text{ others null}. \quad (6.3)$$

Finally, for M_2 we have

$$C_{2,4}^{1,1}=1, \text{ others null.} \quad (6.4)$$

2. Three-body interaction $K_3 \equiv J_{3,2}$

Let α and β denote the sites that are second neighbors (Table II), and γ the nearest neighbor to α and β . Following Eq. (2.15),

$$\begin{aligned} \langle \Pi_{3,2} \rangle &= \langle \hat{S}_\alpha \hat{S}_\beta \hat{S}_\gamma \rangle = q \langle \hat{S}_\beta \hat{S}_\gamma \rangle + q \langle \hat{S}_\alpha \hat{S}_\gamma \rangle + q \langle \hat{S}_\alpha \hat{S}_\beta \rangle \\ &\quad - q^2 \langle \hat{S}_\alpha \rangle - q^2 \langle \hat{S}_\beta \rangle - q^2 \langle \hat{S}_\gamma \rangle + q^3 \\ &= 2q \langle \Pi_{2,1} \rangle + q \langle \Pi_{2,2} \rangle - 2q^3, \quad (6.5) \end{aligned}$$

Using Eq. (6.1) we obtain

$$\langle \Pi_{3,2} \rangle = 2q \langle \Pi_{2,1} \rangle - q^3, \quad (6.6)$$

or

$$C_{3,2}^{2,1} = 2, \quad (6.7)$$

$$C_{3,2}^{1,1} = -1. \quad (6.8)$$

3. Four-body interaction $K_4 \equiv J_{4,2}$

α and β are second neighbors. Thus

$$\begin{aligned} \langle \hat{S}_\alpha \hat{S}_\beta \hat{S}_\gamma \hat{S}_\delta \rangle &= q \langle \hat{S}_\beta \hat{S}_\gamma \hat{S}_\delta \rangle + q \langle \hat{S}_\alpha \hat{S}_\gamma \hat{S}_\delta \rangle + q \langle \hat{S}_\alpha \hat{S}_\beta \hat{S}_\delta \rangle + q \langle \hat{S}_\alpha \hat{S}_\beta \hat{S}_\gamma \rangle \\ &\quad - q^2 \langle \hat{S}_\alpha \hat{S}_\beta \rangle - q^2 \langle \hat{S}_\alpha \hat{S}_\gamma \rangle - q^2 \langle \hat{S}_\alpha \hat{S}_\delta \rangle - q^2 \langle \hat{S}_\beta \hat{S}_\gamma \rangle - q^2 \langle \hat{S}_\beta \hat{S}_\delta \rangle - q^2 \langle \hat{S}_\gamma \hat{S}_\delta \rangle \\ &\quad + q^3 \langle \hat{S}_\alpha \rangle + q^3 \langle \hat{S}_\beta \rangle + q^3 \langle \hat{S}_\gamma \rangle + q^3 \langle \hat{S}_\delta \rangle - q^4. \quad (6.9) \end{aligned}$$

Using Eq. (6.6) for the third and fourth terms, and Eq. (6.1) for the fifth, we obtain

$$\langle \Pi_{4,2} \rangle = 2q \langle \Pi_{3,1} \rangle - q^2 \langle \Pi_{2,1} \rangle. \quad (6.10)$$

Then

$$C_{4,2}^{3,1,1} = 2, \quad (6.11)$$

$$C_{4,2}^{2,1} = -1. \quad (6.12)$$

B. Effective multiatom interactions $\tilde{J}_f(x, V)$ and energies $\Delta \tilde{E}(n, x, V)$

Using these C_ϕ^f and the values of $D_f \equiv D_{k,m}$ of Table II, Eq. (2.21) gives the resummed (effective) interaction energies

$$\tilde{J}_0(x, V) = J_0(V), \quad (6.13a)$$

$$\begin{aligned} \tilde{J}_1(x, V) &= J_1(V) + 3(2x-1)K_2(V) \\ &\quad + 12(2x-1)L_2(V) + 6(2x-1)M_2(V) \\ &\quad - 12(2x-1)^2K_3(V), \quad (6.13b) \end{aligned}$$

$$\begin{aligned} \tilde{J}_2(x, V) &= J_2(V) + 4(2x-1)K_3(V) \\ &\quad - 2(2x-1)^2K_4(V), \quad (6.13c) \end{aligned}$$

$$\tilde{J}_3(x, V) = J_3(V) + 3(2x-1)K_4(V), \quad (6.13d)$$

$$\tilde{J}_4(x, V) = J_4(V). \quad (6.13e)$$

In the next step, we combine the effective interactions $\tilde{J}_k(x, V)$ to obtain the energies $\Delta \tilde{E}(n, x, V)$ of Eq. (2.24). For the $2^4 = 16$ ordered configurations of a lattice with a tetrahedral unit cell, the probabilities P_n are the symbols W_{ijkl} of Kikuchi,⁶⁴ where i, j, k, l may be either zero or one, hence our effective equations of state $\epsilon_n(P, V)$ correspond to the ϵ_{ijkl} . For the disordered phase, the energies and probabilities are equal whenever $i + j + k + l$ are the

same. Therefore, there are just five independent probabilities P_n , equations of state $\epsilon_n(P, V)$, and energies $\Delta \tilde{E}(n, x, V)$:

$$\begin{aligned} \Delta \tilde{E}(0, x, V) &= \tilde{J}_0(x, V) - \tilde{J}_1(x, V) + 6\tilde{J}_2(x, V) \\ &\quad - 8\tilde{J}_3(x, V) + 2\tilde{J}_4(x, V), \quad (6.14a) \end{aligned}$$

$$\begin{aligned} \Delta \tilde{E}(1, x, V) &= \tilde{J}_0(x, V) - \frac{1}{2}\tilde{J}_1(x, V) + 4\tilde{J}_3(x, V) - 2\tilde{J}_4(x, V), \\ &\quad (6.14b) \end{aligned}$$

$$\Delta \tilde{E}(2, x, V) = \tilde{J}_0(x, V) - 2\tilde{J}_2(x, V) + 2\tilde{J}_4(x, V), \quad (6.14c)$$

$$\begin{aligned} \Delta \tilde{E}(3, x, V) &= \tilde{J}_0(x, V) + \frac{1}{2}\tilde{J}_1(x, V) - 4\tilde{J}_3(x, V) - 2\tilde{J}_4(x, V), \\ &\quad (6.14d) \end{aligned}$$

$$\begin{aligned} \Delta \tilde{E}(4, x, V) &= \tilde{J}_0(x, V) + \tilde{J}_1(x, V) + 6\tilde{J}_2(x, V) \\ &\quad + 8\tilde{J}_3(x, V) + 2\tilde{J}_4(x, V). \quad (6.14e) \end{aligned}$$

C. The effective equations of state $\epsilon_n(P, V)$

In the last step one uses Eq. (2.32) to calculate the effective equations of state.

1. Nearest-neighbor (tetrahedron) interaction

When considering just nearest-neighbor interaction^{24,48,58} (assuming all the other interactions to be zero), the effective equations of state (denoted as $M=5$) do not depend on the probabilities $\{P_n\}$ and coincide with the excess energies of the ordered structures 0-4 of Fig. 2, namely

$$\begin{aligned} \tilde{\epsilon}_0^{(5)}(V) &= J_0(V) - J_1(V) + 6J_2(V) - 8J_3(V) + 2J_4(V), \\ &\quad (6.15a) \end{aligned}$$

$$\tilde{\epsilon}_1^{(5)}(V) = J_0(V) - \frac{1}{2}J_1(V) + 4J_3(V) - 2J_4(V), \quad (6.15b)$$

$$\tilde{\epsilon}_2^{(5)}(V) = J_0(V) - 2J_2(V) + 2J_4(V), \quad (6.15c)$$

$$\bar{\epsilon}_3^{(5)}(V) = J_0(V) + \frac{1}{2}J_1(V) - 4J_3(V) - 2J_4(V), \quad (6.15d)$$

$$\bar{\epsilon}_4^{(5)}(V) = J_0(V) + J_1(V) + 6J_2(V) + 8J_3(V) + 2J_4(V). \quad (6.15e)$$

2. Addition of other pair interactions

Next, we add the pair interactions K_2 , L_2 , and M_2 of Table II. In this case, the effective equations of state (denoted as $M=8$) depend on $\{P_n\}$ only through x . They are given by

$$\bar{\epsilon}_0^{(8)}(x, V) = \bar{\epsilon}_0^{(5)}(V) + (2x+1)(1-2x)F_2(V), \quad (6.16a)$$

$$\bar{\epsilon}_1^{(8)}(x, V) = \bar{\epsilon}_1^{(5)}(V) + 2x(1-2x)F_2(V), \quad (6.16b)$$

$$\bar{\epsilon}_2^{(8)}(x, V) = \bar{\epsilon}_2^{(5)}(V) + (2x-1)(1-2x)F_2(V), \quad (6.16c)$$

$$\bar{\epsilon}_3^{(8)}(x, V) = \bar{\epsilon}_3^{(5)}(V) + (2x-2)(1-2x)F_2(V), \quad (6.16d)$$

$$\bar{\epsilon}_4^{(8)}(x, V) = \bar{\epsilon}_4^{(5)}(V) + (2x-3)(1-2x)F_2(V), \quad (6.16e)$$

where

$$F_2(V) = 3K_2(V) + 12L_2(V) + 6M_2(V). \quad (6.16f)$$

3. Additional three- and four-body interactions

Finally, when we also include the interactions K_3 and K_4 , the effective equations of state (denoted as $M=10$) depend on $\{P_n\}$ explicitly, and Eq. (2.32) needs to be solved self-consistently for given temperature T , volume V , and concentration x . While we numerically calculate these self-consistently using the actual, finite temperature CVM probabilities, we give here the simpler expressions at $T = \infty$, when the probabilities are those of random alloy,

$$\bar{\epsilon}_0^{(10)}(x, V, \infty) = \bar{\epsilon}_0^{(8)}(x, V) + 12(2x+1)(2x-1)K_3(V) - 12(2x+1)(2x-1)K_4(V), \quad (6.17a)$$

$$\bar{\epsilon}_1^{(10)}(x, V, \infty) = \bar{\epsilon}_1^{(8)}(x, V) + 6(2x-1)^2K_3(V) + 12(2x-1)K_4(V), \quad (6.17b)$$

$$\bar{\epsilon}_2^{(10)}(x, V, \infty) = \bar{\epsilon}_2^{(8)}(x, V) - 8(2x-1)K_3(V) + 4(2x-1)^2K_4(V), \quad (6.17c)$$

$$\bar{\epsilon}_3^{(10)}(x, V, \infty) = \bar{\epsilon}_3^{(8)}(x, V) - 6(2x-1)^2K_3(V) - 12(2x-1)K_4(V), \quad (6.17d)$$

$$\bar{\epsilon}_4^{(10)}(x, V, \infty) = \bar{\epsilon}_4^{(8)}(x, V) - 12(2x-3)(2x-1)K_3(V) - 12(2x-3)(2x-1)K_4(V). \quad (6.17e)$$

Equations (6.17) can be trivially generalized to include more interactions. These are powerful expressions, affording the use of just five functions $\bar{\epsilon}_n(x, V, T)$ in standard nearest-neighbor Ising model calculations, yet providing results which approximate well distant-neighbor effects. Combined with different choices of structures, one can test the trends and convergence of calculated thermodynamic quantities.

D. The equilibrium condition

Letting $V = V_{\text{eq}}(x, T)$ be the equilibrium volume of the alloy at x and T , the functions $\bar{\epsilon}_n[x, V_{\text{eq}}(x, T), T]$ may be

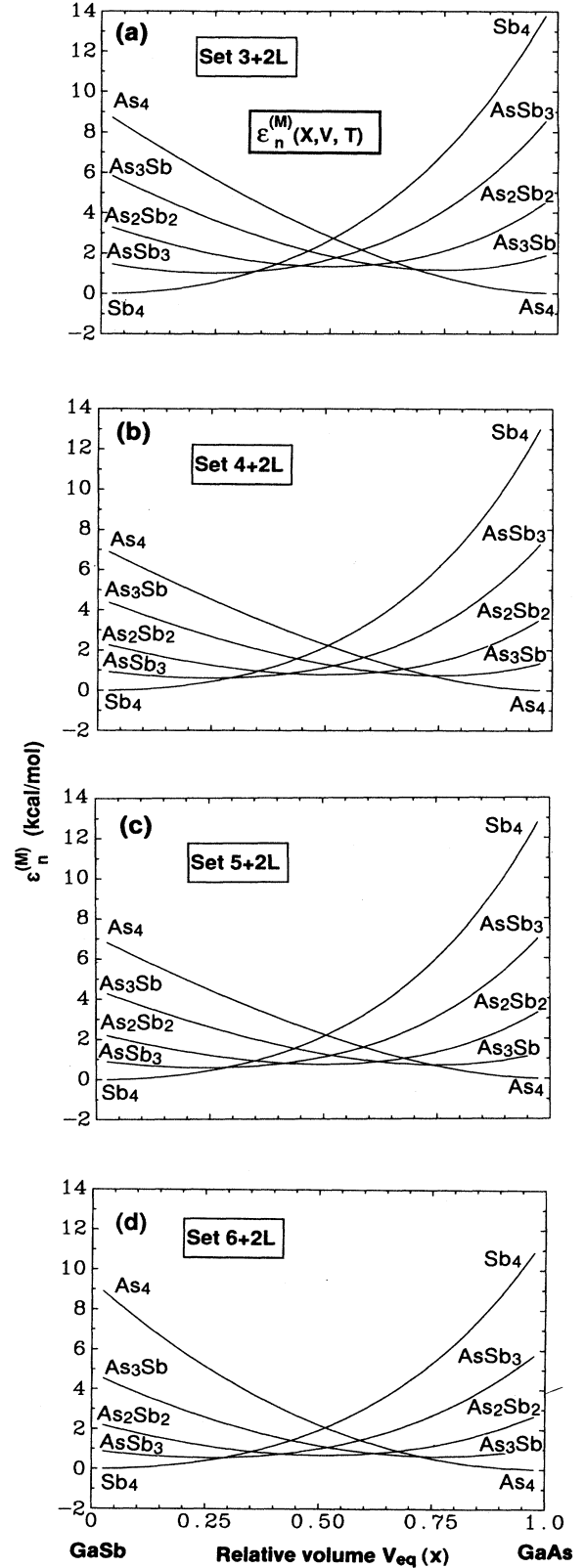


FIG. 4. Effective equation of states for GaAs-GaSb [Eqs. (6.15)–(6.17)].

used, instead of $\bar{\epsilon}_n(P, V)$ to calculate the thermodynamic equilibrium. For instance, the equilibrium volume is given by the equation

$$\sum_n P_n \frac{d\epsilon_n[X(V, T), V, T]}{dV} = \sum_n P_n \frac{\partial x}{\partial V} \frac{\partial \bar{\epsilon}_n}{\partial x} + \sum_n P_n \frac{\partial \bar{\epsilon}_n}{\partial V} = 0 \quad (6.18)$$

because the first term is zero due to Eqs. (2.29) and (2.30), and the second due to Eq. (2.26). Therefore we can work with $\bar{\epsilon}_n[x(V, T), V, T]$ or $\bar{\epsilon}_n[x, V_{\text{eq}}(x, T), T]$ as a temperature-dependent, but state-of-order-independent effective equation of state.

Figure 4 depicts the effective equation of state $\bar{\epsilon}_n[x(V, T), V, T]$ for $\text{GaAs}_x\text{Sb}_{1-x}$, and Fig. 5 depicts $\bar{\epsilon}_n(x, T)$ for $\text{Al}_{1-x}\text{Ga}_x\text{As}$. No lattice mismatch was permitted in the latter case, so that no volume variation can be considered. In both cases, the temperature dependence is so weak that it cannot be seen in the scale of the figures. This implies that (when phonon contributions are neglected) $V_{\text{eq}}(x, T)$ is also nearly temperature independent. One observes in Figs. 4 and 5 that, by increasing the number of ordered structures the energies at the minima (enthalpies of formation) decrease, and the curvatures (or the effective bulk moduli) also decrease. In the case of Fig. 5, the new configurations introduce a re-

markable x dependence in the energies. In this case, the energy maxima occur at the stoichiometric compositions $x = X_n$, as one readily verifies by equating the derivatives of Eqs. (6.16) to zero. In Sec. VIII C, we will further discuss the effective energies $\bar{\epsilon}_n$ of Figs. 4 and 5.

E. Calculated thermodynamic quantities

The folded interaction energies $\{\bar{J}_k(x, V)\}$ of Eq. (6.13) [or the effective equations of state in Eq. (6.23)] can now be used in the context of the generalized Ising problem to solve for the correlation functions $\langle \Pi_f \rangle$ or the probabilities P_n and the equilibrium volumes [Eq. (2.27)]. Evaluating $\langle \Delta E(V) \rangle$ for the various phases enables the calculation of the basic thermodynamic properties of these phases. We next define the main thermodynamic quantities calculated and discussed in Sec. VIII. These include the disordered alloy *excess mixing enthalpy* $\Delta H(x, T)$ of Eq. (1.2) and its "interaction parameter"

$$\Omega_H(x, T) \equiv \Delta H(x, T)/x(1-x). \quad (6.19)$$

The *formation enthalpy* $\Delta H(x)$ of ordered compounds is the equilibrium value $\Delta E(s, V_s)$ of Eq. (2.2). The *free energy* is

$$F(x, T) = \Delta H(x, T) - TS^{(0)}(x) - T \Delta S(x, T) \quad (6.20)$$

(where $S^{(0)}$ is the ideal mixing entropy), the *excess free energy* is

$$\Delta F(x, T) = \Delta H(x, T) - T \Delta S(x, T), \quad (6.21)$$

and its "interaction parameter"

$$\Omega_F(x, T) \equiv \Delta F(x, T)/x(1-x). \quad (6.22)$$

The amount by which the cluster probability P_n of Eq. (2.12) deviates from the (temperature-independent) *random* (R) probability is defined as *degree of nonrandomness*

$$\Delta P_n(x, T) = P_n(x, T) - P_n^{(R)}(x). \quad (6.23)$$

If $\Delta P_n(x, T) < 0$ for the pure A or pure B clusters ($n=0, 4$), the system is said to exhibit "clustering," whereas if $\Delta P_n(x, T) > 0$ for the $n=0, 4$ clusters, the system is said to exhibit "anticlustering."

VII. USEFUL NUMERICAL SIMPLIFICATIONS

The input to the calculation of the phase diagrams consists of the excess energies $\Delta E(s, V)$ for the ordered structures $\{s\}$ over the volume range from $V = V_{AC}$ to $V = V_{BC}$. The results are normally fitted to a convenient analytic form in terms of the bulk modulus B_n , its pressure derivative B_n' , the equilibrium volume V_n , and the formation enthalpy ΔH_n [e.g., Eq. (5.1) and Table III]. Since self-consistent calculations of $\Delta E(s, V)$ over a full volume range are rather time consuming, it is useful to explore approximations which simplify this procedure. One can easily calculate $\{B, B', V\}$ just for the end-point compounds AC and BC using calculated total energies near their respective equilibrium volume, and interpolate the values for ordered compounds. The simplest interpolation is the generalized Vegard rule, i.e.,

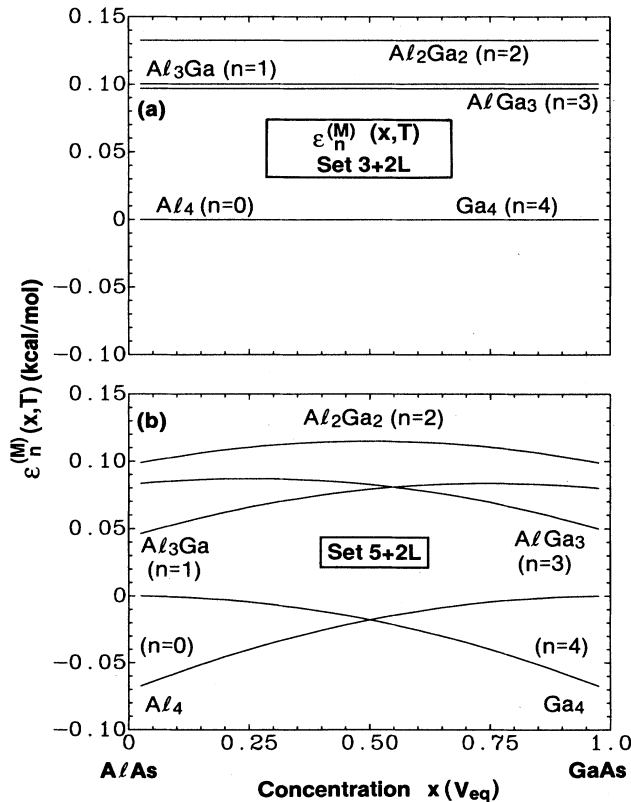


FIG. 5. Effective equation of states for GaAs-AlAs [Eqs. (6.15)–(6.17)].

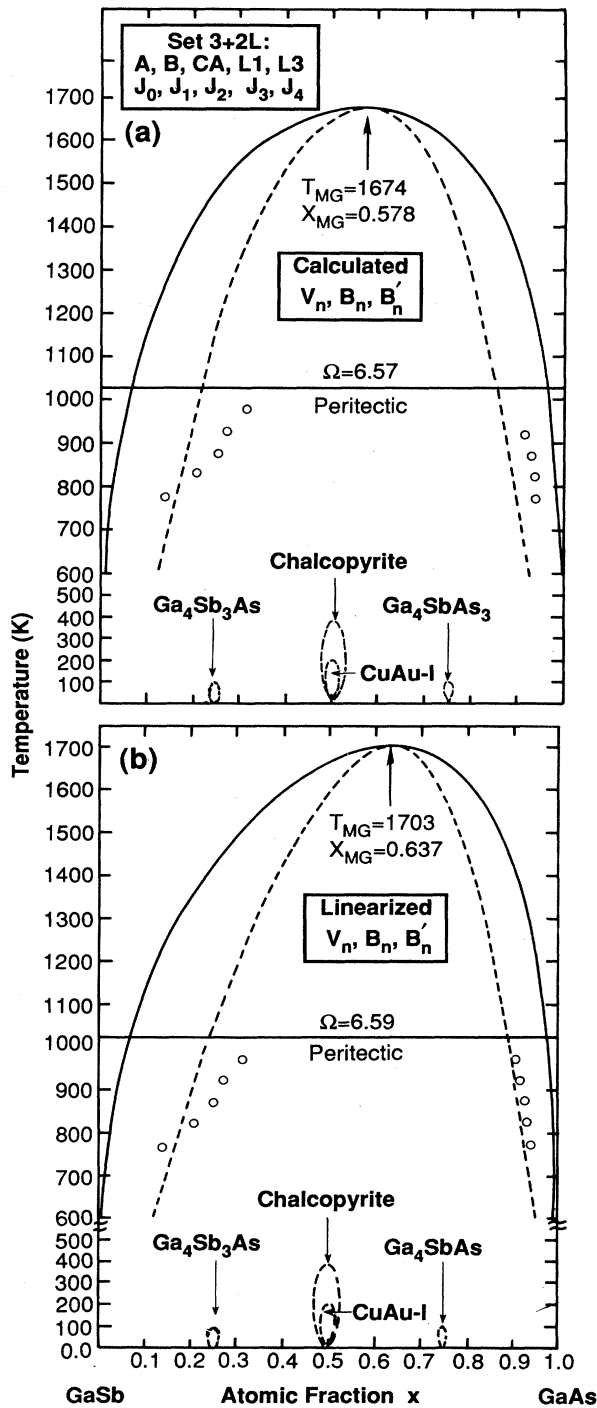


FIG. 6. Phase diagrams of $\text{GaAs}_x\text{Sb}_{1-x}$, illustrating the linear approximation of Eq. (7.1). The dashed line running close to the solid line (binodal) is the spinodal line. This figure also shows the regions of existence of the metastable ordered phases bounded by the spinodal $d^2F/dx^2=0$. To obtain results for CuAu-I we use the structures $A, B, CA, L1$, and $L3$. Ordering temperatures for chalcopyrite are found by using the set $A, B, CH, F1$, and $F3$.

$$\begin{aligned} V_n &= (1-X_n)V_{AC} + X_nV_{BC}, \\ B_n &= (1-X_n)B_{AC} + X_nB_{BC}, \\ B'_n &= (1-X_n)B'_{AC} + X_nB'_{BC}, \end{aligned} \quad (7.1)$$

where X_n is the fraction of atom B in compound n . Obviously, ΔH_n cannot be linearized and are kept with their full n and s dependence. Figures 6 and 7 depict the calculated phase diagram of GaAs-GaSb using as input the directly calculated equation of states of Table II [part (a) of these figures] and the linearized version of Eq. (7.1) [part (b) of these figures], where B'_{AC} and B'_{BC} are obtained using five calculated data points near their respective equilibrium positions (see Table X). In Fig. 6, we give the comparison for a case where no folding is involved, whereas Fig. 7 gives results for seven structures, where folding of higher-order interactions is involved. In all cases, we use the formation enthalpies $\Delta H(n)$ of the ordered phases obtained in *direct* calculation (Table III),

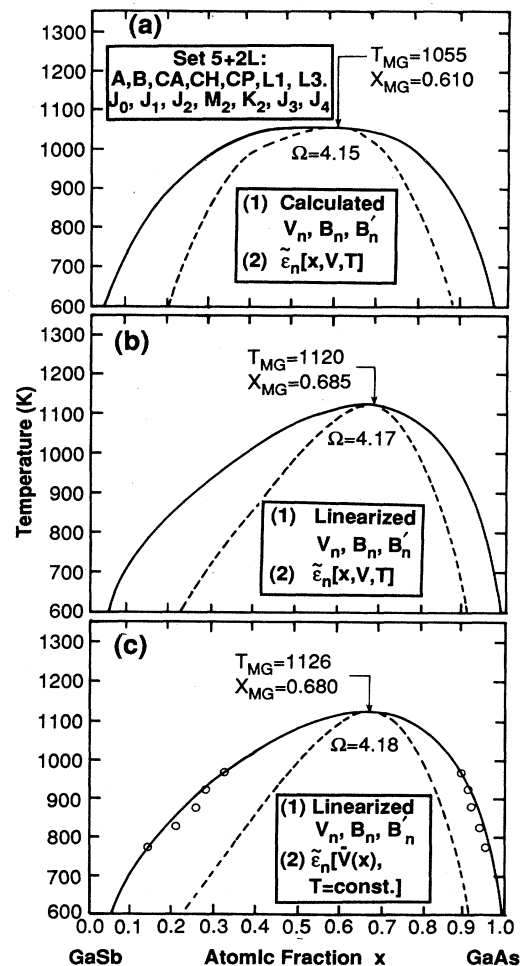


FIG. 7. Phase diagrams of $\text{GaAs}_x\text{Sb}_{1-x}$, illustrating the approximations to the effective energies $\tilde{\epsilon}_n$, discussed in Sec. VII. The dashed line is the spinodal. Data taken from Table X.

TABLE X. Comparison of the input parameters V_n , B_n , B'_n , and ΔH_n [Eq. (5.1)] of the LAPW calculated $\Delta E(s, V)$ excess energies [using Eq. (7.1)] with the effective values obtained by fitting the effective energies $\bar{\epsilon}_n(V)$ of “set 5+2L” to the same equation, (5.1). $A = \text{Sb}$, $B = \text{As}$.

Struct.	V_n (cm ³ /mol)		B_n (GPa)		B'_n		ΔH_n (kcal/mol)	
	Input	Effec.	Input	Effec.	Input	Effec.	Input	Effec.
A_4C_4	34.29	34.29	51.8	36.6	6.78	9.8	0.0	0.00
A_3BC_4	32.62	32.60	57.5	42.8	6.5	8.8	(a)	0.57
$A_2B_2C_4$	30.95	30.92	63.2	48.9	6.3	7.9	(b)	0.72
AB_3C_4	29.28	29.25	68.9	54.8	6.1	7.2	(c)	0.68
B_4C_4	27.62	27.62	74.6	60.6	5.82	6.5	0.0	0.00

^a1.02 for $L1$, 0.69 for $F1$.

^b1.33, 0.60, 1.52, and 1.12 for CA, CH, CP, and Z2.

^c1.15 for $L3$, 0.79 for $F3$.

with no linearization. The results are compared with the recently measured⁸⁶ phase diagram. This shows that the linearization of the parameters B_n , B'_n , and V_n change the miscibility-gap temperature by only $\sim 5\%$, leaving the mixing enthalpy essentially unchanged. Since the extraction of the values of B_n and B'_n for intermediate ordered compounds from the numerically calculated energy $\Delta E(s, V)$ involves larger uncertainties than those underlying Eq. (7.1), we judge approximation (7.1) to be both appropriate and sufficiently accurate for these systems. This reduces dramatically the computational effort required, as the total energy of the inter semiconductor compounds needs to be calculated only at few volumes near their equilibrium (to find ΔH_n), rather than for many more volumes over the full range.

As a further time-saving simplification, we note from Fig. 4 that the effective equations of state $\bar{\epsilon}_n(x, V, T)$ depend but very weakly on T (changing by less than 0.1% near their respective minimum or less than 2% in the whole range for $T = 800\text{--}40\,000$ K), and that the equilibrium volume satisfying Eq. (6.18) is nearly Vegard-like (i.e., linear with x). Hence, we (i) compute $\bar{\epsilon}_n$ only at a single, fixed temperature, and (ii) replace $V_{\text{eq}}(x)$ by its concentration-weighted average \bar{V} . This gives $\bar{\epsilon}_n(x, V, T)$ in a simplified form $\bar{\epsilon}_n(\bar{V})$, which can be readily fitted to an analytic form [Eq. (5.1)] for ease of use. Figure 7 contrasts the phase diagram of GaAs-GaSb obtained with $\bar{\epsilon}_n(x, V, T)$ [Fig. 7(b)] with that obtained with the simplified $\bar{\epsilon}_n(\bar{V})$ and fitting to Murnaghan's equation of state^{78,87} [Fig. 7(c)], showing little loss of accuracy. In what follows, we will present results using this form of $\bar{\epsilon}(\bar{V})$ as well as the linearized parameters of Eq. (7.1) (see Table X).

VIII. RESULTS

A. Convergence of the phase diagram with respect to the range of interaction

Figure 8 depicts the calculated phase diagram of GaAs-GaSb using the sets of interaction parameters (Table VIII) within $M = 3, 4, 5$, and 6 structures [Figs. 8(a)–8(d)], as well as the results obtained by adding the three- and four-body terms J_3 and J_4 , respectively along with the $L1$ and $L3$ structures [shown in Figs. 8(e)–8(h)].

The recent experimental data of Ref. 86 is also given. In each case, we also depict the “interaction parameter” $\Omega_H(x, T)$ of Eq. (6.19) at $T = 1000$ K and the three compositions $x = 0, 0.5$, and 1.0.

Our results show (i) the commonly used set of five (001) structures⁵⁸ [Fig. 8(e)] overestimates the maximum miscibility-gap temperature and the mixing enthalpies by as much as $\sim 60\%$; (ii) the convergence rate of the phase diagram with respect to the interactions included is rather fast, e.g., the maximum miscibility temperature is 1703, 1206, 1126, and 1080 K for $M = 3, 4, 5$, and 6, respectively (the experimentally interpolated value⁸⁸ is $\sim 1100 \pm 100$ K), and the enthalpy “interaction parameter” at $x = 0.5$ is 6.59, 4.41, 4.18, and 4.01 kcal/mol, respectively (the experimentally interpolated value is^{19,20,88(a)} 4.2 ± 0.3 kcal/mol). Our converged Ω value is expected to underestimate Ω by 5–10% since we underestimate lattice mismatch between GaAs and GaSb (calculated to be 0.425 Å compared to experimental data of 0.444 Å). The rapid convergence, implying that even 4–6 well-chosen ordered structures suffice to describe the system over a full temperature and composition range, and the close agreement with experiment of this fully *ab initio* theory are very encouraging. (iii) Inclusion of three- and four-body terms have but a small effect on the maximum miscibility-gap temperature T_{MG} , but change significantly the asymmetry of the binodal and spinodal lines about $x = 0.5$. For $M = 3, 4, 5$, and 6, the value of x at T_{MG} without and with the many-body terms are (0.587, 0.637), (0.612, 0.690), (0.588, 0.680), and (0.545, 0.595), respectively. Note that due to the volume dependence of $J_r(V)$, calculations with pair interactions alone already produce an asymmetric phase diagram. Very recent careful measurements of the GaAs-GaSb phase diagram^{86,88(a)} have confirmed the pronounced asymmetry predicted here, which is, however, absent from simplified models.^{86(b)}

B. Role of sublattice relaxation

As indicated in Sec. V A and shown in Table I, $A_x B_{1-x} C$ alloys and $A_n B_{4-n} C_4$ ordered structures have both cell-internal structural degrees of freedom [i.e., relaxation of the common sublattice C leading to unequal $A\text{—}C$ and $B\text{—}C$ bond lengths⁷³ evident in extended x -

ray-absorption fine-structure (EXAFS) measurements⁸⁹], as well as cell-external degrees of freedom (relaxation of the mixed, A - B lattice leading to unequal A - A , A - B , and B - B distances, also seen in EXAFS measurements⁸⁹). We

have previously shown^{60,61,73} that relaxation of the cell-internal coordinates [i.e., minimizing the total energy $\Delta E(s, V)$ at each V with respect to the coordinates of C] lowers enormously the mixing enthalpy and the miscibili-

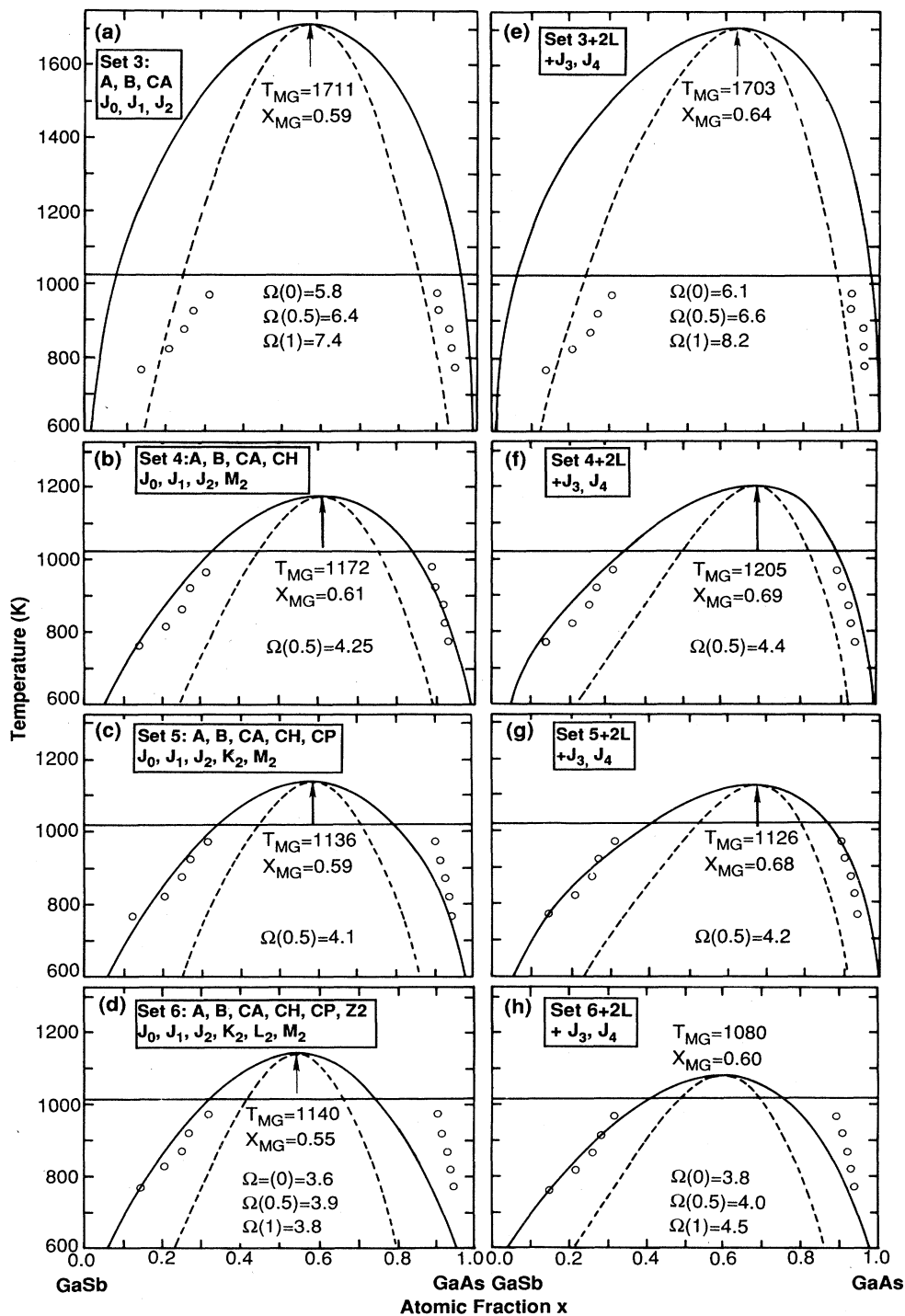


FIG. 8. Calculated phase diagrams and interaction parameters Ω [Eq. (6.19)] for $\text{GaAs}_x\text{Sb}_{1-x}$ using the various sets of structures and interaction energies of Table VIII. The dashed line is the spinodal. Data taken from Table X. Observe the rather fast convergence of the major features. Open circles denote the experimental data of Ref. 86.

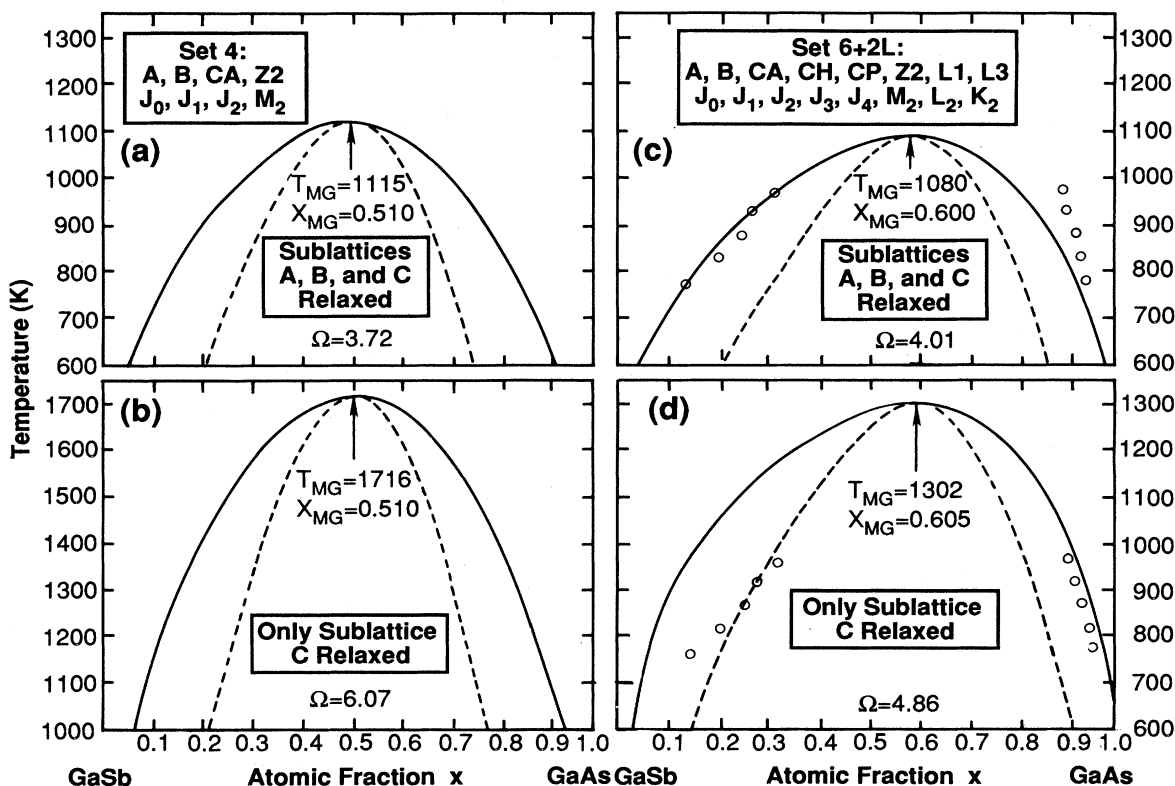


FIG. 9. Phase diagrams of $\text{GaAs}_x\text{Sb}_{1-x}$ illustrating the effects of relaxing the mixed (As-Sb) sublattices.

ty temperature. Here we focus on the more subtle effect of relaxation of the mixed sublattice A - B .

To study this relaxation effect, we have included the $Z2$ structure (exhibiting a mixture of A_4 , B_4 , and A_2B_2 tetrahedra), showing sizeable mixed sublattice relaxation in the A_4, B_4 tetrahedra. All the other structures we have studied have negligible mixed sublattice relaxation. Figure 9 shows the calculated phase diagram of $\text{GaAs}_x\text{Sb}_{1-x}$ using two different sets of structures (both including the “ $Z2$ ” superlattice) where the mixed sublattice in $Z2$ is unrelaxed [Figs. 9(b) and 9(d)] or relaxed [Figs. 9(a) and 9(c)]. In both cases, the common sublattice C is fully relaxed. Our results show that relaxation of the mixed sublattice is important in reducing the mixing enthalpy and maximum miscibility temperature, and bringing it into close agreement with experiment.

C. How do the effective energies $\bar{\epsilon}_n(V)$ differ from the real energies $\Delta E(n, V)$

It is interesting to observe how the renormalization of a “large” set of energies $\{\Delta E(n, V)\}$ into five simple effective energy functions $\bar{\epsilon}_n(V)$, $0 \leq n \leq 4$, alters the latter. Table X gives for set “ $5+2L$ ” (Table VIII) the parameters \bar{V}_n , \bar{B}_n , \bar{B}'_n , and $\Delta\bar{H}_n$ obtained by fitting the numerically calculated effective equation of state $\bar{\epsilon}_n(\bar{V})$ into the same analytic form [Eq. (5.1)] used to represent the ordinary excess energy $\Delta E(n, V)$. We have used in this

calculation the numerical simplifications outlined in Sec. VII. For comparison, we give the real equilibrium volume V_n , bulk modulus B_n and its pressure derivative B'_n , and formation enthalpy ΔH_n obtained by similarly fitting the LAPW calculated excess energies $\Delta E(n, V)$. We see that renormalization of distant-neighbor interactions into five effective energies significantly lowers B_n and ΔH_n .

In a previous work,^{24,48,61} we have used the five canonical structures A , $L1$, CA , $L3$, and B (set $3+2L$), observing^{48,61} that the effects of cell-internal and cell-external relaxation could be mimicked by permitting the *equilibrium* volume V_n of cluster n to depend on the composition x in which it is embedded. To first order in a Taylor series

$$V_n(x) = V_n(X_n) + K_n[V(x) - V_n(X_n)] + \dots, \quad (8.1)$$

where $V_n(X_n) = V_n$ is the actual equilibrium volume of cluster n in isolation and K_n is a relaxation parameter. If $K_n = 0$, the system is unrelaxed and $V_n(x) = V_n(X_n)$ for all x 's. Full relaxation corresponds to $K_n = 1$ where all clusters experience the same equilibrium volume $V(x)$ as the medium. Since for small volume changes the alloy energy scales as $[V(x) - V_n(x)]^2$ Eq. (8.1) shows that the effective energy of a cluster embedded in an alloy of volume $V = V(x)$ is

$$\Delta\bar{E}(n, V) = \Delta H_n + \frac{1}{2} \frac{B_n}{V_n} (1 - K_n)^2 (V - V_n)^2 + \dots \quad (8.2)$$

This is equivalent to scaling the B_n/V_n ratio of ordered structures by $(1 - K_n)^2$:

$$\frac{\tilde{B}_n}{\tilde{V}_n} = (1 - K_n)^2 \frac{B_n}{V_n} \quad (8.3)$$

In our previous work,^{48,61} we absorbed all relaxation into changes of B_n/V_n , using K as an adjustable parameter, but assumed the formation enthalpies

$$\Delta\tilde{H}_n = (1 - \chi_n)^2 \Delta H_n \quad (8.4)$$

are unaltered ($\chi_n = 0$). Our present calculation permits reflection on our previous approach. From Table IX and Eq. (8.3) we find that the actual relaxation constants are $K_n = 0.16, 0.14, 0.12, 0.11$, and 0.10 for $n = 0, 1, 2, 3$, and 4 , respectively (and indeed, having but a weak n dependence), but that the enthalpy relaxes too (relative to $L1$, CA , and $L3$), with $\chi_n = 0.25, 0.26$, and 0.23 , for $n = 1, 2$, and 3 , respectively. While we could fit⁶¹ the results for semiconductor alloys using $K \approx 0.3$ and $\chi = 0$, our present approach supercedes the previous one in that rigorous effective equations of states $\tilde{\epsilon}_n(V)$, incorporating directly relaxation effects, are now readily calculable.

D. Relative stability of ordered and disordered phases

Figure 10 depicts the calculated excess enthalpies $\Delta H(x, T)$ of both ordered and disordered $Al_{1-x}Ga_xAs$ and $GaAs_xSb_{1-x}$ structures at $x = 0.5$ with respect to the equilibrium, phase-separated constituents $AC + BC$. These results are best discussed by considering separately systems with a large size mismatch between the constitu-

ents (e.g., GaAs-GaSb, showing a 7.6% relative difference in their lattice parameters) and the system showing a very small size mismatch (GaAs-AlAs, with relative difference of only 0.1%).

When a small size mismatch exists [Fig. 10(a)], we find that the disordered phase as a *lower* enthalpy than all short-period ordered phases considered. We hence expect at low temperatures a competition between phase separation (the ground state) and the disordered phase, but no ordering of simple structures. The observation of partial CuAu-I-like ordering in $Ga_xAl_{1-x}As$ alloys³¹ is hence not explainable in our calculation as a bulk effect, and is likely to be induced during growth by a surface-related effect.

When a large size mismatch exists [Fig. 10(b)], we find that at low temperatures the chalcopyrite (CH) structure has a lower enthalpy than the disordered phase of the same composition. Hence, while both the ordered and the disordered phases have $\Delta H > 0$ and would phase separate at the $T = 0$ equilibrium, if such a phase separation were to be kinetically hindered at low temperatures (where atomic mobilities are small), we expect to find metastable ordering, as observed experimentally.³⁰ Using the $6+2L$ set, we find an order-disorder transition (for the chalcopyrite structure) of 285 K. Our subsequent work (see Sec. VD) on other lattice-mismatch alloys has shown that CH always has a lower enthalpy than the disordered phase, and is hence likely to be a universal metastable ordered phase in isovalent semiconductor alloys. The CuPt structure does not have this property (Fig. 10).

The convergence of our energy expansion of Eq. (2.2) for the lattice-matched system means that as we increase the repeat period of the ordered structure [e.g., from $(AC)_1(BC)_1$ to $(AC)_p(BC)_p$, $p > 1$], their energy *per atom* would decrease.⁸⁵ Hence, for sufficiently long-period superlattices, the energy of the random alloy must be above that of the superlattice. We next discuss the physical factors underlying the different behavior of short-period ordered structures in lattice-matched and -mismatched semiconductor alloys.

Recall that our description of the excess enthalpy $\Delta H(x, T)$ [Eq. (1.2)] centers on its expansion [Eq. (2.13)] in terms of the energies $\Delta E(n, V)$ of ordered structures n :

$$\Delta H(x, T) = \sum_n P_n(x, T) \Delta E[n, V_{eq}(x)] \quad (8.5)$$

where $V_{eq}(x)$ minimizes $\langle \Delta E(\sigma, V) \rangle$ with respect to V , and that the decomposition of $\Delta E(n, V)$ of Eqs. (5.7)–(5.10) leads to the form

$$\Delta H(x, T) = \sum_n P_n(x, T) \epsilon_n + G(x) \quad (8.6)$$

Using Eqs. (5.7)–(5.10),

$$\epsilon_n = \Delta E_{CE}(n, V_n) + \Delta E_S(n, V_n)$$

and

$$(8.7)$$

$$G(x) = \sum_n P_n(x, T) \Delta E_{VD}[n, V_{eq}(x)]$$

When the equilibrium volume at a fixed composition x does not depend on the state of order (generally, an excellent approximation for many metal and semiconductor

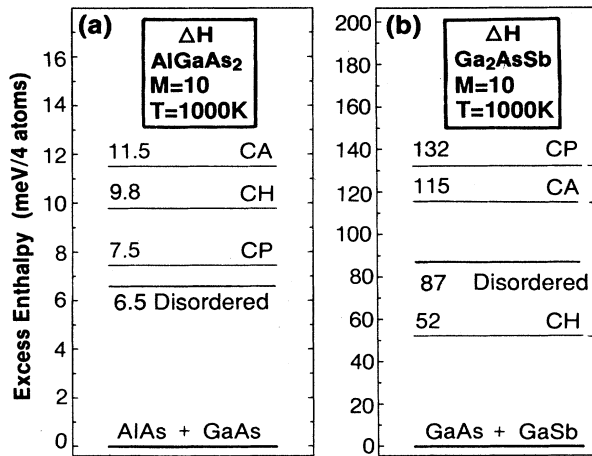


FIG. 10. Calculated excess enthalpies at $T = 1000$ K for (a) $AlGaAs_2$ and (b) Ga_2AsSb . Observe in (a) that the disordered phase (at $x = 0.5$) is lower in energy than all ordered LL phases, where as in (b) the chalcopyrite structure has a lower energy than the disordered phase.

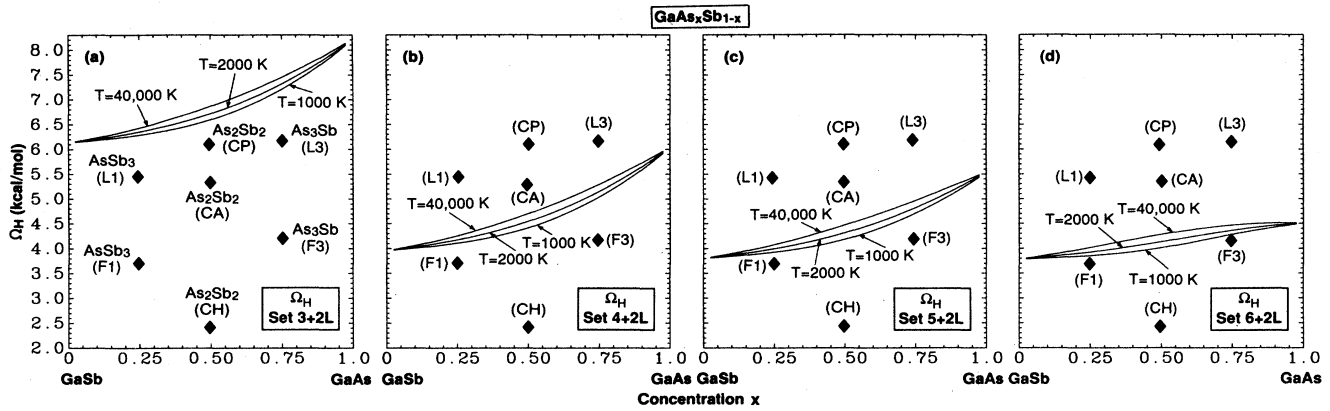


FIG. 11. Enthalpy interaction parameter [Eq. (6.19)] for ordered and disordered phases of GaAs-GaSb at $T=1000, 2000,$ and $40\,000$ K ($40\,000$ K represents numerically the near-random limit). The diamond-shaped symbols give the ($T=0$) values for ordered compounds.

alloys²⁶), Ref. 26 showed that ε_n depends only on the configuration n (but not on V or x), whereas $G(x)$ (“elastic energy”) depends on x , but not on n . For an ordered compound with stoichiometry X_n , Eq. (8.6) gives

$$\Delta H_n = \varepsilon_n + G(X_n), \quad (8.8)$$

where $G(X_n)$ is the value of $G(x)$ at $x=X_n$. Equations (8.6) and (8.8) show that while the magnitude of the excess enthalpies depends both on the “chemical” energy ε_n and on the “strain” energy $G(x)$, order-disorder transformations at a fixed composition depend on ε_n alone as $G(x)$ is common to both ordered and disordered phases at a fixed $x=X_n$.

Many approaches used in metallurgy to construct phase diagrams in terms of an Ising model^{37,38,47,50,54–56,63,67,74} assumes fixed interaction energies ε_n neglecting $G(x)$. While such models are able to fit the observed order-disorder transition temperatures by adjusting⁷⁴ ε_n , calculating enthalpies with these ε_n ’s grossly misrepresents²⁶ ΔH_n and $\Delta H(x, T)$ (as $G > 0$ is neglected). In their simple form, retaining just pair interactions in ε_n , these models predict either a phase-separating behavior when $\varepsilon_n > 0$ (an Ising ferromagnet), or an ordering behavior when $\varepsilon_n < 0$ (an Ising antiferromagnet); the phase diagram is symmetric with respect to $x = \frac{1}{2}$. Our results (Figs. 6–8) show that retention of both chemical and elastic energies leads to correct transition temperatures, enthalpies, asymmetry, and can exhibit phase separation and ordering in the same phase diagram.

The standard approach used in semiconductor physics to construct phase diagrams^{19–22} retains the elastic energies $G(x)$ (assumed proportional to $Ba\Delta a^2$), but neglects the chemical energies ε_n . Since $G(x) \geq 0$, these approaches must universally predict a phase-separating behavior and fail to distinguish ordered from disordered phases.

Our analysis shows that while the mixing enthalpy $\Delta H(x, T)$ of *disordered* semiconductor alloys and the formation enthalpy ΔH_n of *ordered* intersemiconductor

compounds are both positive, this is consistent with having either attractive ($\varepsilon_n < 0$, $\text{GaSb}_{1-x}\text{As}_x$) or repulsive ($\varepsilon_n > 0$, $\text{Al}_{1-x}\text{Ga}_x\text{As}$) “chemical” energies (Fig. 3). In *lattice mismatched* systems, the sublattice relaxation energy [$\Delta E_S(n, V)$ of Eq. (5.9)] makes ε_n negative, whereas in *lattice-matched* systems, $\Delta E_S(n, V) \approx 0$ and $\Delta E_{CE}(n, V) \geq 0$ make ε_n slightly positive. Valence force field calculations⁶⁰ for 18 III-V alloys and 18 II-VI alloys as well as simple electrostatic energy calculations⁸² show that this is a general result for such isovalent ternary semiconductors. This has a significant implication for the relative magnitude of the energies of ordered versus disordered phases: for systems dominated by pair interactions, if $\varepsilon_n < 0$ then $\varepsilon_2 < \sum_n P_n \varepsilon_n$, hence the ordered phase can have a lower enthalpy than the disordered phase at the same composition, while if $\varepsilon_n > 0$, the opposite is true. These cases are illustrated by Fig. 10.

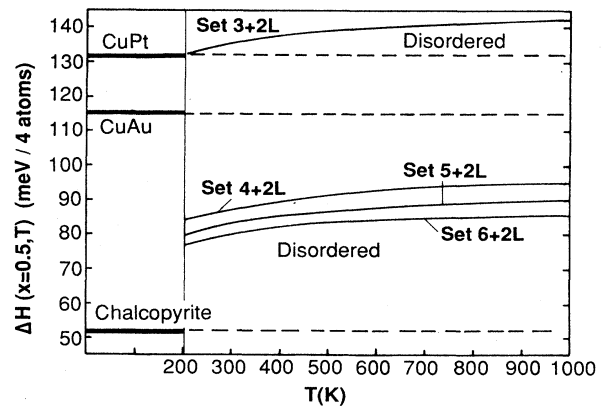


FIG. 12. Temperature dependence of the mixing enthalpy (at $x=0.5$) of $\text{GaAs}_{0.5}\text{Sb}_{0.5}$ for different sets M of structures (Table VIII). Also given are the formation enthalpies of ordered structures at $x=0.5$ and $T=0$.

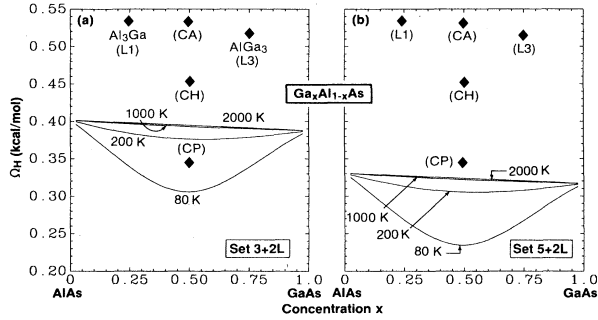


FIG. 13. Enthalpy interaction parameter [Eq. (6.19)] for $\text{Ga}_x\text{Al}_{1-x}\text{As}$. The diamond-shaped symbols give the values for ordered compounds.

For $\epsilon_n < 0$ ($\text{GaAs}_x\text{Sb}_{1-x}$), Fig. 11 demonstrates that there are some short-period ordered phases with lower enthalpies than the disordered phase. Figure 12 shows these enthalpies at $x = 0.5$ as a function of temperature, demonstrating that the above conclusion holds for a certain temperature range. This implies that while due to $\Delta H > 0$, the thermodynamic ground state corresponds to phase separation, the inequality $\Delta H_n < \Delta H(X_n, T)$ will give at stoichiometric compositions X_n long-range-ordered phases which are stabler below a critical temperature than a disordered alloy of the same composition. This is seen in the calculated phase diagram $\text{GaAs}_x\text{Sb}_{1-x}$ depicted in Fig. 6.

For $\epsilon_n > 0$ ($\text{Al}_{1-x}\text{Ga}_x\text{As}$), Fig. 13 shows that the disordered phase has a lower enthalpy than all ordered structures. Since the configurational entropy term $-T\Delta S$ further stabilizes the disordered phase, we do not expect to find long-range ordering of simple, short-period structures (Table I) at any temperature. Figure 14 shows the phase diagram for $\text{Al}_{1-x}\text{Ga}_x\text{As}$, confirming this expectation. (We find $T_{\text{MG}} = 84$ K using the parameter sets 3+2L and $T_{\text{MG}} = 70 \pm 10$ K for the larger sets, hence we show only a single phase diagram for this system.) Ironically, the standard semiconductor model,^{19–22} predicting universally a phase-separating behavior such as that seen in Fig. 14, applies only to such lattice-matched systems

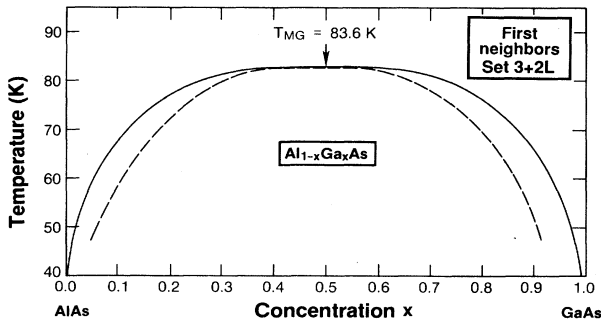


FIG. 14. Calculated phase diagrams for $\text{Al}_{1-x}\text{Ga}_x\text{As}$. The dashed line is the spinodal.

($\text{Al}_{1-x}\text{Ga}_x\text{As}$ and $\text{Cd}_{1-x}\text{Hg}_x\text{Te}$).

For $\text{GaAs}_x\text{Sb}_{1-x}$, our calculated maximum miscibility-gap temperature is $\sim 1100\text{K}$ (Fig. 8). The experimental T_{MG} value is difficult to assess in this system since the alloy melts peritectically (solid horizontal line in Fig. 8) below T_{MG} . Extrapolation of the observed miscibility line^{87,88} suggest $T_{\text{MG}} \approx 1100 \pm 100$ K. In his empirical model, Stringfellow⁸⁸ finds a symmetric phase diagram ($x_{\text{MG}} = 0.5$) with $T_{\text{MG}} = 1023$ K.

For GaAs-AlAs , we find $T_{\text{MG}} = 70 \pm 10$ K. The experimental value^{21,22} of T_{MG} for $\text{Al}_{1-x}\text{Ga}_x\text{As}$ is uncertain, since T_{MG} is smaller than the growth temperature characteristic of any of the semiconductor growth techniques. Neglecting chemical effects, Stringfellow¹⁹ estimates $T_{\text{MG}} = 3$ K from strain effects alone, whereas Balzarotti *et al.*⁹⁰ calculated from their semiempirical quasi-chemical model $T_{\text{MG}} = 360$ K. We do not find any metastable ordered phases in the $\text{Al}_{1-x}\text{Ga}_x\text{As}$ phase diagram consistent with the results of Fig. 10.

E. Equilibrium lattice parameters

Figure 15 depicts the calculated excess equilibrium lattice parameter⁹¹ $\Delta a(x, T)$ of $\text{GaAs}_x\text{Sb}_{1-x}$ alloys,

$$\Delta a(x, T) = a(x, T) - xa_{\text{GaAs}} - (1-x)a_{\text{GaSb}}, \quad (8.9)$$

neglecting phonon (hence, thermal expansion) effects. The solid horizontal line at $\Delta a = 0$ corresponds to the prediction of Vegard's rule. In calculating $\Delta a(x, T)$, we have not used the linearization of Eq. (7.1) (which would bias the small effect seen in Fig. 15) but rather the unmanipulated data of Table III. We find that (i) deviations from Vegard's rule (maximum of $\sim 0.004 \text{ \AA}$) are very small. The deviation is larger and positive on the GaSb side and smaller (negative) on the GaAs side. These deviations reflect mostly anharmonic effects. In the pure harmonic theory the strain energy at $x = \frac{1}{2}$ is proportional to

$$\Delta E_{\text{strain}} \propto B_{AC}(a_{\text{eq}} - a_{AC})^2 + B_{BC}(a_{\text{eq}} - a_{BC})^2, \quad (8.10)$$

where B_i are the bulk moduli. Minimization of ΔE_{strain} gives

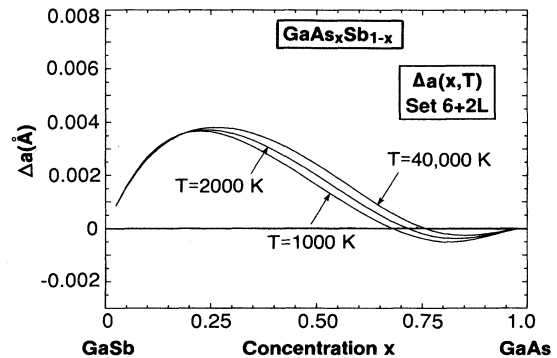


FIG. 15. Deviations $\Delta a(x, T)$ from Vegard's rule [Eq. (8.9)] for $\text{GaAs}_x\text{Sb}_{1-x}$ calculated from the $M = 6+2L$ set (Table VIII) and the data of Table III.

$$\frac{\delta a}{\bar{a}} = \frac{a_{\text{eq}} - \bar{a}}{\bar{a}} = \frac{\Delta B \Delta a}{4\bar{B}\bar{a}}, \quad (8.11)$$

where

$$\begin{aligned} \bar{a} &= \frac{1}{2}(a_{AC} + a_{BC}), \\ \bar{B} &= \frac{1}{2}(B_{AC} + B_{BC}), \\ \Delta a &= (a_{BC} - a_{AC}), \end{aligned} \quad (8.12)$$

and

$$\Delta B = (B_{BC} - B_{AC}).$$

Since ΔB and Δa have opposite signs for semiconductors,¹⁶ δa is always negative in the harmonic theory. In reality, however, the pressure derivative B' of bulk modulus is positive. The bulk modulus of the compound with large lattice constant will have a sharp increase when it is compressed and the one with smaller lattice constant will have a decreasing B when it is expanded. This indicates that the deviation δa should be smaller than what harmonic theory would predict (i.e., a_{eq} is closer to Vegard's rule) and could be positive as found in our study for Ga(As,Sb).

F. Mixing enthalpies and free energies

In contrast with the predictions of contemporary semiconductor alloy models,^{17–22} we find (Figs. 11 and 13) that Ω_H is composition dependent. Its values at the limiting concentrations $x \rightarrow 0$ and $x \rightarrow 1$ provide the “limiting partial heats of solution,” showing that it is considerably more difficult to dissolve the larger atom (Sb) in GaAs [$\Omega(\text{GaAs:Sb}) \sim 4.5$ kcal/mol] than to dissolve the smaller As atom in GaSb [$\Omega(\text{GaSb:As}) \sim 3.8$ kcal/mol]. The dependence on x is considerably weaker in the lattice-mismatched $\text{Al}_{1-x}\text{Ga}_x\text{As}$ system (Fig. 13; note the finer scale relative to Fig. 11).

No *direct* experimental measurements of Ω_H or Ω_H exists for semiconductor alloys. The currently available values^{17–22} are fit to the data of the liquidus and solidus lines (hence, are appropriate to high temperatures), assuming simple thermodynamic models in the fit procedures. In cases where different fit methods were attempted for the same system,^{17–22,92} Ω_H of 4–4.5 kcal/mol are obtained for $\text{GaAs}_x\text{Sb}_{1-x}$. This is in very good agreement with our calculated value (Fig. 11) of

~ 4.0 kcal/mol at $x = 0.5$ and a temperature $T = 1000$ K (the average of the melting temperatures of the constituents). Various authors have used empirical models to estimate $\Omega_H(x = 0.5)$ for GaAs–GaSb. These include the recent model of Sher *et al.*⁵¹ ($\Omega_H = 3.67$ kcal/mol), the elastic model of Martins and Zunger⁷³ ($\Omega_H = 4.58$ kcal/mol), the phenomenological delta lattice parameter (DLP) model of Stringfellow¹⁹ ($\Omega_H = 3.35$ kcal/mol), and the empirically adjusted model of Fedders and Muller⁹³ ($\Omega_H = 2.76$ kcal/mol).

For $\text{Al}_{1-x}\text{Ga}_x\text{As}$ our calculated value is $\Omega_H(0.5, T) = 0.3$ kcal/mol at $T = 1000$ K, compared with experimental estimates^{20,21} of 0–1.6 kcal/mol. Calculated values range from Ω_H of -0.07 kcal/mol by Sher *et al.*⁵¹ to 0.11 kcal/mol by Van Vechten.⁹⁴ Balzarotti *et al.*⁹⁰ estimate $\Delta E(n) = n(4-n)W$ from diffused x-ray scattering,⁴⁰ yielding in this pair-interaction model $\Omega(0.5) = \frac{3}{4}\Delta E^{(2)} = 3W = 1.6$ kcal/mol.

The enthalpy and free-energy interaction parameters of Figs. 11–13 and 16 show a marked temperature dependence. This dependence is neglected in regular and quasiregular solution models and represented phenomenologically as $\Omega(0.5, T) = a - bT$ in other⁹² models. The nonideal entropy ΔS of Eq. (6.20) is always negative (as the actual system is more ordered than the random system), contributing a positive $-T\Delta S$ term to the free energy. Interestingly, the excess enthalpy $\Delta H(x, T)$ becomes *less positive* as the temperature is lowered (Figs. 11 and 12). To understand the mechanism by which the system reduces the positive (“destabilizing”) effect of ΔH as T decreases, we consider next the excess probabilities of Eq. (6.23).

G. Excess cluster probabilities

Figure 17 depicts the excess cluster probabilities $\Delta P_n(x, T)$ of Eq. (6.23) for $\text{GaAs}_x\text{Sb}_{1-x}$, whereas Fig. 18 shows analogous information for $\text{Al}_{1-x}\text{Ga}_x\text{As}$.

In the case of $\text{GaAs}_x\text{Sb}_{1-x}$ ($\epsilon_n < 0$) we see in Fig. 17 *clustering of the mixed species*, i.e., a deficiency of the As_4 and Sb_4 clusters and an excess of clusters AsSb_3 , As_2Sb_2 , and As_3Sb at $X_n = \frac{1}{4}$, $\frac{1}{2}$, and $\frac{3}{4}$, respectively. Since in this system $\epsilon_n < 0$, the energy ϵ_n of a single cluster is *lower* than the energy of a phase exhibiting a few clusters. As the temperature is lowered, hence the entropy term $-T\Delta S$ becomes less important, the system acts to *enrich*

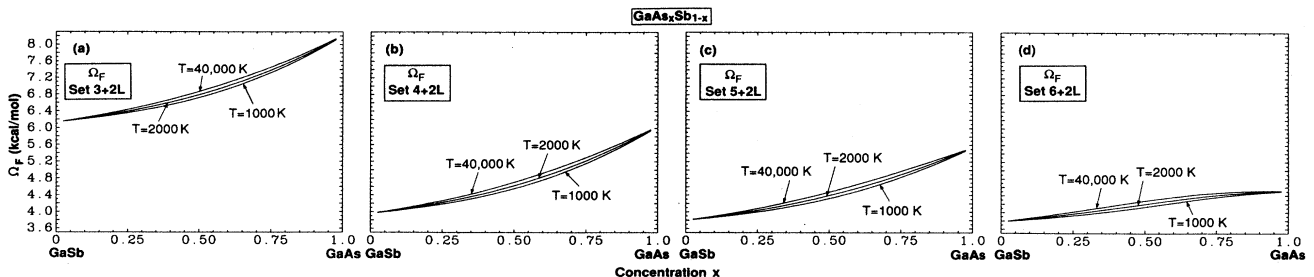


FIG. 16. Free-energy interaction parameter [Eq. (6.22)] for $\text{GaAs}_x\text{Sb}_{1-x}$.

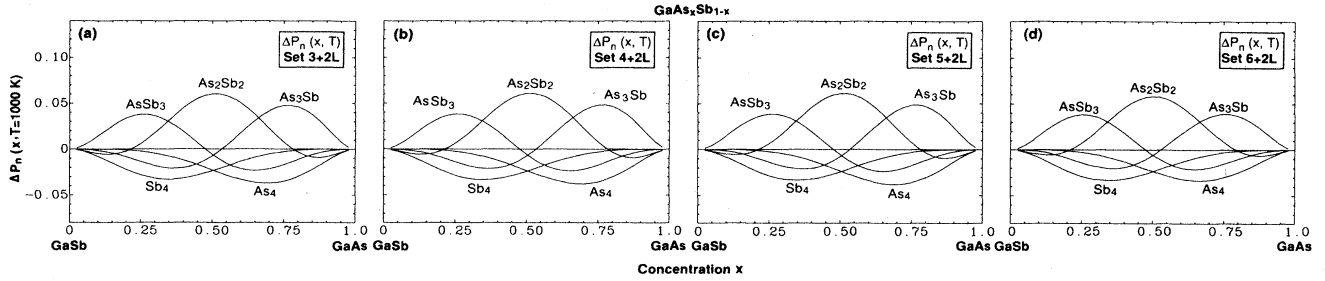


FIG. 17. Excess cluster probabilities [Eq. (6.23)] for $\text{GaAs}_x\text{Sb}_{1-x}$.

the concentrations of single mixed species (around their corresponding compositions X_n), hence reducing $\Delta H(x, T)$, as seen in Fig. 11. Since in the absence of clustering the enthalpy of the disordered phase is higher (see the high-temperature curves in Fig. 11, corresponding to random disorder), we might say that in this case the disordered alloy stabilizes itself (hence, delays phase separation) by performing a natural selection of the “fittest” clusters.

In the case of $\text{Al}_{1-x}\text{Ga}_x\text{As}$ ($\epsilon_n > 0$) we see in Fig. 18 anticlustering of the mixed species, i.e., the clusters GaAl_3 , Ga_2Al_2 , and Ga_3Al are deficient relative to what random statistics would grant near X_n , whereas the Al_4 and Ga_4 clusters are in excess. Since in this system $\epsilon_n > 0$, the energy associated with a single pure cluster is higher than the energy of a collection of clusters, hence, when the temperature is lowered, the system acts to suppress the mixed clusters, enriching itself by the lower-energy Al_4 and Ga_4 clusters. This reduces the mixing enthalpy relative to that characteristic of the random phase.

H. Nearest-neighbor lengths

In analogy with the calculation of ΔE for a random alloy [Eq. (5.15)], we may write the average bond length $\bar{R}_{AC}(x)$ of the disordered phase as

$$\bar{R}_{AC}(x) = \frac{1}{W(x)} \sum_s Q_s(x) \omega_{AC}(s) \bar{R}_{AC}[s, V_{\text{eq}}(x)], \quad (8.13)$$

where the weights $Q_s(x)$ are given by Eq. (5.16), $\omega_{AC}(s)$ is the average number of AC bonds in structure s [for the five canonical structures (0–4) in Table II $W_{AC}(n) = 4 - n$], $\bar{R}_{AC}[s, V_{\text{eq}}(x)]$ are the AC bond lengths calculated at $V_{\text{eq}}(x)$, and

$$W(x) = \sum_s Q_s(x) \omega_{AC}(s) \quad (8.14)$$

is the normalization factor. Similar expressions pertain to $\bar{R}_{BC}(x)$.

Figure 19 depicts the calculated nearest-neighbor bond lengths $\bar{R}_{\text{Ga-Sb}}(x)$ and $\bar{R}_{\text{Ga-As}}(x)$ as a function of concentration x and interaction range M . We have simplified the calculation by calculation $\bar{R}_{\text{Ga-Sb}}(x)$ and $\bar{R}_{\text{Ga-As}}(x)$ at $x = \frac{1}{2}$ and assuming that these bond lengths are linear with x . The bond lengths for the ordered structures at equilibrium are given in Table IV and are reproduced in Fig. 19 for (001) (solid square) and (201) structures (open square). We find from Fig. 19 the following.

(i) $\bar{R}_{\text{Ga-As}}(x)$ and $\bar{R}_{\text{Ga-Sb}}(x)$ in both ordered and disordered alloys are closer to their ideal bond lengths $R_{\text{Ga-As}}^0(1)$ and $R_{\text{Ga-Sb}}^0(0)$ than to the linear averaged value $(\sqrt{3}/4)a(x)$ even though Vegard’s rule for $a(x)$ is obeyed well. The bimodal distribution in the alloy is con-

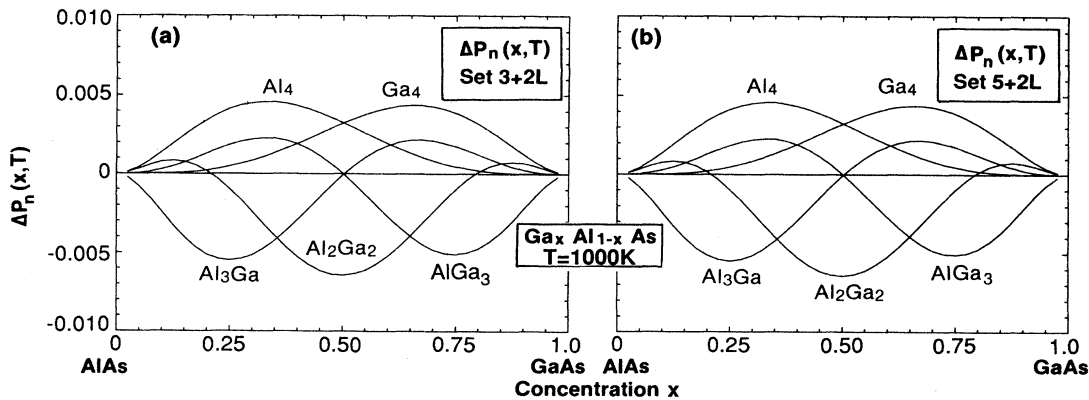


FIG. 18. Excess cluster probabilities [Eq. (6.23)] for $\text{Ga}_x\text{Al}_{1-x}\text{As}$.

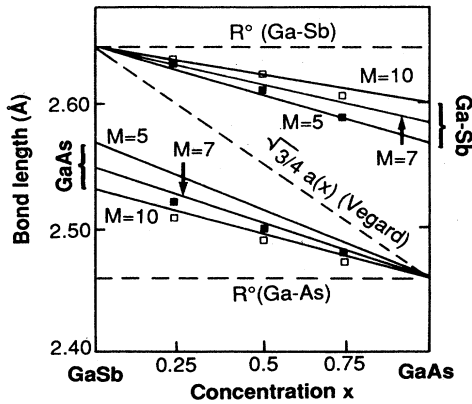


FIG. 19. Alloy-averaged bond lengths [Eq. (8.13)] for $\text{GaAs}_x\text{Sb}_{1-x}$ using three different structure sets: $3+2L$, $5+2L$, and $6+2L+2F$, denoted as $M=5$, 7 , and 10 , respectively. Solid squares, (001) ordered compounds; open squares, (201) ordered compounds.

sistent with the observed EXAFS measurements for various semiconductor alloys.⁸⁹

(ii) For $M=3+2L$ of Table VIII, the deviations $\bar{R}(x)-R^0$ are relatively large, reflecting the large strain energy associated with these (001) structures. $\bar{R}(x)$ is also closer to Vegard's line than are the ordered ternary compounds since in this model the nearest-neighbor bond lengths for pure A_4C and B_4C clusters coincide with Vegard's rule.

(iii) Considerable bond relaxation is observed in going from $M=3+2L$ to $M=5+2L$ and $M=6+2L+2F$: for $M=5+2L$ $\bar{R}(x)$ is closer to R^0 . This larger relaxation is mainly caused by the more effective cell-internal relaxation associated with the (201) structures (chalcopyrite and famatinitite). In going from $M=5+2L$ to $M=6+2L+2F$ $\bar{R}(x)$ gets even closer to R^0 due to further relaxation of the mixed sublattice.

(iv) Our calculated results do not agree with the available experimental EXAFS data for⁹⁵ $\text{GaAs}_x\text{Sb}_{1-x}$, which show essentially $\bar{R}(x) \approx R^0$, i.e., complete relaxation. Our results, however, are consistent with the calculation of Qteish *et al.*⁹⁶ for the same system. Our previous calculations for some II-VI alloys⁷² show reasonable agreement with experimental data. As pointed out in Ref. 96, the EXAFS data⁹⁵ on $\text{GaAs}_x\text{Sb}_{1-x}$ taken in the transmission mode for dilute system may have considerable error.

IX. COMPARISON WITH PREVIOUS APPROACHES TO SEMICONDUCTOR SOLID SOLUTIONS

Many of the previous approaches to semiconductor solid solutions failed to distinguish ordered from disordered phases, focusing only on the latter. This can be traced back to the failure to recognize explicit configuration-dependent terms [e.g., ϵ_n to Eq. (6.8)] in the interaction energy. Most previous attempts at the problem can be classified as (i) macroscopic phenomenology, (ii) microscopic phenomenology, and (iii) microscopic theories of alloy bonding.

Models based on *macroscopic phenomenology* have parametrized the interaction parameter of Eq. (6.19) as

$$\Omega = \Omega_0[1 + A(x - 0.5)] - BT[1 + C(x - 0.5)], \quad (9.1)$$

and attempted to fit it to various data. The limit $\Omega_0 = A = B = C = 0$ corresponds to the ideal solution model, deemed early on²² as inappropriate for semiconductors. The limit $A = B = C = 0$ corresponds to the regular solution model used by Panish and Ilegems,²² where Ω_0 was treated as an adjustable parameter fit to liquidus and solidus data. The limit $A = C = 0$ corresponds to the quasiregular solution model where $\Omega = \Omega_0 + BT$; Brebrick⁹² used this model, again fitting Ω_0 and B to experiment (finding $B > 0$ for $\text{GaAs}_x\text{Sb}_{1-x}$ as found in Fig. 12). The use of the full expression (9.1) is denoted as the "subregular solution model" discussed by Brebrick.⁹²

Attempts to calculate Ω from *microscopic phenomenology* (e.g., continuum elastic models) were made by Fedders and Muller⁹³ who considered the elastic energy associated with compression and dilation of AC and BC into the average lattice constant \bar{a} , finding $\Omega = \frac{9}{2}BV(\Delta a)^2/\bar{a}^2$ (a result which is ~ 4 times larger than the experimental value, for reasons discussed by Ferreira *et al.*²⁶). Stringfellow¹⁹ calculated Ω in his (DLP) model by assuming a universal scaling of the elastic energy of the solids A , B or AB of the type $-K/a^{2.5}$; when used in Eqs. (1.2) and (6.19) this gives $\Omega = 4.375K(\Delta a)^2/\bar{a}^{4.5}$, where K is a constant. Least-squares fit to the data produces a robust value for K for a large range of alloys; this value was explained later in a microscopic approach by Ferreira *et al.*²⁶ Bublick and Leikin²⁰ have parametrized Ω as $W + xE_{AC} + (1-x)E_{BC}$, where W is a "chemical" energy extracted from diffused x-ray scattering and E_α is the elastic energy associated with volume deformations of $\alpha = AC, BC$, calculated from elastic constants. For $\text{GaAs}_{1-x}\text{Sb}_x$, they find $W = 0$ and $\Omega = 0.6x + 3.6$ kcal/mol, hence $\Omega(0) = 3.6$, $\Omega(0.5) = 3.9$, and $\Omega(1) = 4.2$, in good agreement with our *ab initio* results (Fig. 8) of 3.8, 4.0, and 4.5 kcal/mol, respectively. For $\text{Al}_{1-x}\text{Ga}_x\text{As}$, they find²⁰ $\Omega = W = 1.6$ kcal/mol, a surprisingly large chemical energy for a mixed-cation isovalent alloy with small difference in atomic electronegativity and radii (our result is 0.3 kcal/mol).

The common theme in all of the phenomenological models of semiconductor alloys is that $\Omega > 0$ is a *statement* of absence of ordering; the known instability of the disordered phase ($\Omega > 0$) is taken to imply that its constituent clusters A_nB_{4-n} are unstable [$\Delta E(n) > 0$] too (for the same reason, namely strain), hence the system is driven to show a *deficiency* of $A_{4-n}B_n$ ($n = 1, 2$, and 3) clusters and eventually to phase separation at low temperature. It appears that this point of view has been discouraged, until recently,²⁷⁻³³ experimental searches for ordering in semiconductor alloys. Our work²⁴ showed that the strain resulting from an attempt to accommodate dissimilar $A-C$ and $B-C$ bond lengths leads to $\Delta H > 0$, yet also to a preference for ordering of some structures over disorder at the same (x, T) . This is so because a coherently ordered arrangement of a *single* type of local bonding environment A_nB_{4-n} around C can better reduce the strain energy than a disordered arrangement of a *few* $\{A_nB_{4-n}\}$ clusters. In this case, ϵ_n is negative. At $T > T_{MG}$ when a single phase exists, the system is

driven to short-range clustering (i.e., in excess) of the mixed clusters A_3B , A_2B_2 , and AB_3 , and a deficiency of A_4+B_4 clusters. At low temperatures, in the rarely achieved situation of perfect thermodynamic equilibrium, the system will fully phase separate into AC-rich and BC-rich regions, otherwise it will tend to order below T_c into $A_nB_{4-n}C_4$ compounds. Both (incoherent) phase separation and long-range ordering reduce the strain energy, hence the two phenomena are not mutually exclusive as earlier thought. Indeed, recent experiments have now observed metastable long-range (2,0,1) ordering in size-mismatched semiconductor alloys^{29,30} (note that CuPt ordering³³ is not predicted here to be a bulk effect and is likely to represent growth-induced ordering).

A number of alloy models based on a microscopic theory of bonding have been advanced. In a series of papers, Ito⁹⁷ used a pseudopotential perturbation theory (with local Heine-Abarenkov potentials adjusted to fit the properties of compound semiconductors), calculating Ω within the virtual-crystal approximation^{97(a)} (VCA). The resulting Ω was 2–3 times larger than the observed values, prompting Ito to add to Ω a correction $-\alpha\bar{a}^{-2.5}$ with $\alpha > 0$ fit to experiment. In another work,^{97(b),97(d)} he used Eq. (2.13) with $M=3+2L$ ordered structures, calculating their energies within the pseudopotential perturbation expansion. He finds that ordered compounds have smaller lattice parameters than disordered alloys and $\Delta H_n < \Delta H^D(x, T)$, as found here (Fig. 13). However, in contrast with our results (Fig. 19 and Table IV) he finds that the alloy bond lengths are closer to their concentration-weighted average than to their (“ideal”) values in the end-point compounds. In agreement with our work (Fig. 11), he finds^{97(a)} that the disordered alloy energy (modeled by the VCA) is far higher than that of ordered chalcopyrite.

Equation (2.13) with $M=3+2L$ ordered structures and various empirical parametrizations of $\Delta E(n, V)$ has been used also in a series of papers by Ichimura and Sasaki⁹⁸ and Balzarotti *et al.*⁹⁹ Ichimura and Sasaki⁹⁸ represented $\Delta E(n, V)$ by the empirical valence force field where Balzarotti *et al.*⁹⁹ have added also a constant chemical energy W taken from Bublick and Leikin.²⁰ Both groups contain the probabilities $P_n(x, T)$ and the entropy using a simple quasichemical approximation. The calculated Ω for lattice-mismatched systems was considerably larger than the experimental value, as expected from the $M=3+2L$ set [compare Fig. 8(b) to Fig. 8(h)]. Both groups find clustering of A_3B , A_2B_2 , and AB_3 for all lattice-mismatched alloys, as seen in Fig. 17 and bimodal bond-length distribution (like in Fig. 19). Czyzyk *et al.*^{99(c)} find a five-branched spinodal curve for lattice-mismatched alloys which is absent from all of our first-principles calculations. Sher *et al.*¹⁰⁰ have used a similar approach except that $\Delta E(n, V)$ for $0 \leq n \leq 4$ is calculated by combining VFF for the elastic energy with a chemical term calculated within Harrison’s empirical tight-binding model. Two to three shells of bonds surrounding the central atom are included. All authors using the superposition approach of Eq. (2.13) failed to find any metastable long-range ordering.

Qteish *et al.*⁹⁶ have also used Eq. (2.13) with

$M=3+2L$ ordered structures and calculated the energies $\Delta E(n, V)$ within the first-principles pseudopotential formalism; the probabilities P_n were found within the quasichemical approximation. When this model was applied to $\text{Ga}_x\text{As}_{1-x}\text{Sb}$, it yielded $\Omega=6$ kcal/mol and a very high miscibility-gap temperature in accord with our results of Fig. 8(e) and in conflict with experiment. (Their probabilities calculated for this model are, however, qualitatively different from ours; we suspect that they are in error). To improve agreement with experiment, Qteish *et al.*⁹⁶ adopted a relaxation model similar to that we have previously developed⁴⁸ [Eqs. (8.1) and (8.2)], retaining the relaxation parameter from a Monte Carlo simulation with an empirical potential. This improves considerably the agreement with experiment (e.g., $\Omega=4.75$ kcal/mol). The basic differences with respect to our earlier approach⁴⁸ and the present one are (i) instead of relaxing the value of the equilibrium volume $V_n(x)$, they have relaxed the external volume $V(x)$. Working with lattice parameters instead of volumes, they assume that at a given composition x , the physical dimension $a(x, n)$ of each cluster n changes from the value $a(x)$ (the equilibrium alloy lattice parameter) to

$$a(x, n) = a(x) - k[a(x) - a_n(X_n)] . \quad (9.2)$$

The equilibrium lattice parameter $a_n(X_n)$ of each cluster is assumed unchanged. This incorrectly yields an elastically soft alloy bulk modulus, $(1-k)^2$ times the actual value. (Finding $k=0.3$, their predicted bulk modulus is about half the actual value.) This is to be contrasted with Eq. (8.1) where relaxation is taken to leave the physical dimension of each cluster unchanged (hence, the bulk modulus is unchanged), altering only the equilibrium value of cluster n . (ii) We include distant-neighbor interactions and sublattice relaxation on equal footing—by adding lower energy structures to the $M=3+2L$ set and increasing the number of J s—whereas Qteish *et al.* treat the nearest-neighbor interactions (included in the set $M=3+2L$) like we do, yet distant-neighbor relaxations are treated separately in a calculation involving an empirical valence force field. Their model does not distinguish CA from CH, or $L1$ from $F1$, etc. (iii) The results of the model of Qteish *et al.* depend on the choice of the five units used to calculate $\Delta E(n, V)$ (e.g., CA or CH), whereas the present approach produces a unique solution. (iv) The model of Qteish *et al.* produces anticlustering (preference for A_4 and B_4) whereas the present model predicts clustering (preference for mixed clusters). This reflects the fact that the reduction of $\Delta H(x, T)$ by relaxation is achieved in their model by reducing all cluster energies $\Delta E(m, V_n)$ for $m \neq n$, keeping, however, $\Delta E(n, V_n)$ unchanged. This is an artifact of this model when applied to pseudobinary $A_xB_{1-x}C$ systems. Direct inclusion of distant-neighbor relaxation in our description reduces $\Delta E(n, V)$ nearly uniformly for all clusters (as seen in Table X), hence the tendency for clustering is not reversed relative to the unrelaxed model.

X. SUMMARY

We have presented a first-principles method for calculating the temperature-composition phase diagrams for

fcc-based phase-separating alloys. The method requires calculation of the excess total-energy functions $\Delta E(s, V)$ for an optimal set of ordered structures $\{s\}$ (e.g., from the local-density formalism). These energies are used in Eq. (2.3) to find the interaction parameters $J_f(V)$ (using the inverse of the matrix given in Table II). These interaction parameters are then inserted in Eq. (6.17) to find five effective equations of state $\bar{\epsilon}_n(V)$. Finally, these effective equations of state are used as input to any standard method for solving the nearest-neighbor (tetrahedron) Ising model (e.g., the CVM). The method is simple and enables a controlled and converged calculation of the

phase diagram and all thermodynamic properties directly from an *ab initio* electronic Hamiltonian.

ACKNOWLEDGMENTS

This work supported by the Office of Energy Research, Division of Materials Science, the Office of Basic Energy Sciences of the U.S. Department of Energy, under Contract No. DE-AC02-77-CH00178. We are grateful for a special grant of supercomputer time from the Grand Challenge program, which made this work possible. We thank Dr. S. Froyen for enlightening discussions on effective interaction energies.

- ¹P. Villars and L. D. Calvert, *Pearson's Handbook of Crystallographic Data for Intermetallic Phases* (American Society for Metals, Metals Park, OH, 1985).
- ²*Binary Alloy Phase Diagrams*, edited by J. L. Murray, L. H. Bennett, and H. Barker (American Society for Metals, Metals Park, OH, 1986).
- ³*Crystal and Solid State Physics*, Vol. III/6 of *Landolt-Börnstein, Numerical Data and Functional Relationships in Science and Technology*, edited by P. Eckerlin and H. Kandler (Springer-Verlag, Berlin, 1971).
- ⁴W. G. Moffatt, *The Handbook of Binary Phase Diagrams* (Gernium, Schenectady, NY, 1984).
- ⁵R. Hultgren, P. D. Desai, D. T. Hawkins, M. Gleiser, and K. K. Kelley, *Selected Values of the Thermodynamic Properties of Binary Alloys* (American Society for Metals, Metals Park, OH, 1973).
- ⁶P. M. Hansen, *Constitution of Binary Alloys* (McGraw-Hill, New York, 1958).
- ⁷W. B. Pearson, *Development in the Structural Chemistry of Alloy Phases*, edited by B. C. Glessen (Plenum, New York, 1969).
- ⁸L. Pauling, *The Nature of the Chemical Bond* (Cornell University Press, Ithaca, 1960).
- ⁹W. Hume-Rothery and G. V. Raynor, *The Structure of Metals and Alloys* (Institute of Metals, London, 1957).
- ¹⁰W. B. Pearson, *The Crystal Chemistry and Physics of Metal Alloys* (Wiley Interscience, New York, 1972).
- ¹¹L. S. Darken and R. W. Gurry, *Physical Chemistry of Metals* (McGraw-Hill, New York, 1953).
- ¹²A. R. Miedema, *J. Less-Common Met.* **32**, 117 (1973); **46**, 67 (1976); A. R. Miedema, R. Boom, and F. R. DeBoer, *J. Less-Common Met.* **41**, 283 (1975).
- ¹³J. St. John and A. N. Bloch, *Phys. Rev. Lett.* **33**, 1095 (1974); A. Zunger, *Phys. Rev. B* **22**, 5839 (1980); J. R. Chelikowsky and J. C. Phillips, *ibid.* **17**, 2453 (1978).
- ¹⁴A recent review of results of total and structural energy calculation is given in *Electronic Structure, Dynamics, and Quantum Structural Properties of Condensed Matter*, edited by J. T. Devreese and D. Van Camp (Plenum, New York, 1985).
- ¹⁵E. M. Levin, C. R. Robbins, and H. B. McMurdie, *Phase Diagrams for Ceramists* (American Ceramic Society, OH, 1964).
- ¹⁶*Landolt-Börnstein, Numerical Data and Functional Relationships in Science and Technology*, edited by O. Madelung, M. Schulz, and H. Weiss (Springer-Verlag, Berlin, 1982), Vol. 17a,b.
- ¹⁷A. Langres, *Rev. Phys. Appl.* **8**, 259 (1973).
- ¹⁸L. M. Foster, *J. Electrochem. Soc.* **121**, 1662 (1974); L. M. Foster and J. F. Woods, *ibid.* **119**, 504 (1972).
- ¹⁹G. B. Stringfellow, *J. Phys. Chem. Solids* **34**, 1749 (1973); *J. Cryst. Growth* **27**, 21 (1974).
- ²⁰V. T. Bublik and V. N. Leikin, *Phys. Status Solidi A* **46**, 365 (1978).
- ²¹L. M. Foster, J. E. Scardefield, and J. F. Woods, *J. Electrochem. Soc.* **119**, 765 (1972).
- ²²M. B. Panish and M. Ilegems, *Prog. Solid State Chem.* **7**, 34 (1972).
- ²³L. Kaufman, J. Nell, K. Taylor, and F. Hayes, *CALPHAD* **5**, 185 (1981).
- ²⁴G. P. Srivastava, J. L. Martins, and A. Zunger, *Phys. Rev. B* **31**, 2561 (1985); **38**, 12 694(E) (1988).
- ²⁵A. A. Mbaye, L. G. Ferreira, and A. Zunger, *Phys. Rev. Lett.* **58**, 49 (1987).
- ²⁶L. G. Ferreira, A. A. Mbaye, and A. Zunger, *Phys. Rev. B* **37**, 10 547 (1988); **35**, 6475 (1987).
- ²⁷A. Ourmazd and J. C. Bean, *Phys. Rev. Lett.* **55**, 765 (1985).
- ²⁸S. Mahajan, D. E. Laughlin, and H. M. Cox, *Phys. Rev. Lett.* **58**, 2567 (1987).
- ²⁹H. Nakayama and H. Fujita, in *GaAs and Related Compounds 1985*, *Inst. Phys. Conf. Ser. No. 79*, edited by M. Fujimoto (Hilger, Bristol, 1986).
- ³⁰H. R. Jen, M. H. Cherng, and G. B. Stringfellow, *Appl. Phys. Lett.* **48**, 1603 (1986); H. R. Jen, M. J. Cherng, M. J. Jou, and G. B. Stringfellow, *GaAs and Related Compounds 1986*, *Inst. Phys. Conf. Ser. 83*, edited by W. T. Lindley (IOP, Bristol, 1987), p. 159; Y. E. Ihm, N. Otsuka, J. Klem, and H. Morkoç, *Appl. Phys. Lett.* **51**, 2013 (1987).
- ³¹T. S. Kuan, T. F. Kuech, W. I. Wang, and E. L. Wilkie, *Phys. Rev. Lett.* **54**, 210 (1985).
- ³²T. S. Kuan, W. I. Wang, and E. L. Wilkie, *Appl. Phys. Lett.* **51**, 51 (1987).
- ³³A. Gomyo, T. Suzuki, K. Kobayashi, I. Hino and T. Yuasa, *Appl. Phys. Lett.* **50**, 673 (1987); A. Gomyo, T. Suzuki, and S. Iijima, *Phys. Rev. Lett.* **60**, 2645 (1988).
- ³⁴E. N. Khabarov, *Acta. Cryst.* **31A**, S92 (1975); N. A. Semikolenova and E. N. Khabarov, *Fiz. Tekh. Poluprovodn.* **8**, 2240 (1974) [*Sov. Phys.—Semicond.* **8**, 1459 (1975)].
- ³⁵V. A. Singh and A. Zunger, *Phys. Rev. B* **25**, 907 (1982); J. R. Chelikowsky, *ibid.* **19**, 686 (1979); J. A. Alonso and S. Simozar, *ibid.* **22**, 5583 (1980).
- ³⁶C. Domb, in *Phase Transition and Critical Phenomena*, edited by C. Domb and H. S. Green (Academic, London, 1974), Vol. 3, p. 357; D. M. Burley, *ibid.*, Vol. 2, p. 329.
- ³⁷D. de Fontaine, in *Solid State Physics*, edited by H. Ehrenreich, F. Seitz, and D. Turnbull (Academic, New York, 1979), Vol. 34, p. 73.
- ³⁸T. Muto and Y. Takagi, *The Theory of Order-Disorder Transi-*

- tions in Alloys (Academic, New York, 1955).
- ³⁹Equations (1.9) follow from the orthogonality of the products $\Pi_f, \sum_{\sigma} \Pi_f(l_f, \sigma) \Pi_{f'}(l'_f, \sigma) = 2^N \delta_{f, f'} \delta_{l_f, l'_f}$. If (f, l_f) does not coincide with (f', l'_f) there are unpaired spin variables \hat{S}_i in the left-hand side of the above equation. The orthogonality results from summing over all the spin variables \hat{S}_i (1 and -1). See Ref. 40 for details.
- ⁴⁰J. M. Sanchez, F. Ducastelle, and D. Gratias, *Physica* **128A**, 334 (1984).
- ⁴¹R. Kikuchi, *Phys. Rev.* **81**, 988 (1951).
- ⁴²J. A. Barker, *Proc. R. Soc. London* **216**, 45 (1953).
- ⁴³T. Morita, *J. Phys. Soc. Jpn.* **12**, 753 (1957).
- ⁴⁴D. G. Pettifor, *J. Phys. C* **5**, 97 (1972); **19**, 285 (1986); **19**, 315 (1986); C. H. Hodges, *J. Phys. C* **12**, 2965 (1979); J. E. Inglesfield, *J. Phys. C* **9**, 1551 (1979); M. Cyrot and F. Cyrot-Lackmann, *J. Phys. F* **6**, 2257 (1976); J. Friedel, *J. Magn. Magn. Mater.* **17-19**, 38 (1980).
- ⁴⁵W. L. Bragg and E. J. Williams, *Proc. R. Soc. London Ser. A* **145**, 699 (1934).
- ⁴⁶H. A. Bethe, *Proc. Soc. London Ser. A* **150**, 552 (1935).
- ⁴⁷(a) F. Ducastelle and F. Gautier, *J. Phys. F* **6**, 2039 (1976); A. Bieber and F. Gautier, *J. Phys. Soc. Jpn.* **53**, 2061 (1984); *Acta Metall.* **35**, 1839 (1987); (b) P. Turchi, M. Sluiter, and D. de Fontaine, *Phys. Rev. B* **36**, 3161 (1987).
- ⁴⁸S.-H. Wei, A. A. Mbaye, L. G. Ferreira, and A. Zunger, *Phys. Rev. B* **36**, 4163 (1987); A. Zunger, S.-H. Wei, A. A. Mbaye, and L. G. Ferreira, *Acta Metall.* **36**, 2239 (1988).
- ⁴⁹E.g., see D. A. Papaconstantopoulos, *Handbook of the Band Structure of Elemental Solids* (Plenum, New York, 1986).
- ⁵⁰C. Sigli and J. M. Sanchez, *Acta Metall.* **36**, 367 (1988). These authors suggested incorrectly that the neglect of explicit volume dependence of the interaction energies is legitimate for systems satisfying Vegard's rule. Reference 26 shows that this is not so.
- ⁵¹A. Sher, M. van Schilfgarde, A. B. Chen, and W. Chen, *Phys. Rev. B* **36**, 4279 (1988).
- ⁵²J. Ihm, A. Zunger, and M. L. Cohen, *J. Phys. C* **12**, 4409 (1979).
- ⁵³(a) H. Krakauer, M. Posternak, and A. J. Freeman, *Phys. Rev. Lett.* **43**, 1885 (1979); E. Wimmer, H. Krakauer, M. Weinert, and A. J. Freeman, *Phys. Rev. B* **24**, 864 (1981); (b) S.-H. Wei and H. Krakauer, *Phys. Rev. Lett.* **55**, 1200 (1985); (c) D. Singh, H. Krakauer, and C. S. Wang, *Phys. Rev. B* **34**, 8391 (1986).
- ⁵⁴C. M. van Baal, *Physica (Utrecht)* **64**, 571 (1973); D. F. Styer, M. K. Phani, and J. Lebowitz, *Phys. Rev. B* **34**, 3361 (1986).
- ⁵⁵F. Ducastelle, in *Phase Transformations in Solids*, edited by T. Tsakalakos (North-Holland, New York, 1984), p. 375.
- ⁵⁶J. M. Sanchez and D. de Fontaine, *Phys. Rev. B* **21**, 216 (1980); **25**, 1759 (1982).
- ⁵⁷J. Kanamori and Y. Kakehashi, *J. Phys. (Paris) Colloq.* **38**, C7-274 (1977).
- ⁵⁸(a) J. W. D. Connolly and A. R. Williams, *Phys. Rev. B* **27**, 5169 (1983); (b) K. Terakura, T. Oguchi, T. Mokri, and K. Watanabe, *ibid.* **35**, 2169 (1987); (c) R. Podloucky, H. J. F. Jansen, X. Q. Guo, and A. J. Freeman, *ibid.* **37**, 5478 (1988); (d) A. E. Carlsson, *ibid.* **35**, 4858 (1987).
- ⁵⁹J. E. Bernard and A. Zunger, *Phys. Rev. B* **36**, 3199 (1987).
- ⁶⁰J. E. Bernard, L. G. Ferreira, S.-H. Wei, and A. Zunger, *Phys. Rev. B* **38**, 6338 (1988).
- ⁶¹A. A. Mbaye, D. M. Wood, and A. Zunger, *Phys. Rev. B* **37**, 3008 (1988); *Appl. Phys. Lett.* **49**, 782 (1986); D. M. Wood and A. Zunger, *Phys. Rev. Lett.* **61**, 1501 (1988).
- ⁶²A. E. Carlson has shown [*Phys. Rev. B* **35**, 4858 (1987)] how many-atom interactions within nearest neighbors ($m = 1$) can be renormalized into effective pair potentials, not treating, however, interactions beyond nearest neighbors.
- ⁶³J. M. Sanchez and D. de Fontaine, *Phys. Rev. B* **17**, 2926 (1978).
- ⁶⁴R. Kikuchi, *J. Chem. Phys.* **60**, 1071 (1974).
- ⁶⁵See *Local Density Approximations in Quantum Chemistry and Solid State Physics*, edited by J. P. Dahl and J. Avery (Plenum, New York, 1984).
- ⁶⁶*Density Functional Methods in Physics*, edited by R. M. Dreizler and J. D. Providencia (Plenum, New York, 1985).
- ⁶⁷C. Sigli and J. M. Sanchez, *CALPHAD* **8**, 221 (1981).
- ⁶⁸B. L. Gyorffy and G. M. Stocks, *Phys. Rev. Lett.* **50**, 374 (1983).
- ⁶⁹G. Treglia, F. Ducastelle, and F. Gautier, *J. Phys. F* **8**, 1437 (1978).
- ⁷⁰R. C. Kittler and L. M. Falicov, *Phys. Rev. B* **18**, 2506 (1978); **19**, 291 (1979); M. O. Robbins and L. M. Falicov, *ibid.* **25**, 2343 (1982).
- ⁷¹O. H. Nilsen and R. M. Martin, *Phys. Rev. Lett.* **50**, 697 (1983); *Phys. Rev. B* **32**, 3780 (1985); **35**, 9308(E) (1987).
- ⁷²S.-H. Wei and A. Zunger, *Phys. Rev. B* **37**, 8958 (1988); *Phys. Rev. Lett.* **56**, 2391 (1986); *J. Vac. Sci. Technol.* **6A**, 2597 (1988).
- ⁷³J. L. Martins and A. Zunger, *Phys. Rev. B* **30**, 6217 (1984).
- ⁷⁴R. Kikuchi, in *Noble Metal Alloys*, edited by T. B. Massalski, W. B. Pearson, L. H. Bennett, and Y. A. Chang (Metallurgical Society, Warrendale, PA, 1986), p. 63.
- ⁷⁵See A. G. Khachatryan, *Theory of Structural Thermodynamics in Solids* (Wiley, New York, 1983).
- ⁷⁶D. M. Ceperly and B. J. Alder, *Phys. Rev. Lett.* **45**, 566 (1980); J. P. Perdew and A. Zunger, *Phys. Rev. B* **23**, 5048 (1981).
- ⁷⁷L. Hedin and B. I. Lundqvist, *J. Phys. C* **4**, 2063 (1971).
- ⁷⁸F. D. Murnaghan, *Proc. Natl. Acad. Sci. (U.S.A.)* **30**, 244 (1944).
- ⁷⁹S. Froyen, *Phys. Rev. B* **39**, 3168 (1984), and references therein.
- ⁸⁰J. L. Martins and A. Zunger, *Phys. Rev. Lett.* **56**, 1400 (1986); *J. Mater. Res.* **1**, 523 (1986); P. B. Littlewood, *Phys. Rev. B* **34**, 1363 (1986).
- ⁸¹S.-H. Wei and A. Zunger, *Phys. Rev. B* **35**, 2340 (1987).
- ⁸²D. M. Wood, S.-H. Wei, and A. Zunger, *Phys. Rev. B* **37**, 1342 (1987).
- ⁸³S.-H. Wei, *Phys. Rev. Lett.* **59**, 2613 (1987).
- ⁸⁴S.-H. Wei and A. Zunger, *Phys. Rev. B* **39**, 3279 (1989).
- ⁸⁵S.-H. Wei and A. Zunger, *Phys. Rev. Lett.* **61**, 1505 (1988); (b) N. E. Christensen, S.-H. Wei, and A. Zunger, *Phys. Rev. B* **40**, 1642 (1989).
- ⁸⁶K. Ishida, T. Shumiya, T. Nomura, H. Ohtani, and T. Nishizawa, *J. Less Common Met.* **142**, 135 (1988).
- ⁸⁷For the fitting we used the calculated data $\bar{\epsilon}_n(\bar{V}(x))$ at $X_n - 0.125 < x < X_n + 0.125$ with step size $\Delta x = 0.025$; that is, 11 values for each n .
- ⁸⁸(a) M. F. Grattion and J. G. Woolley, *J. Electron. Mater.* **2**, 455 (1973); *J. Electrochem. Soc.* **127**, 55 (1980); (b) J. R. Pessetto and G. B. Stringfellow, *J. Cryst. Growth* **62**, 1 (1983).
- ⁸⁹J. C. Mikkelsen and J. B. Boyce, *Phys. Rev. Lett.* **49**, 1412 (1982).
- ⁹⁰A. Balzarotti, P. Letardi, and N. Motta, *Solid State Commun.* **56**, 471 (1985).
- ⁹¹C. Y. Fong, W. Weber, and J. C. Phillips, *Phys. Rev. B* **14**, 5387 (1976).

- ⁹²R. F. Brebrick and R. J. Panlener, *J. Electrochem. Soc.* **121**, 932 (1974); R. F. Brebrick, C. H. Su, and P. K. Liao, in *Semiconductors and Semimetals*, edited by R. K. Willardson and A. C. Beer (Academic, New York, 1983), p. 171.
- ⁹³P. A. Fedders and M. W. Muller, *J. Phys. Chem. Solids* **45**, 685 (1984).
- ⁹⁴J. A. Van Vechten, in *Semiconductor Handbook*, edited by S. P. Keller (North-Holland, Amsterdam, 1980), Vol. 3, p. 1.
- ⁹⁵A. Marbeut, F. Karouta, H. Dexpert, P. Lagarde, and A. Joullie, *J. Phys. (Paris) Colloq.* **47**, 369 (1986).
- ⁹⁶A. Qteish, N. Motta, and A. Balzarotti, in *Proceedings of the 19th International Conference on the Physics of Semiconductors, Warsaw, 1988*, edited by W. Zawadzki (Institute of Physics, Polish Academy of Sciences, Warsaw, 1988), Vol. 2, p. 865; *Phys. Rev. B* **39**, 5987 (1989).
- ⁹⁷(a) T. Ito, *Phys. Status Solidi B* **129**, 559 (1985); (b) *Jpn. J. Appl. Phys.* **26**, 256 (1987); **26**, L1330 (1987); **26**, 1625 (1987); (c) *Phys. Status Solidi B* **135**, 493 (1986); (d) in *Proceedings of the 18th International Conference on Semiconductor Physics, Stockholm*, edited by O. Engström (World Scientific, Singapore, 1987), p. 1225.
- ⁹⁸M. Ichimura and A. Sasaki, *J. Appl. Phys.* **60**, 3850 (1986); *Superlatt. Microstruct.* **3**, 127 (1987); *Jpn. J. Appl. Phys.* **26**, 246 (1987); **26**, 1296 (1987); **26**, 2061 (1987).
- ⁹⁹(a) A. Balzarotti, M. T. Czyzyk, A. Kisiel, P. Letardi, N. Motta, M. Podgorny, and M. Zimnal-Starnawska, *Festkörperprobleme* **25**, 689 (1985); (b) P. Letardi, N. Motta, and A. Balzarotti, *J. Phys. C* **20**, 2853 (1987); (c) M. T. Czyzyk, M. Podgorny, A. Balzarotti, P. Letardi, N. Motta, A. Kisiel, and M. Zimnal-Starnawska, *Z. Phys. B* **62**, 153 (1986).
- ¹⁰⁰A. Sher, M. Van Schilfgaarde, A. B. Chen, and W. Chen, *Phys. Rev. B* **36**, 4279 (1987).